Multi-Scale Dynamical Modeling of Correlated Systems Based on Dynamical Mean-Field Theory

Zhijie Fan
Beijing, China

BS Physics,
Hong Kong University of Science and Technology,
Hong Kong, China, 2016

A Dissertation Presented to
the Graduate Faculty of the University of Virginia
in Candidacy for the Degree of
Doctor of Philosophy

Department of Physics
University of Virginia
August, 2021

Abstract

In this thesis, we introduce a novel scheme of adiabatic quantum molecular dynamics (QMD), in which the electron degrees of freedom are integrated out on the fly by the dynamical mean-field theory (DMFT) calculation. Compared with the QMD based on the popular density functional theory, our new scheme is able to describe phenomena due to strong electron correlation, such as Mott metal-insulator transition (MIT). Moreover, our DMFT-QMD also provides information on the incoherent non-quasi-particle electronic excitations, thus significantly generalizing the capability of Gutzwiller/Slave-boson-based QMD recently developed by our group. We use this new MD method to study the Mott transition in an atomic liquid of hydrogen-like atoms. We observe a reentrant phase transition driven by Coulomb repulsion and obtain various nontrivial atomic and electronic properties of the system.

Additionally, we combine exact diagonalization with molecular dynamics simulation to study the correlated liquid model in the strong coupling limit, in which the local moments on atoms dominate. We discover a tendency of dimer formation in the system and the dimers undergo a dissociation process driven by Coulomb repulsion.

Our work opens a new avenue for multi-scale dynamical simulations and modeling of strongly correlated electron systems. Our results provide unique insights into the dynamics and the electronic properties of the MIT in correlated liquid systems.

Acknowledgements

First and foremost, I would like to express my deepest gratitude to my supervisor Prof. Gia-Wei Chern for his continuous support and guidance during my Ph.D. study. Prof. Chern has provided me with invaluable advice and abundant resources along with my academic researches. I have learned a lot from his deep insight, immense knowledge, and plentiful experiences in physics research and various aspects.

Moreover, my gratitude extends to the defense committee members Prof. Keivan Esfarjani, Prof. Joe Poon, and Prof. Israel Klich for their insightful questions and suggestions. I would also like to thank Prof. Keivan Esfarjani, Prof. Mona Zebarjadi, and Prof. Bellave Shivaram for their instruction during our collaborations. In addition to that, thanks to Dr. Shi-Zeng Lin of Los Alamos National Lab and Prof. Adolfo del Campo of the University of Luxembourg for their assistance to our fruitful researches.

Besides that, I would like to express my appreciation to the students and faculties of the Physics Department. They have given me great support during my stay in Charlottesville. Their presence makes my life in the U.S. enjoyable.

Finally, I am extremely grateful to my parents and grandparents for their unwavering support and belief in me. I would also like to express my deepest love and thanks to my girlfriend, Emma. Without her understanding and encouragement in the past few years, it would be impossible for me to complete my Ph.D. study.

Contents

List of Figures

Chapter 1

Introduction

Modern condensed matter physics dedicates to explain all kinds of physical phenomena in various materials. Over the last 100 years, physicists have developed many successful theories to predict the properties of simple metals and some semiconductors and insulators. Typically, effective single-electron pictures, in which electrons are considered to be non-interacting with each other, are sufficiently accurate for these materials. Among all the properties of materials, electronic properties are probably one of the most important classes since they are closely related to the development of novel electronic technologies. Therefore, numerous theories, including band theories and Fermi liquid theory, have been developed to extensively investigate the electronic properties of materials, such as band structure, magnetism, and electronic transportation [1, 2]. Perhaps, one of the most successful and most widely-used theories is the density functional theory (DFT) that is based on the Kohn–Sham equations [3, 4], within which the ground state properties of many simple elements and semiconductors, and even of some insulators are accurately described. With the powers of the local density approximation (LDA) [5], the generalized gradient approximation (GGA) [6], and the LDA+U method [7], the magnetic and electron orbital properties and the crystal structures of many materials have been successfully predicted in the framework of the DFT [8, 9].

Despite the great success of these theories in many materials, the situation turns out to be complicated when attempting to explain the physics of systems with strong mutual electron-electron interactions. In this case, the effects of interacting (correlated) electrons are too conspicuous for them to be treated as independent particles. Such strong electron correlations can often be identified in transition metals, such as vanadium, iron, and corresponding oxides. In these materials, open d and f electron shells exist, and electrons occupy narrow orbitals. Thus, the electrons experience strong Coulombic repulsion due to the spatial confinement in those narrow orbitals, triggering a dramatic increase in the problem's complexity. For instance, in transition metal oxides, there are two competing forces acting on the electrons - the Coulombic repulsion that tends to localize individual electrons at atoms and the hybridization with the oxygen p electron states that tend to delocalize electrons. Because of this competition, a rich amount of physics are produced [1]. Additionally, at low temperatures, the internal degrees of freedom - spin ($S = \pm 1/2$), charge ($-e$), and orbital moment - of the d and f electrons and their coupled dynamics can lead to complex phases, such as liquid-like, crystal-like, and liquid-crystal-like states of electrons, and phenomena, like the electronic phase separation and the pattern formation [1, 10, 11].

On the one hand, for weakly correlated materials, such as silicon or aluminum, the DFT method and other non-interacting treatments can be a good starting point to capture the nature of the system using perturbation theories [12]. On the other hand, those theories, even the powerful DFT, fail to accurately describe the electronic and structural properties of strongly correlated systems because they miss the strong correlation effects in those systems [1, 9, 12, 13]. Take nickel oxide and manganese oxide as an example. They are insulators with relatively low magnetic-ordering temperatures but large insulating gaps; nevertheless, the conventional band theory fails to make the correct insulating prediction when the long-range magnetic order is missing [12]. It is suggested by Nevill Mott that those insulators can be better understood from a real-space picture by considering the solid as a system consisting of localized electrons bounded to atoms via open shells. Excitations in this system are achieved by simply adding and removing electrons from an atom [14, 15]. Furthermore, the modeling of the strongly correlated system is challenging when the system is away from the two well-understood limits and has electrons that are neither fully mobile (wave-like) nor fully localized (particle-like). Because of this dual nature of electrons in the system, it is vital to combine both the real-space and momentum-space pictures to describe the complete physics of the system [12].

In particular, one of the simplest models of correlated electronic systems that can demonstrate such competition is the famous Hubbard Model,

$$H = -\sum_{i,j,\sigma} h_{ij} \left(c^{\dagger}_{i,\sigma} c_{j,\sigma} + c^{\dagger}_{j,\sigma} c_{i,\sigma} \right) + U \sum_{i} n_{i,\uparrow} n_{i,\downarrow}, \tag{1.1}$$

where the matrix element h_{ij} describes the hopping of electrons with spin σ between orbitals at sites i and j; the constant U is the local Coulomb repulsion between two electrons on the same site i; $n_{i,\sigma} = c^{\dagger}_{i,\sigma} c_{i,\sigma}$ is the density of electrons at site i with spin σ. Although the Hamiltonian has a relatively simple form, the Hubbard model can lead to profound physics, which makes it very difficult to solve [16]. In the Hubbard model, the kinetic energy and the interaction energy are characterized by the hopping term h_{ij} and the local Coulomb repulsion U, respectively. Hence, the competition between the inter-orbital electron hopping h_{ij} and the intra-orbital Coulomb repulsion U can be described by this minimal model, which is at the very heart of the electronic many-body problems. Although a variety of physical properties can be derived from this simple model, the properties of the system are governed by some rather fundamental parameters, namely the ratio between the Coulomb repulsion U and the bandwidth W that is determined by the hopping matrix h_{ij}, the temperature T, and the filling fraction of electrons n.

Moreover, the Hubbard model described in Eq.(1.1) is a single orbital Hubbard model, in which the electron hoppings and the local Coulomb interactions are limited to one single orbital on each atom, whereas multi-orbital hopping and coupling are actually common in real systems, in which interacting electrons can occupy d and f shells that have multiple orbitals and exhibit complex interactions within these shells. This is the multi-orbital Hubbard model. For example, if interacting electrons occupy the d-orbitals, namely $d_{z^2}, d_{x^2-y^2}, d_{xy}, d_{yz}$ and d_{xz} orbitals, the Coulomb repulsion will be described using a 5 by 5 interaction matrix U_{mn} depending on both Coulomb repulsion

U and Hund's coupling J [9, 17, 18]. In fact, this interaction matrix could be simplified to reduce the complexity of problems using various approximations, like focusing on only the orbitals with dominating influence to obtain a smaller U_{mn}, or ignoring the off-diagonal terms in the interaction matrix U_{mn} that might not be significant to the overall physics.

Despite the difficulties encountered when studying even the simplest strongly correlated system, physicists are constantly interested in investigating a wide variety of physical properties of these systems. A major topic of strongly correlated system physics is the metal-insulator transition (MIT), which could be one of the oldest, yet one of the fundamentally least understood problems in condensed matter physics and materials science [12, 14]. As stated above, the two limits - good insulators and good metals - have been well explained using simple theories developed long ago, but understanding the intermediate regime between them remains challenging because it is difficult to reconcile the wave-particle duality nature of electrons in materials. In a metal, electrons are well described by Bloch waves, but in an insulator, they are better understood from a real-space picture as localized particles occupying atomic orbitals [14, 15]. The MIT driven by strong electron correlation are of most importance, in which itinerant electrons (metallic) become localized (insulating) due to strong on-site Coulomb repulsion. This phenomenon is also called the Mott transition [19]. Understanding the nature of MIT and attempting to master the MIT has become the major driving force behind the discoveries of many novel phenomena in materials science.

Searching for high-temperature superconductivity plays an important role in modern physics researches, and the discovery of cuprates superconductors with exceptionally high transition temperature [20] revived people's interest in strongly correlated systems because they are closely related to the Hubbard model. Cuprates superconductors are layered, consisting of superconducting planes of copper oxide separated by intermediate layers of ions. From a phenomenological angle, it is widely accepted that the "parent state" in the cuprates is a quasi-2D antiferromagnetic insulator, and the Hubbard model on the square lattice is the simplest possible model of a doped antiferromagnetic state. Further connections between the cuprates and the Hubbard model were made by the surprisingly good matches between theoretical studies and experimental results. Many of the properties of the Hubbard model obtained from theoretical investigations turn out to resemble the characteristic features of the electronic states of the cuprates [16, 21, 22].

Another widespread interest in copper oxides and other correlated-electron systems is the colossal magnetoresistance (CMR) phenomenon [23, 24]. Magnetoresistance is the phenomenon that the material exhibits a change of resistance in the presence of an applied magnetic field. In contrast, in materials with colossal magnetoresistance, a small increase in the external magnetic field will lead to a gigantic decrease in resistivity [1]. The ability to control MIT in an unconventional way offers hope that correlated-electron systems may provide a basis for the development of next-generation low-power, high-speed electronics technology [1]. For instance, researchers are developing the so-called Mott transistors that utilize the collective response of electrons in the MIT for switching. The Mott transistors are much faster than the con-

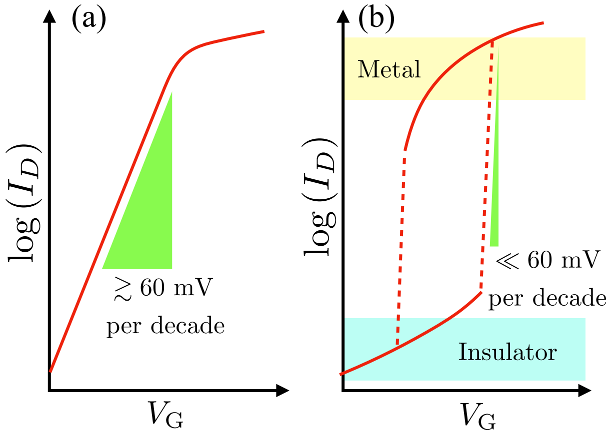

Figure 1.1: Schematic current-voltage curve of (a) the MOSFET and (b) the Mott-transistor. The switching of the Mott-Transistor is through a MIT induced by a gate voltage, which can be much faster than the Boltzmann limit 60mV/decade.

ventional metal-oxide-semiconductor field-effect transistors (MOSFET) with a switching speed bounded by the Boltzmann limit [29, 30, 31, 32, 33, 34, 35].

Aside from the material with CMR, another promising candidate for Mott transistors is the vanadium dioxide VO_2, which is one of the prototypical correlated materials [36]. The metal-insulator transition temperature of vanadium dioxide is slightly above the room temperature, and across the MIT, it exhibits a huge change in resistivity. These properties attracted enormous attention from both physicists and engineers. Based on the unique properties of VO_2, prototypes of novel electronics has been developed [30, 31, 32, 33, 34, 35]. An important phenomenon observed during the recent studies of the MIT in the real correlated compounds such as VO_2 and $NdNiO_3$ is the existence of structural distortions and highly inhomogeneous electronic states during the MIT. In particular, several near-field spectroscopy and nano-imaging experiments

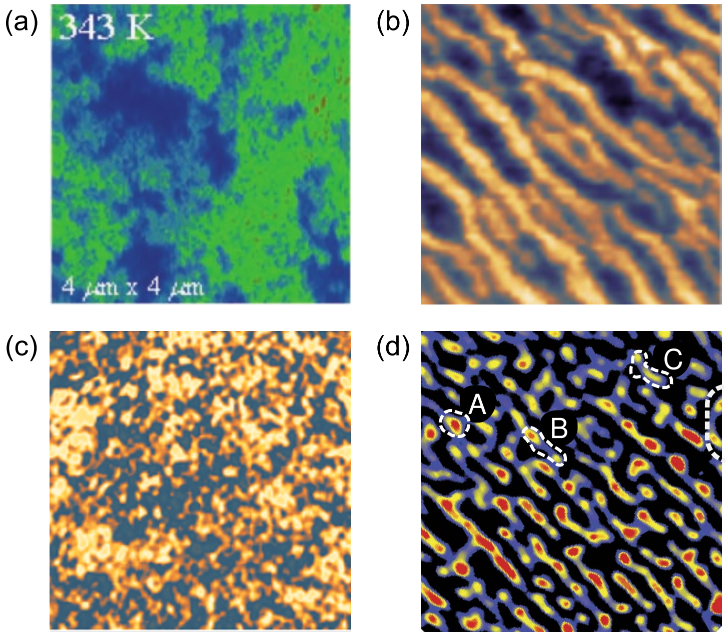

Figure 1.2: Mesoscopic textures revealed by the near-field nano-imaging during the metal-insulator transition (MIT): (a),(b) temperature-driven MIT in VO_2 [25, 26] without and with external strain, respectively. Panels (c) and (d) show the nano-scale phase separation at the MIT of another function Mott material $NdNiO_3$ [27, 28]. The color gradient indicates the local metallicity of the sample.

have uncovered complex nano-scale textures during the MIT of these strongly correlated material as shown in Fig. 1.2 [30, 31, 32, 33, 34, 35]. All these properties of the strongly correlated system make the prospects for developing applications from correlated-electron materials exciting. However, the richness of the phenomena, and the sensitivity to microscopic details such as structural distortions and spatial inhomogeneity, make their experimental and analytical study more difficult.

In order to study the wide variety of physical properties in strongly correlated systems and understand the MIT, numerous numerical techniques and analytical methods have been used. A traditional approach of studying a correlated system is to model and solve the corresponding Hamiltonian of the system; however, in practice, it is a highly complex problem itself to reduce the fully many-body Hamiltonian to a solvable model that can preserve the characteristic features and the physics of the original system. Without reducing the degree of freedom, the solution of the original Hamiltonian, whose Hilbert space grows exponentially, is not feasible. For instance, mean-field theories (MFT) can be utilized to give an approximate overall description of the physical properties of many-body models. In a mean-field theory, the fluctuating field created by the many-body interactions in the actual Hamiltonian is approximated by an averaged effective field, namely the mean-field, such as the Weiss mean-field approach in the Ising model. Thus, the original many-body lattice problem reduces (or maps) to a single-site problem with effective parameters [9].

The well-known Hartree-Fock (HF) mean-field methods can be applied to the Hubbard model. Adopting the Hartree approximation, correlations can be eliminated by factorizing the local interaction term $n_{i,\uparrow} n_{i,\downarrow}$.

$$U \sum_i n_{i,\uparrow} n_{i,\downarrow} \approx U \sum_i \left(n_{i,\uparrow} \langle n_{i,\downarrow} \rangle + \langle n_{i,\uparrow} \rangle n_{i,\downarrow} - \langle n_{i,\uparrow} \rangle \langle n_{i,\downarrow} \rangle \right) \tag{1.2}$$

In this approximation, correlations of the fluctuations are neglected and the mean field is static, thus it is not accurate enough to described the physical nature of the strongly correlated systems, especially near the metal-insulator transition (MIT) driven by the Coulomb repulsion U [14].

More advanced many-body techniques were later developed to handle the strong electron correlations in lattice models, such as Quantum Monte Carlo methods [37, 38] and variational methods [39]. Among all these numerous methods, the Gutzwiller variational method is perhaps the most efficient approach that can successfully capture the essential correlation effects. The basic idea of the Gutzwiller approximation (GA) method is to apply an operator to a Slater determinant which reduces the probability amplitude of doubly occupied states, and double occupancy probability is optimized variationally [39, 40]. The GA method not only provides us an effective single-particle picture but also captures the crucial correlation effects of the system, such as band narrowing and electron localization. Combined with *ab initio* methods, such as the LDA, the GA method has proven to be successful in studying real correlated materials [41, 42, 43]. It was recently combined with molecular dynamics methods to investigate the dynamics and the electronic properties of a strongly correlated liquid system [44, 45].

Further progress in studying strongly correlated systems was made by the development of the dynamical mean-field theory [13, 46]. The essence of a mean-field theory is to map a many-body lattice problem to a single-site problem with effective parameters. Likewise, in the dynamical mean-field theory, the many-body lattice problem is simplified by mapping it onto a single-impurity model embedded in a medium that has to be determined self-consistently. The impurity model is connected to the original many-body problem via a set of self-consistent equations. In contrast to Hartree-Fock-type approximations, the mean-field in the DMFT is dynamical, whereby the local quantum fluctuations are fully taken into account. The dynamical mean-field theory has opened new perspectives for investigating strongly correlated electron systems and greatly improved our understanding of correlation effects in models and materials. Furthermore, extensions of DMFT, such as cluster DMFT, inhomogeneous DMFT, and nonequilibrium DMFT, were developed to capture more sophisticated interactions and characteristics in the strongly correlated systems, including short-range quantum fluctuations, spatial inhomogeneity, and nonequilibrium dynamics of the electrons [47, 48, 49, 50, 51].

In addition to the methods introduced above, other new techniques have been developed and been applied to the strongly correlated system, such as the self-energy functional theory [52, 53], the density matrix renormalization group (DMRG) [54] and the numerical linked-cluster expansions methods [55, 56, 57, 58, 59]. With the help of all these newly developed theories and methods, people are getting closer to the great goal of understanding and mastering the metal-insulator transition.

Nowadays, one major research topic in the field of strong correlation physics is to combine the *ab initio* calculations and DMFT methods to predict the properties of real materials [2]. Another focus of the community is to describe the quantum fluctuations better using more complex extensions of DMFT method [47] or calculate more accurate results for challenging models using better impurity solvers. Unfortunately, there are currently only a limited amount of studies on the multi-scale modeling of the strongly correlated systems that can include both the microscopic many-body physics of the strongly correlated electrons and the macroscopic modeling of complex phase transition kinetic. As revealed in the experiments, the spatial inhomogeneity can be found in the vicinity of the MIT of real materials such as VO_2 [34, 35], which is closely related to the development of correlation-based electronics. However, it is currently relatively less focused. The formation of these nano-textures and their dynamical properties remain unanswered, and a comprehensive and microscopic understanding of MIT dynamics is further required. To summarize, the difficulty of developing such an understanding is partly due to the multi-scale and multi-faceted nature of the MIT kinetics. On the one hand, accurate modeling of strongly correlated electrons requires advanced many-body techniques, most of which are computationally too expensive to be directly combined with large-scale dynamical simulations. On the other hand, the mesoscale electronic inhomogeneities associated with the MIT are reminiscent of the complex systems dominated by nonlinear and nonequilibrium processes.

In this thesis, we are interested in bridging this gap. We propose a multi-scale dynamical simulations scheme and modeling of strongly correlated electron systems based on the molecular dynamics and the dynamical mean-field theory. This novel scheme provides information on the incoherent non-quasi-particle electronic excitations during the molecular dynamics, thus significantly generalizing the capability of Gutzwiller/Slave-boson-based QMD recently developed by our group [44, 45]. Moreover, we proposed a second scheme combining molecular dynamics with the exact diagonalization to dynamically simulate correlated systems in the strongly correlated limit where local magnetic moments dominate and interact via exchange interactions. It allows us to investigate the interplay between the correlation and the kinetics of the local moments, which is also crucial in developing a relatively complete understanding of MIT [60]. These two methods were applied to a strongly correlated liquid system to illustrate the physical pictures on both sides of the Mott transition in a liquid system.

Chapter 2

Dynamical Mean Field Theory

In this chapter, we give a summary of the dynamical mean-field theory (DMFT) and related topics. Meanwhile, some basic notations are established for the succeeding chapters.

The dynamical mean-field theory discussed in this chapter is the conventional homogeneous DMFT (single-site DMFT). Although it is not designed to capture the spatial inhomogeneity in the Hubbard model that we are most interested in, it can serve as a good demonstration of the basic ideas of the DMFT, such as the mapping from the Hubbard model to an effective impurity problem and the self-consistent loop of DMFT. As the foundation of all other extensions of DMFT methods, the homogeneous DMFT can help one understand the inhomogeneous DMFT method introduced in the later chapter since their central ideas are similar. Additionally, basic properties of the Hubbard model, such as the first-order U driven MIT and the doping δ driven MIT, are also discussed based on the numerical results obtained from DMFT, such as spectral functions and quasi-particle weights. The impurity solvers used in our simulations are also briefly discussed.

The dynamical mean-field theory is derived for the case of the single-band Hubbard mode (1.1) in this chapter. It is assumed, for simplicity, that no symmetry breaking occurs, which means that we only consider the paramagnetic phase without any long-range order. Note that, to capture the long-range order of the Hubbard model, such as the antiferromagnetic state in the Mott phase, one should apply the extensions of DMFT, like cluster DMFT [47]. The above Hamiltonian made no assumption to the atomic system in which the Hubbard model resides. Thus, it can be on various systems, from liquid systems without a well-defined lattice to solid systems with translational invariant crystal structures in d-dimension.

The numerical results displayed in this chapter are obtained by solving a homogenous Hubbard model on the Bethe lattice using DMFT. The Hubbard model on the Bethe lattice has been extensively studied using DMFT methods [13, 61, 62]. Indeed, the simple form of its non-interacting (bare) density of state (DOS) is convenient for the DMFT calculation, which is given by

$$\rho_0\left(\omega\right) = \frac{2}{\pi}\sqrt{1-\left(\frac{\omega}{D}\right)^2} \tag{2.1}$$

where $D = 2t$ is the half bandwidth. In this chapter, the energies are in units of D, and we set $D = 1$ for clarity.

2.1 Dynamical Mean Field Theory

As outlined in the introduction, the central idea of a mean-field theory is to reduce the full many-body model to an effective single-particle model. Similarly, in the dynamical mean-field theory framework, a particular site i is chosen and the degree of freedom of all other sites are integrated out, which results in an effective local action [9, 13, 63]:

$$
\begin{aligned}
S_{\text{eff}} = &- \int_0^\beta d\tau \int_0^\beta d\tau' \sum_\sigma c^\dagger_{0\sigma}(\tau)\, \mathcal{G}_0^{-1}(\tau-\tau') c_{0\sigma}(\tau') \\
&+ U \int_0^\beta d\tau n_{0\uparrow}(\tau) n_{0\downarrow}(\tau)
\end{aligned}
\tag{2.2}
$$

where the bare Green's function $\mathcal{G}_0(\tau-\tau')$ is given by

$$
\mathcal{G}_0^{-1}(i\omega) = i\omega + \mu - \Delta(i\omega) \tag{2.3}
$$

In this expression, the Green's function is transformed to the Matsubara frequencies iw_n domain,

$$
\mathcal{G}_0(i\omega_n) = \int_0^\infty d\tau \mathcal{G}_0(\tau) e^{i\omega_n \tau}, \quad \omega_n = \frac{(2n+1)\pi}{\beta} \tag{2.4}
$$

where β is the inverse temperature; $\Delta(i\omega)$ is the hybridization function that describes the coupling of the local site i with the rest of the system. Here the bare Green's function $\mathcal{G}_0(\tau-\tau')$ corresponds to the Weiss effective field in the conventional mean-field theories in statistical mechanics [13]. The physical constant of $\mathcal{G}_0(\tau-\tau')$ is that of an effective amplitude for an electron to be created on the impurity site i at imaginary time τ and being destroyed at time τ', namely, an electron coming from the external bath at τ and going back to the bath at τ'. In contrast to the classical mean-field theory, where the quantum fluctuations are ignored and thus being static, this effective "Weiss field" $\mathcal{G}_0$ takes full account of the temporal fluctuations. Therefore, the local temporal fluctuations are fully taken into account in the DMFT, and this is from where the name "dynamical" comes. Furthermore, it can be seen that the effective action in Eq. (2.2) is a purely local problem. Therefore, one can identify this action S_{eff} as that of a local impurity problem; consequently, the many-body model is then mapped to an impurity problem which has an action of the same form of the effective local action S_{eff}. Moreover, this requires the local Green's function of the Hubbard model G_{local} to coincide with the impurity Green's function G_{imp}

$$G_{\text{imp}}\left(i\omega\right) = G_{\text{local}}\left(i\omega\right) \tag{2.5}$$

The relation between local Green's function G_{imp} and the Weiss field $\mathcal{G}_0$ can be expressed in the form of a Dyson's equation

$$\begin{aligned} G^{-1}_{\text{imp}}(i\omega_n) &= \mathcal{G}^{-1}_0(i\omega_n) - \Sigma(i\omega) && (2.6) \\ &= i\omega + \mu - \Delta(i\omega) - \Sigma\left(i\omega\right), && (2.7) \end{aligned}$$

$\Sigma(i\omega_n)$ is the self-energy of the local impurity problem which is also the self-energy of the Hubbard model. Then, by assuming this self-energy to be strictly local [13, 46, 63], i.e. momentum-independent, the system Green's function of the original many-body system is given by,

$$G^{-1}(k, i\omega) = \omega + \mu - \epsilon_k - \Sigma_{\text{new}}(i\omega), \tag{2.8}$$

Finally, the local green's function can be recovered using system Green's function $G(k, \omega)$ via a Hilbert transformation,

$$G_{\text{imp}}(i\omega) = G_{\text{local}}(i\omega) = \sum_k G(k, i\omega) \tag{2.9}$$

The above equations form a self-consistent loop that establish the mapping from the Hubbard model to impurity model. These equations can also be written on the real-axis, by simply replacing $i\omega_n$ with ω. Once the algorithm of solving the impurity problem S_{eff} is known, one can solve the correlated system self-consistently,

$$\Sigma \to G \to \mathcal{G}_0 \to \Sigma \tag{2.10}$$

Starting from a self-energy Σ, the full Green's function (Green's function of the Hubbard model) G is calculated. Then, the local Green's function G_{local} and corresponding Weiss field $\mathcal{G}_0$ are obtained from G and Σ. Finally, a new self-energy Σ_{new} can be obtained by solving the impurity problem defined by $\mathcal{G}_0$ and acts as the initial self-energy of the next iteration. The algorithm converges when the input self-energy and the output self-energy are identical $\Sigma = \Sigma_{\text{new}}$.

2.2 Impurity solvers

The most complicated step in the DMFT calculation is to solve the impurity problems defined by the action S_{eff}. In practice, the local Green's function is obtained by solving the impurity problem in a Hamiltonian formulation instead of solving the action S_{eff} directly. For the Hubbard model, the corresponding impurity model is a single-impurity Anderson model (SIAM) consisting of an impurity f coupled to a bath of conducting electron $c_{k,\sigma}$. The Hamiltonian of SIAM is given by [13],

$$H_{\text{SIAM}} = \epsilon_f \sum_{\sigma} f_{\sigma}^{\dagger} f_{\sigma} + \sum_{k,\sigma} \epsilon_{k,\sigma} c_{k,\sigma}^{\dagger} c_{k,\sigma} \tag{2.11}$$

$$+ \sum_{k,\sigma} V_k \left(c_{k,\sigma}^{\dagger} f_{\sigma} f_{\sigma}^{\dagger} c_{k,\sigma} \right) + U f_{\uparrow}^{\dagger} f_{\uparrow} f_{\downarrow}^{\dagger} f_{\downarrow} \tag{2.12}$$

In this Hamiltonian, $c_{k,\sigma}^{\dagger}(c_{k,\sigma})$ corresponds to band states in a non-interacting bath with spin σ and energy ϵ_k, and $f_{\sigma}^{\dagger}(f_{\sigma})$ corresponds to impurity states with energy ϵ_f.

Fortunately, Anderson impurity problems have been extensively studied in the past, and various solvers have been developed. For instance, one of the most powerful and widely used impurity solvers is the continuous-time quantum Monte-Carlo algorithm (CTQMC), which in principle can provide exact results for the impurity problem [13]. Indeed, it is subject to several drawbacks, such as the famous sign problems and its huge computational cost. Nevertheless, it has been widely used in the LDA+DMFT calculations in which the strong correlations during the *ab initio* calculation are handled using DMFT [2, 17].

We developed two impurity solvers during our study: a real-axis iterative perturbation theory solver and a numerical renormalization group solver. They will be briefly explained below.

2.2.1 Iterative Perturbation Theory

The Iterative Perturbation Theory (IPT) is an approximation method that relies on the interpolation from 2nd order perturbation theory for the Anderson impurity problem. The interpolation preserves the correct high-frequency limit for the self-energy and is exact in both the non-interacting and the atomic limits [13, 61, 64].

The self-energy in the IPT is parametrized by,

$$\Sigma(\omega) \approx U\frac{n}{2} + \frac{A\Sigma^{(2)}(\omega)}{1 - B\Sigma^{(2)}(\omega)} \tag{2.13}$$

where,

$$\begin{aligned}\Sigma^{(2)}(\omega) = U^2 \int_{-\infty}^{0} d\varepsilon_1 \int_{0}^{\infty} d\varepsilon_2 d\varepsilon_3 \frac{\rho^{(0)}(\varepsilon_1)\rho^{(0)}(\varepsilon_2)\rho^{(0)}(\varepsilon_3)}{\omega + \varepsilon_1 - \varepsilon_2 - \varepsilon_3 - i\eta} && (2.14)\\ + U^2 \int_{0}^{\infty} d\varepsilon_1 \int_{-\infty}^{0} d\varepsilon_2 d\varepsilon_3 \frac{\rho^{(0)}(\varepsilon_1)\rho^{(0)}(\varepsilon_2)\rho^{(0)}(\varepsilon_3)}{\omega + \varepsilon_1 - \varepsilon_2 - \varepsilon_3 - i\eta} && (2.15)\end{aligned}$$

with $\rho^{(0)} = \frac{1}{\pi}\text{Im}G_0$. Here the bare Green's function is defined by,

$$G_0(\omega) = \frac{1}{\omega + \mu_0 - \Delta(\omega)} \tag{2.16}$$

Note that this bare Green's function is equivalent to the $\mathcal{G}_0$ in the DMFT formulism. The parameter μ_0 is a fictitious chemical potential. In the half-filling case $\mu_0 = 0$, but for the arbitrary filling case, it is yet to be fixed. The constants A and B are given by,

$$A = \frac{n(1-n)}{n_0(1-n_0)}, \tag{2.17}$$

$$B = \frac{(1-n)U + \mu_0 - \mu}{n_0(1-n_0)U^2} \tag{2.18}$$

Here n_0 is a fictitious particles number determined from G_0,

$$n_0 = -\int d\omega \frac{1}{\pi} f(\omega) \mathrm{Im} G_0(\omega) \tag{2.19}$$

Here $f(\omega)$ is Fermi distribution function. As stated above, for the arbitrary filling case, the parameter μ_0 is yet to be fixed. There exist different ways to determine it [61, 64]. In our simulation, we compute μ_0 by setting the fictitious particles number to the physical particle number n of the impurity problem,

$$n = -\int d\omega \frac{1}{\pi} f(\omega) \mathrm{Im} G(\omega) \tag{2.20}$$

The interacting Green's function of the impurity problem follows from,

$$G(\omega) = \frac{1}{G_0(\omega) - \mu_0 + \mu - \Sigma(\omega)} \tag{2.21}$$

Numerically, this can be done via standard root-finding algorithms, such as Newton's methods and bisection methods. When incorporating to the DMFT,

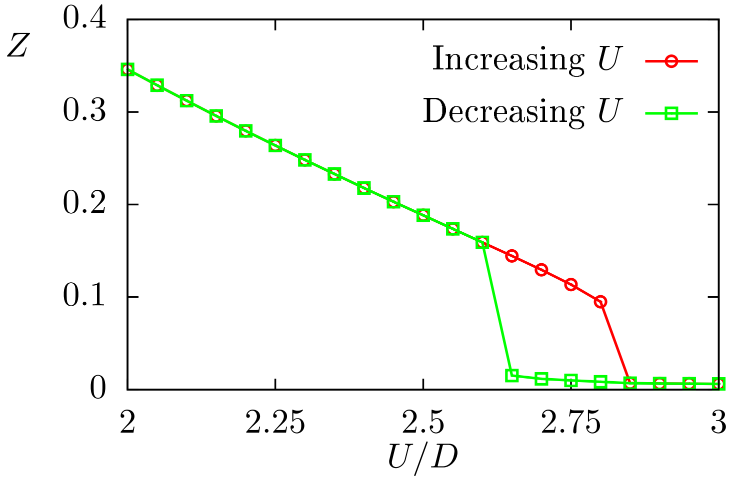

Figure 2.1: Quasi-particle weight as a function of U/D on a half-filled Bethe lattice at $T = 0.03$. D is half bandwidth of the bare density of state. The red curve is obtained from increasing U simulation and the green curve is from a decreasing U simulation. The clear hysteresis near the transition suggested that the U driven metal-insulator transition in Hubbard model is of first-order. It can be estimated from the plots that $U_{\mathrm{c}1} \sim 2.6D$ and $U_{\mathrm{c}2} \sim 2.8D$.

this $G(\omega)$ is equivalent to the local Green's function $G_{\mathrm{loc}}(\omega)$, therefore the μ_0 can also be fixed using the particle number calculated from $G_{\mathrm{loc}}(\omega)$.

One important quantity that can be obtained from the DMFT calculation is the quasi-particle weight also known as the mass renormalization factor Z, which is defined as,

$$Z = \frac{m}{m^*} = \left(1 - \left.\frac{\partial \mathrm{Re}\Sigma(\omega)}{\partial \omega}\right|_{\omega \to 0}\right)^{-1} \tag{2.22}$$

where m is the physical mass of electron and m^* is the effective mass of electron. It can act as a criterion for identifying metal-insulator transition. In a metallic system, there is a finite quasi-particle weight, while Z vanishes when the system becomes insulating.

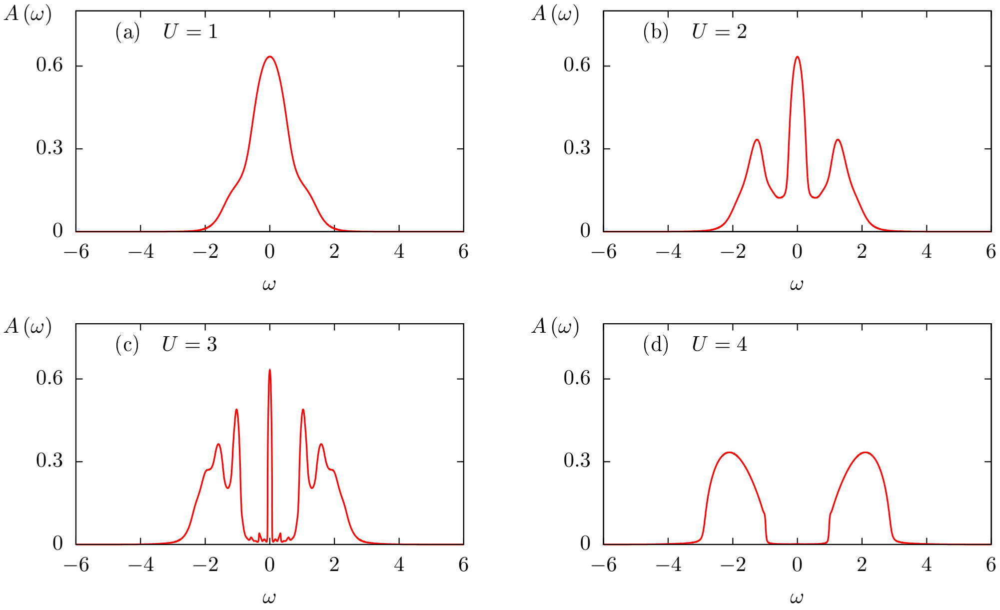

Figure 2.2: The spectral functions of half-filled Hubbard model on Bethe lattice at various U, at $T = 0.01$, obtained from a real-axis IPT solver. The unit of U is $D = 1$. The panel (b) shows the typical three peaks structure, when the localization and delocalization effects are comparable. The panel (d) shows a Mott state where two Hubbard bands can be found at $\pm U/2$.

In Fig. 2.1, the quasi-particle weight is plotted as a function of U/D on a half-filled Bethe lattice at $T = 0.03$. $D = 1$ is the half bandwidth of the bare density of states. As the U increases (decreases), dramatic changes of Z can be observed. The critical U for the transition can be estimated from the plots: $U_{\mathrm{c}1} \sim 2.6D$ and $U_{\mathrm{c}2} \sim 2.8D$. An evident hysteresis appears near the transition suggesting that the U driven metal-insulator transition in the Hubbard model is first-order.

The spectral function which contains the information of the incoherent non-quasi-particle electronic excitations of electron, is another quantity of interest when studying the strongly correlated system. It can be obtained from the imaginary part of the Green's function,

$$A(\omega) = -\frac{1}{\pi}\mathrm{Im}\left(G(\omega)\right) \tag{2.23}$$

The MIT can be monitored using the features of a spectral function. For instance, in a metallic phase, a quasi-particle peak appears at the Fermi level $\omega = 0$ (the Fermi level is usually shifted to 0 during the DMFT calculation); however, a gap opens at $\omega = 0$, and two Hubbard bands grow out at $\pm U/2$ when the system enters a Mott insulating phase. The spectral functions of a half-filled Hubbard model on Bethe lattice at various U, at $T = 0.01$ are shown in Fig. 2.2.1. It can be seen that as the strength of Coulomb repulsion U increases, the quasi-particle peak at $\omega = 0$ vanishes when the system enters the Mott state and the spectral weight of central peak shifts to the two Hubbard bands at $\pm U/2$. The spectral functions of doped Hubbard models on Bethe lattice are shown in Fig. 2.2.1. The system is at $T = 0.01$. The doping factor is given by $\delta = 1 - 2n$. By observing Fig. 2.2.1(d) and Fig. 2.2.1(b) and Fig. 2.2.1(c), one can see that at low temperature doping-driven transition from insulating phase to a metallic phase can occur. The original Mott state at $U = 4$ has a gap at the Fermi level, while a small doping $\delta = 0.04$ to the system results in a metallic state with a clear quasi-particle peak at $\omega = 0$. In a word, the insulting system can transit a metal after doping. The doping in these simulations is directly controlled using the chemical potential μ. In experiments, the chemical potential can be controlled by applying a gate voltage. Such ability to control the doping-driven MIT can help scientists to develop Mott transistors [30].

The major advantage of this method is that it has a relatively low computational cost, and the calculation is performed directly on the real-axis (no analytical continuation is required), which makes it suitable for solving multiple impurity problems in the real space extension of DMFT. Although IPT provides an approximate solution to the impurity problem, its results are qualitatively accurate and can offer valuable insights into the correlated system [61].

2.2.2 Numerical Renormalization Group

The numerical renormalization group (NRG) solver is a state-of-the-art impurity solver, which is also considered as an exact method [50, 62, 65]. Similar to the IPT solver, the NRG solver works on the real frequency axis directly. The central of this method, the anderson impurity problem (2.11) is mapped to a semi-infinite chain,

$$
\begin{aligned}
H =&\epsilon_f \sum_{\sigma} f_{\sigma}^{\dagger} f_{\sigma} + U f_{\uparrow}^{\dagger} f_{\uparrow} f_{\downarrow}^{\dagger} f_{\downarrow} && (2.24)\\
&+ \sqrt{\frac{\xi_0}{\pi}} \sum_{\sigma} (f_{\sigma}^{\dagger} c_{0\sigma} + c_{0\sigma}^{\dagger} f_{\sigma}) && (2.25)\\
&+ \sum_{\sigma n=0}^{\infty} [\epsilon_n c_{n\sigma}^{\dagger} c_{n\sigma} + t_n (c_{n\sigma}^{\dagger} c_{n+1\sigma} + c_{n+1\sigma}^{\dagger} c_{n\sigma})] && (2.26)
\end{aligned}
$$

This Hamiltonian is then solved by iterative diagonalization technique: the semi-infinite chain is solved by adding one site to the chain at a time [62, 65].

The spectral functions of the half-filled Hubbard model on Bethe lattice at various U, at $T = 1e^{-6}$ are shown in Fig. 2.2.2. Similar to the IPT results, as the strength of Coulomb repulsion U changes, the system undergoes a standard Mott transition. At $U = 2.5$, both metallic and insulating solutions can coexist. In the coexistence regime, the final result of a DMFT simulation is sensitive to the initial condition.

This method can achieve very high accuracy at low energy regime; however, it suffers from low resolution at high frequency due to logarithmic discretization of hybridization function [62].

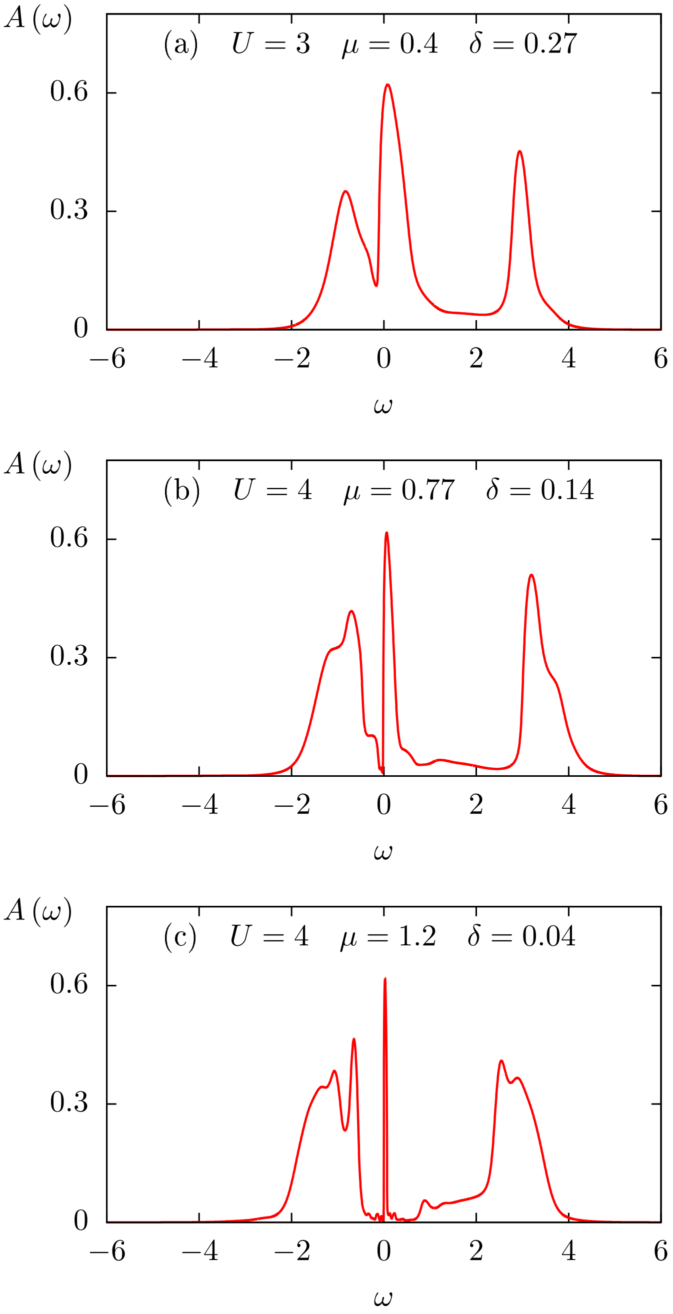

Figure 2.3: The spectral functions of various doped Hubbard model on Bethe lattice at $T = 0.01$, obtained from a real-axis IPT solver. Finite doping at low temperature can drive a Mott insulating phase to a metallic phase.

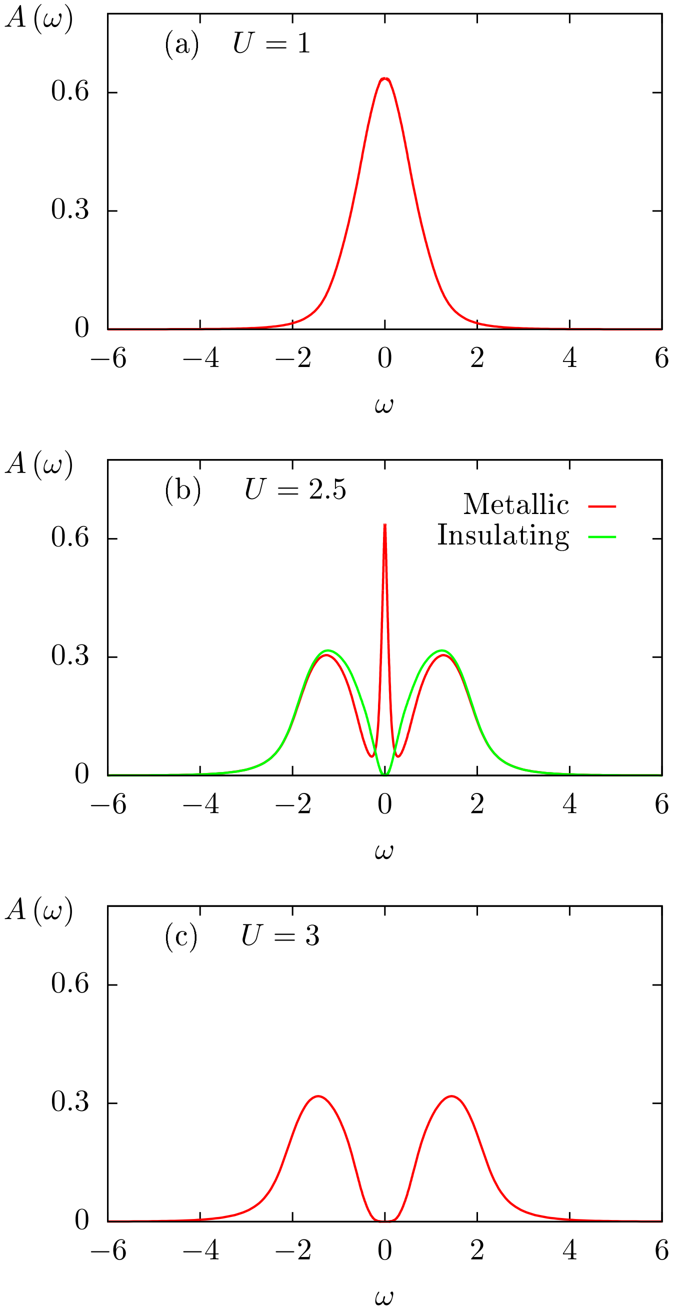

Figure 2.4: The spectral functions obtained from DMFT+NRG. The calculations are performed on half-filled Hubbard models on Bethe lattice at $T = 1e^{-6}$. In penal (b), both metallic and insulating solutions coexist. In the coexistence regime, the final results is sensitive to the initial condition.

Chapter 3

Molecular Dynamics with Dynamical Mean Field Theory

Metal-insulator transition (MIT) continues to be an essential subject in modern condensed matter physics even after more than sixty years of study [14, 66]. Unlike conventional phase transitions that can be characterized by broken symmetries, the MIT originates from the different dynamical behaviors, itinerancy versus localization, of electrons. There are two basic mechanisms that cause electron localization. It was shown by Anderson that disorder or strong spatial fluctuations result in well-localized electron wave function even in the absence of interactions [67, 68]. On the other hand, in the Mott transition scenario, localization of electrons is driven by strong short-range Coulomb repulsion [19, 69]. The interplay of these two scenarios lead to interesting phenomena such as disordered-induced local moment formation and electronic Griffiths phase [60, 70, 71, 72, 73, 74, 75].

While extensive efforts have been devoted to understanding the effects of quenched disorder on correlated lattice models, much less is known about the Mott transition in an atomic liquid, which in a sense can be viewed as correlated electrons subject to a dynamical disorder. In fact, fluid systems, such as liquid mercury and alkali metals, had played a crucial role in our understanding of MIT in disordered medium [76, 77, 78, 79, 80]. Early theoretical models, however, assumed electron interactions are negligible in atomic liquids and focused on the disorder effect [77, 81, 82]. Assuming no particular short-range order of atoms, such theories for MIT in liquid are not much different from those developed to describe amorphous solids. For example, Mott's theory for liquid semiconductors and mercury posited a disorder-induced pseudogap within which the electron states are localized through the Anderson mechanism [77]. A metal-to-insulator transition occurs when the density of states at the Fermi level is below a threshold, and the pseudogap opens near the Fermi energy [83, 84].

Theoretical approaches to liquid-state MIT based on Anderson localization mechanism often implicitly assume an atomic configuration similar to that of amorphous solid, an assumption which is not always justified. On the other hand, models based on percolation theory have been proposed that link the atomic structure to the MIT in liquid. For example, a lattice gas system has been used to model the percolation MIT in the super-critical regime of fluid metals [85, 86, 87]. Percolation scenarios were also obtained from reverse Monte Carlo modeling on neutron diffraction data of expanded alkali fluid [88]. As the atomic density is decreased, atoms start to fragment into clusters which can be associated with a strong tendency to maintain metallic bonding. Close to the critical point, a conducting network remains where finite clusters are connected through weak atomic links. The resultant MIT is suggested to be driven by a process similar to bond percolation [88, 89, 90].

The importance of disorder for the electron localization in liquid metals does not preclude the correlation effect as a driving force for MIT, especially for transition-metal or rare-earth compounds. For example, the first-order phase transition in liquid metallic cerium is mainly driven by the localization of f electrons [91]. Moreover, in the percolation picture discussed above, finite metallic droplets stabilized by the binding force from delocalized electrons could be rather resilient during a density-driven MIT in an atomic liquid. Electron localization driven by correlation effects thus could be the dominant mechanism for the break up of atomic clusters in this scenario. Of particular interest is the MIT in expanded metallic alkali fluids. Early theoretical works already emphasized the importance of electron correlation for the MIT in such monovalent liquid systems [92, 93]. Various experimental studies also hinted at a correlation-driven metal-nonmetal transition in supercritical alkali liquid [94, 95, 96, 97, 98, 99]. In particular, experiments on liquid cesium observed an enhancement of magnetic susceptibility close to the critical density [97, 98, 99], a telltale sign of Mott-Hubbard type transition.

It is worth noting that discussions of MIT in liquid systems are often based on the Born-Oppenheimer approximation, which assumes that electron relaxation is much faster than atomic motion. Consequently, the problem of electronic structure and electron transport in an atomic liquid can be treated assuming a quasi-static atomic configuration. However, since the structure of an atomic liquid is determined by the interatomic forces, which in turn depend on the electronic properties, a consistent approach is required in order to account for the subtle interrelation between atomic structure and electron wave function. For example, the formation of metallic atomic clusters embedded in the expanded fluid, as discussed above, results from the nontrivial interplay between atom dynamics and electron delocalization. The appearance of molecules during MIT is another important and unique aspect of the liquid system.

The evolution of atomic configuration can be efficiently modeled by the molecular dynamics (MD) simulation [100, 101, 102], which has a long history dating back to the famous Fermi-Pasta-Ulam-Tsingou nonlinear chain simulation in 1953 [103]. By providing a general approach to understand and analyze material functionalities in terms of dynamics at the atomic level, MD essentially plays the role of a computational microscope. Although conceptually, MD simulation is simply the integration of Newton's equation of motion for a large number of atoms, the challenging part is the calculation of interatomic forces. In the widely used classical MD methods, these interatomic forces are computed from predetermined empirical potentials or force fields [104]. Since the evolution of the electronic subsystem is not consistently accounted for, such classical approaches certainly cannot describe electronic phase transitions such as MIT.

The scope and predictive power of MD methods are greatly enhanced by using the quantum approach for force calculation [105, 106, 107, 108, 109, 110].

In such quantum MD (QMD) schemes, the forces acting on atoms are obtained by solving the many-electron Schrödinger equation on the fly as the atomic trajectories are generated. The validity and limitation of a QMD scheme then depend on the approximations used in solving the many-body problem. For example, the well-known Hartree-Fock (HF) mean-field methods were used in the early development of *ab initio* MD methods [111, 112]. The most popular QMD methods nowadays are based on density functional theory (DFT) [3, 4, 113, 114], or more specifically, the Kohn-Sham (KS) approach. By recasting the intractable complexity of the many-electron interactions into the form of effective one-electron energy that is a unique functional of the electron density, the KS method achieves a desirable tradeoff between accuracy and efficiency. Assisted by high-performance computers and advanced algorithms, DFT-MD is now firmly established as an essential research tool in physics, chemistry, biology, and materials sciences.

Although DFT is in principle exact, its accuracy in practical implementation depends on approximations used for the exchange-correlation functional, whose exact universal expression is not known. The local density approximation (LDA) and its variants are among the most popular methods [6, 115, 116]. One particular limitation of these approximations is their inability to describe phenomena that is due to strong electron correlation. While modified methods such the self-interaction correction or DFT+U have proven useful for some applications [7, 117, 118, 119], it is still very difficult to capture generic electron correlation effects and particularly the Mott metal-insulator transition in the KS approach.

On the other hand, several many-body techniques have been developed to handle strong electron correlation in lattice models such as the Hubbard and Anderson Hamiltonians [16, 120]. Among them, the Gutzwiller variational method is perhaps the most efficient approach that successfully captures the essential correlation effects [39, 40, 121]. For example, the Brinkman-Rice theory [122] of the Hubbard model, which is based on the Gutzwiller method, had offered important insight on the Mott transition. Contrary to a single Slater-determinant underlying either the HF or KS methods, the Gutzwiller wave function is a multi-Slater-determinant that is variationally optimized to balance the kinetic energy gain due to electron delocalization against the local Coulomb repulsion when two electrons reside at the same orbital [123].

In an effort to develop MD methods for correlated electron materials, a new QMD scheme [44, 45, 124] was recently proposed that is based on the Gutzwiller wave function and the Gutzwiller approximation (GA). Interatomic forces in such GA-MD simulations are computed from a Gutzwiller wave function that has to be iteratively optimized at every time step. Crucially, similar to other self-consistent approaches such as HF or KS methods, the GA also reduces the intractable many-body problem into an effective single-electron one in terms of a renormalized tight-binding Hamiltonian, which is to be solved self-consistently. Indeed, in its modern formulation in terms of slave bosons, GA can be viewed as a mean-field theory for the Mott transition with amplitudes of slave-bosons serving as the order parameters [125, 126, 127, 128]. Consequently, the computational cost of GA-MD simulation is similar to that of DFT-MD.

It is worth noting that MD methods based on a self-consistent independent-electron approach, including HF, KS, and GA, can only describe the behavior of quasi-particles of the electronic system. The quasi-particles basically are solutions of the self-consistent single-electron Schrödinger equation. Importantly, while the HF or KS quasi-particles are electrons whose single-particle states have been renormalized by interactions, but whose effective mass and Fermi distribution remain unchanged with respect to the non-interacting case, the quasi-particles described by the GA are Landau quasi-particles with an enhanced mass m^* [123]; the divergence of m^* signals the localization of electrons and the onset of Mott transition.

The quasi-particle weight in GA is directly related to the renormalization of inter-site hopping and the electron bandwidth. Although GA provides a qualitatively, and often quantitatively, correct description for correlated metals through the concept of renormalized quasi-particles, it fails to account for the incoherent electronic excitations and the appearance of Hubbard bands. Moreover, the non-Fermi liquid behavior and electronic Griffiths phase [73, 74, 75] that result from the interplay of disorder and electron correlation are also beyond the capability of GA-MD methods.

In this chapter, we propose a new quantum MD scheme that goes beyond self-consistent independent-electron picture for strongly correlated electron systems. Our approach is based on an efficient integration of the tight-binding molecular dynamics method with the dynamical mean-field theory (DMFT) [2, 12, 13, 129]. Contrary to most quantum MD methods that rely on solving an effective single-particle Schrödinger equation, the DMFT-MD scheme is entirely based on the self-consistent solution for the electron Green's function, thus offering the capability of computing the complete spectral function that includes the quasi-particle peaks and the incoherent excitations represented by the Hubbard bands. Within DMFT, the Mott transition results from the transfer of spectral weight from the quasi-particle peak to the Hubbard bands.

The central idea of DMFT is the approximation of a local self-energy, which, in the case of translation-invariant system, assumes that the electron self-energy is momentum-independent $\Sigma(\omega, \mathbf{k}) \approx \Sigma(\omega)$. This locality approximation is shown to be exact in the limit of infinite dimensions $d \to \infty$ [46, 130, 131], although DMFT often gives rather accurate results already for $d = 3$. Importantly, DMFT can be generalized to inhomogeneous systems by allowing a site-dependent but still local self-energy. In this approach, often called the real-space or statistical DMFT [49, 50, 51, 132, 133, 134, 135, 136], the interacting many-body problem is mapped to a set of quantum impurity models, one for each atom, which is solved self-consistently. The real-space DMFT methods have been used to study Mott transitions in, e.g., Anderson-Hubbard model, correlated cold-atom systems, and heterostructures of correlated materials. Importantly, our new QMD scheme is also built on the real-space DMFT in order to treat random atom configurations in liquid metals.

We apply the DMFT-MD to simulate the MIT in a model system for correlated s-band liquid metal. Conceptually, this model is perhaps the most intuitive generalization of the Hubbard model to an atomic liquid, allowing one to study the generic interplay of dynamical disorder and electron correlation. It is worth noting that the Hubbard liquid model also serves as a minimum model for MIT in alkali fluids. Our DMFT-MD simulations, on the one hand, allow us to investigate how electron correlation affects the atom distribution and transport behaviors, confirming several of the results obtained in previous GA-MD simulations [44]. On the other hand, by going beyond the GA, we are able to compute, for the first time, the electron spectral function and examine the evolution of quasi-particle peak and Hubbard bands in an atomic liquid that undergoes a Mott transition. Three distinct liquid phases are identified in this model based on the atomic structure and electronic properties.

3.1 The Hubbard liquid model

The repulsive-interaction Hubbard model is one of the canonical models for strongly correlated electron systems [16, 39, 137, 138, 139]. It is perhaps the simplest model that encodes the competition between electron delocalization and on-site electron correlation. Despite its simplicity, it exhibits a wide range of correlated electron behavior, including interaction-driven metal-insulator transitions, superconductivity, and magnetism [140, 141]. Originally proposed as a model system to describe correlation-driven MIT, a renewed interest in the 2D Hubbard model was spurred by the discovery of high-temperature cuprate superconductors [16]. Several recent comparative studies based on a wide variety of state-of-the-art numerical methods have also been performed for the two-dimensional Hubbard model [142, 143, 144].

The Hubbard model can be solved exactly only in the one-dimensional case, although no Mott transition is found in this special limit [145]. On the other hand, Mott transition has been demonstrated in the infinite limit of the Hubbard model [46, 130, 131], which also inspires the development of the approximation methods such as GA and DMFT. In particular, the frustrated Hubbard model at half-filling is the testbed for studying the correlation-induced MIT. Here we present a natural generalization of the Hubbard model to an atomic liquid, which is then studied using the DMFT-MD simulations to be discussed below. The Hubbard liquid model is defined as

$$\begin{aligned}\mathcal{H} &= \sum_{i,j}\sum_{\sigma} h(|\mathbf{R}_i - \mathbf{R}_j|)\, c^{\dagger}_{i,\sigma} c_{j,\sigma} + U \sum_{i} n_{i,\uparrow} n_{i,\downarrow}, \\ &\quad + \frac{1}{2}\sum_{i\neq j} \phi(|\mathbf{R}_i - \mathbf{R}_j|) + \sum_{i} \frac{\mathbf{P}_i^2}{2M}, \qquad (3.1)\end{aligned}$$

where $\mathbf{R}_i$ and $\mathbf{P}_i$ are the position and momentum vectors, respectively, of the i-th atom, $c^{\dagger}_{i,\sigma}$ ($c_{i,\sigma}$) creates (annihilates) an electron of spin $\sigma = \uparrow, \downarrow$ at atom-i, $n_{i,\sigma} = c^{\dagger}_{i,\sigma} c_{i,\sigma}$ is the electron number operator, $h_{ij} = h(|\mathbf{R}_i - \mathbf{R}_j|)$ denotes the hopping amplitude between a pair (ij) of atoms, $U > 0$ is the Hubbard term due to on-site Coulomb repulsion, and $\phi(|\mathbf{R}_i - \mathbf{R}_j|)$ is a classical pairwise repulsive potential between atoms. The first two terms in Eq. (3.1) correspond to a Hubbard model with random hoppings h_{ij} that is determined by the instantaneous atomic configuration $\{\mathbf{R}_i\}$. The last term describes the classical kinetic energy of atoms with mass M. For clarity, here, we use the uppercase letters to denote position, momentum, and mass for nuclei, while lowercase letters are used for electrons.

To complete the model, one needs to specify the dependence of the hopping amplitude $h(R_{ij})$ and pair potential $\phi(R_{ij})$ on the relative distance $R_{ij} =$

$|\mathbf{R}_j - \mathbf{R}_i|$ between two atoms. The fact that these two functions depend only on the distance R_{ij} is due to the isotropy of the s-orbital. The hopping of these s-orbitals gives rise to the formation of σ-bonds. In terms of Wannier functions as the basis for the s-band, the transition amplitude is given by the integral

$$h_{ij} = \int w_i(\mathbf{r}) \left[-\frac{\hbar^2 \boldsymbol{\nabla}^2}{2m} + V_{\text{nuclei}}(\mathbf{r}) \right] w_j(\mathbf{r}) \, d^3\mathbf{r} \tag{3.2}$$

where $w_j(\mathbf{r})$ is the Wannier function centered at atom-i, m is the electron mass, and $V_{\text{nuclei}}(\mathbf{r})$ is the potential field created by the nuclei and the inert core electrons, which can be implemented using the pseudo-potentials. The challenging part is the calculation of the basis of Wannier functions. One approach is to start from atomic-like orbitals obtained by solving the single-atom Schrödinger equation with appropriate pseudo-potentials to account for the effects of inner core electrons. The Wannier functions $w_i(\mathbf{r})$ are then obtained from proper orthogonalization of the atomic-orbital functions. Generally speaking, the Wannier functions are well localized at the individual atoms, which means the transfer integral h_{ij} decays rapidly with increasing separation R_{ij}.

Given the Wannier functions, one can compute the following interaction parameters

$$V_{ijkl} = \int\!\!\int \frac{e^2 w_i^*(\mathbf{r}) w_j^*(\mathbf{r}) w_k(\mathbf{r}') w_l(\mathbf{r}')}{|\mathbf{r} - \mathbf{r}'|} \, d^3\mathbf{r} \, d^3\mathbf{r}'. \tag{3.3}$$

The Hubbard parameter, which in general depends on atom index, is given by $U_i = V_{iiii}$. It is worth noting that, while the off-site Coulomb interactions, such as V_{iijj} or V_{ijij}, are not included in the tight-binding (TB) Hubbard model Eq. (3.1), they can be included into the effective single-electron Schrödinger equation, from which the Wannier functions $w_i(\mathbf{r})$ are obtained, through a conventional HF treatment. Finally, the atomic pair potential is given by the integral

$$\phi_{ij} = \int\int \frac{e^2 \rho_i(\mathbf{r}) \rho_j(\mathbf{r}')}{|\mathbf{r} - \mathbf{r}'|} d^3\mathbf{r} d^3\mathbf{r}', \tag{3.4}$$

where $\rho_i(\mathbf{r}) = \delta(\mathbf{r} - \mathbf{R}_i) - |w_i(\mathbf{r})|^2$ is charge density of the nucleus at the i-th atom screened by the s-orbital electron. Since the net charge associated with $\rho_i(\mathbf{r})$ is zero, the integral ϕ_{ij} also decays rapidly with increasing atomic distance R_{ij}.

Although the approach described above can, in principle, be used to construct the TB-Hubbard model, it is computationally very demanding to be incorporated into quantum MD simulations, especially since this has to be done at every MD step. Practically, in order to efficiently carry out the multiple integrals listed above, one usually starts with Gaussian approximations for the eigenfunctions of the atomic pseudo-potentials. However, even with the Gaussian functions, the calculation of parameters for the instantaneous TB-Hubbard model is still very time-consuming. The advantage of this procedure is that the Hubbard parameter U can be unambiguously obtained from the first principles. A more efficient procedure is to use the DFT as the starting point to construct the effective TB-Hubbard model, similar to that used for the LDA+DMFT method for realistic correlated electron materials. Although the Wannier functions can be more efficiently computed in such approaches, the determination of the Hubbard U is quite tedious. Further approximations, such as the double-counting method, are often used for practical calculations.

In this work, we do not attempt to obtain the *ab initio* TB-Hubbard model for liquid alkali metals. Moreover, for QMD simulations of the Hubbard liquid, the DMFT solver, to be discussed in the next section, already requires huge computational overhead. Instead, we treat the Hubbard liquid model Eq. (3.1) as a minimum model system to capture the Mott-Hubbard physics in an atomic liquid system and investigate the new physics that arise from the interplay between electron correlation and atomic dynamics. To this end, further approximations are introduced. First, the Hubbard parameter U is treated as a model parameter, which is independent of atoms. Explicit calculations in the case of hydrogen liquid show that the variation of U among atoms is indeed small.Second, as discussed above, the hopping integral is a strongly decaying function with distance thanks to the well-localized Wannier functions. For simplicity, we assume an exponential decay function for the hopping constant

$$h(R) = h_0 \exp(-R/\xi), \tag{3.5}$$

where h_0 and ξ are two model parameters characterizing the amplitude and range of electron hopping. Finally, since the atomic pair potential describing the Coulomb repulsion between screened nuclei is also short-ranged, we assume it also decays exponentially

$$\phi(R) = \phi_0 \exp(-R/\ell). \tag{3.6}$$

Here ϕ_0 and R are also parameters of the model system. We emphasize that, because of these approximations, our results are not expected to quantitatively describe MIT in realistic alkali fluids or other liquid metals. Instead, similar to the spirit of the lattice Hubbard model, our goal is to study the behaviors (e.g., phase diagram, different scenarios of phase transitions) of this model correlated system with different parameters. We believe the main results of this model study will not be qualitatively affected by these approximations.

3.2 Molecular dynamics with DMFT

Next, we discuss the formulation of a QMD scheme that employs DMFT to solve the many-electron problem. QMD or, more specifically, *ab initio* MD (AIMD) can be classified into adiabatic or non-adiabatic approaches [109]. The representative example of adiabatic QMD is the Born-Oppenheimer molecular dynamics (BOMD) which assumes that electrons adjust instantaneously to the slower motion of the nuclei so that the motion of the latter is governed by a single adiabatic potential energy surface (PES). On the other hand, electronic transitions between multiple PESs are taken into account in non-adiabatic MD simulations [146]. In this work, we will focus on the adiabatic limit, which is also the starting point of most DFT-based MD methods.

3.2.1 Quantum molecular dynamics based on electron Green's functions

The governing equations of adiabatic MD are often obtained from certain ansatz for the total wave function, as detailed in Ref. [109]. Such approaches have also been the basis of most QMD simulations that are based on the effective independent-electron methods. Since the DMFT-MD is formulated in terms of electron Green's functions, instead of wave functions, we first discuss such QMD formalism and outline the corresponding adiabatic approximation. We start with the dynamical equation for the nuclei. In order to properly obtain the electronic force, we consider the Heisenberg equation of motion for the nuclei position operator $d\hat{\mathbf{R}}/dt = [\hat{\mathbf{R}}, \mathcal{H}]/i\hbar$. Following standard procedures, the expectation value of this equation gives the classical Newton equation of motion

$$M\frac{d^2\mathbf{R}_i}{dt^2} + \gamma\frac{d\mathbf{R}_i}{dt} = -\left\langle \frac{\partial \mathcal{H}}{\partial \mathbf{R}_i} \right\rangle + \boldsymbol{\eta}_i(t), \tag{3.7}$$

where M is mass of the nuclei, $\mathbf{R}_i = \langle \hat{\mathbf{R}}_i \rangle$ is now a classical position vector. We have included the dissipation force and thermal noise as in the Langevin dynamics; here γ is a damping coefficient and $\boldsymbol{\eta}_i(t) = (\eta_i^x, \eta_i^y, \eta_i^z)$ denotes a vector whose components are normal-distributed random variables with zero mean:

$$\begin{aligned} \langle \eta_i^\alpha(t) \rangle &= 0, \qquad (3.8) \\ \langle \eta_i^\alpha(t)\eta_j^\beta(t) \rangle &= 2\gamma k_B T \delta_{\alpha\beta}\delta_{ij}\delta(t-t'). \end{aligned}$$

The standard second-order velocity-Verlet method is used to integrate the above equation of motion. It is worth noting that the deterministic force, the first term on the right hand side of Eq. (3.7), is not given by the conservative form $-\partial\langle\mathcal{H}\rangle/\partial\mathbf{R}_i$. The equivalence of these two expressions is due to the Hellmann-Feynman theorem under certain approximations. Substituting the Hamiltonian Eq. (3.1) into the above expression, we obtain two contributions to the force

$$\mathbf{F}_i = -\left\langle \frac{\partial\mathcal{H}}{\partial\mathbf{R}_i} \right\rangle = \mathbf{F}_i^p + \mathbf{F}_i^e, \tag{3.9}$$

where the superscript p and e indicates contributions from the pair potential and the electrons, respectively. The first term, which describes the short-range repulsion between atoms, is given by

$$\mathbf{F}_i^p = -\sum_j \frac{\partial\phi_{ij}}{\partial\mathbf{R}_i} = \sum_j \phi'(R_{ij})\,\hat{\mathbf{n}}_{ij}, \tag{3.10}$$

where $\phi'(R) = d\phi(R)/dR$ and $\hat{\mathbf{n}}_{ij}$ is a unit vector pointing in the direction of vector $\mathbf{R}_{ij} = \mathbf{R}_j - \mathbf{R}_i$. This classical force is easy to compute for the Hubbard liquid model. The electron part is

$$\begin{aligned}\mathbf{F}_i^e &= -\sum_{j,\sigma} \frac{\partial h_{ij}}{\partial\mathbf{R}_i}\langle(c^\dagger_{i\sigma}c_{j\sigma} + \text{h.c.})\rangle \\ &= 2\sum_{j,\sigma} h'(R_{ij})\,\hat{\mathbf{n}}_{ij}\,\mathrm{Re}[\rho_{j\sigma,i\sigma}]. \end{aligned}\tag{3.11}$$

The electronic force depends on the single-electron (reduced) density matrix

$$\rho_{i\sigma,j\sigma'}(t) = \langle c^\dagger_{j\sigma'}(t) c_{i\sigma}(t)\rangle. \tag{3.12}$$

It is worth noting that both forces as well as the reduced density matrix vary with time. For effective independent-electron approaches, such as HF or GA, this density matrix is computed from the eigen-solution of the effective one-particle Hamitlonian $H^{\rm eff}_{i\sigma,j\sigma'}[\{\mathbf{R}_i(t)\}]$, which depends on time through the nuclei coordinates. Specifically, let $U^m_{i,\sigma}$ be the normalized eigenvector of the one-electron Hamiltonian with eigenenergy ϵ_m, the density matrix is $\rho_{i\sigma,j\sigma'} = \sum_m f(\epsilon_m) U^{m\,*}_{i\sigma} U^m_{j\sigma'}$, where $f(\epsilon_m)$ is the Fermi-Dirac function for the occupation probability of the m-th eigenstate.

As discussed above, contrary to the effective independent-electron QMD methods, the DMFT-MD is formulated in terms of the electron Green's function. Of particular importance is the lesser Green's function

$$G^<_{i\sigma,j\sigma'}(t_1,t_2) = i\langle c^\dagger_{j\sigma'}(t_2) c_{i\sigma}(t_1)\rangle. \tag{3.13}$$

The reduced density matrix is given by the equal-time lesser Green's function: $\rho_{i\sigma,j\sigma'}(t) = -iG^<_{i\sigma,j\sigma'}(t,t)$. Also important are the retarded Green's function defined

$$G^R_{i\sigma,j\sigma'}(t_1,t_2) = -i\theta(t_1-t_2)\langle\{c_{i\sigma}(t_1), c^\dagger_{j\sigma'}(t_2)\}\rangle, \tag{3.14}$$

and the associated advanced Green's function $G^A_{i\sigma,j\sigma'}(t_1,t_2) = [G^R_{j\sigma',i\sigma}(t_2,t_1)]^\dagger$.

In terms of the lesser Green's function, the electronic force becomes

$$\mathbf{F}_i^e(t) = 2\sum_{j,\sigma} t'(R_{ij}(t))\, \hat{\mathbf{n}}_{ij}(t)\, \mathrm{Im}\, G^<_{j\sigma,i\sigma}(t,t). \tag{3.15}$$

Here we have explicitly included all the time dependences. A consistent dynamical description thus requires the equation of motion for the lesser Green's function. This can be achieved by the nonequilibrium Green's function (NEGF) theory. For example, a complete dynamical theory can be obtained by combining the Newton equation of motion (3.7) for nuclei with the Kadanoff-Baym equations for Green's functions.

$$\begin{aligned}\left[i\frac{\partial}{\partial t_1} + \mu - \mathbf{h}(t_1)\right] \mathbf{G}^<(t_1,t_2) = \\ \int dt_3 \Big[\mathbf{\Sigma}^R(t_1,t_3)\mathbf{G}^<(t_3,t_2) + \mathbf{\Sigma}^<(t_1,t_3)\mathbf{G}^A(t_3,t_2)\Big],\end{aligned} \tag{3.16}$$

$$\begin{aligned}\left[i\frac{\partial}{\partial t_1} + \mu - \mathbf{h}(t_1)\right] \mathbf{G}^{R/A}(t_1,t_2) &= \delta(t_1-t_2)\,\mathbf{I} \\ &+ \int dt_3 \mathbf{\Sigma}^{R/A}(t_1,t_3)\mathbf{G}^{R/A}(t_3,t_2).\end{aligned} \tag{3.17}$$

Here bold symbols are used to denote matrices in the atom-spin basis, $\mathbf{\Sigma}^<$ and $\mathbf{\Sigma}^{R/A}$ are the lesser, retarded, and advanced self-energies, respectively, μ is the electron chemical potential, and the time-varying matrix $\mathbf{h}(t)$ describes the electron hopping of the Hamiltonian in Eq. (3.1),

$$h_{i\sigma,j\sigma'}(t) = \delta_{\sigma\sigma'}\, h(|\mathbf{R}_i(t) - \mathbf{R}_j(t)|). \tag{3.18}$$

For many-body interacting systems, after introducing suitable approximations such as Born approximation or HF to relate the self-energy Σ to Green's functions, the Kadanoff-Baym equation can then be integrated along with the Newton equation of motion [147, 148, 149, 150]. However, even without the atom dynamics, numerical integration of the inhomogeneous Kadanoff-Baym equation is computationally very demanding. So far, its implementation is restricted to small systems.

The calculation can be much simplified when the nuclei and electrons evolve on significantly different time scales, allowing the system to split into fast (electron) and slow (nuclei) degrees of freedom. To this end, we transform the Kadanoff-Baym equations to the Wigner space where fast and slow time scales are easily identifiable. We define the average and relative time parameters: $t = (t_1 + t_2)/2$ and $\tau = t_1 - t_2$, and introduce the Wigner representation of the Green's functions,

$$\begin{aligned} \mathbf{G}(\omega, t) &= \int e^{i\omega\tau} \mathbf{G}\left(t_1, t_2\right)\, d\tau, \\ \mathbf{G}(t_1, t_2) &= \frac{1}{2\pi} \int e^{-i\omega\tau} \mathbf{G}(\omega, t)\, d\omega. \end{aligned} \tag{3.19}$$

A coupled set of differential equations for the Green's functions in the Wigner representation is obtained by applying the same transformation to Eqs. (3.16) and (3.17). Working in the Wigner space allows one to perform a systematic adiabatic expansion by using variation with respect to the central time t as a small parameter. Similar approaches have recently been extensively investigated in the context of current-induced forces in quantum transport and nonequilibrium BOMD simulations [151, 152, 153, 154, 155]. Formally, we introduce a adiabaticity parameter ϵ which is of the order of $\epsilon \sim |d\mathbf{R}_i/dt|$, and expand the Green's functions in a power series, $\mathbf{G} = \mathbf{G}^{(0)} + \epsilon \mathbf{G}^{(1)} + \epsilon^2 \mathbf{G}^{(2)} + \cdots$. The Kadanoff-Baym equations can then be solved systematically for each order of ϵ.

The adiabatic limit, which is also most relevant to our work, is given by the zero-th order results. For the retarded/advanced Green's functions, the zero-th order solutions are

$$\mathbf{G}^{R/A}(\omega, t) = \left[(\omega + \mu)\, \mathbf{I} - \mathbf{h}(t) - \mathbf{\Sigma}^{R/A}(\omega, t) \right]^{-1}. \tag{3.20}$$

Here the self-energies $\mathbf{\Sigma}^{R/A}$ only depend on the zeroth-order Green's functions through some many-body scheme, which in our case is the DMFT to be discussed below. This is essentially the "equilibrium" Green's functions one would obtain for the Hubbard Hamiltonian defined by the instantaneous atomic configuration $\{\mathbf{R}_i(t)\}$. The zeroth-order lesser Green's function, which is needed for the force calculation in Eq. (3.15) is given by

$$\mathbf{G}^{<}(\omega, t) = \mathbf{G}^{R}(\omega, t)\, \mathbf{\Sigma}^{<}(\omega, t)\, \mathbf{G}^{A}(\omega, t), \tag{3.21}$$

which is the Keldysh equation for the lesser Green's function in the steady state. Higher-order terms in the adiabatic expansion can be found in, e.g., Refs. [151, 155]. To summarize, the adiabatic limit of the Green's functions in the Wigner representation is equivalent to imbuing a static equilibrium solution parameterized by the central time t. This result is consistent with the intuitive picture of the Born-Oppenheimer approximation, where electrons are assumed to stay in the equilibrium state of the instantaneous Hamiltonian. Also importantly, the adiabatic expansion of the Kadanoff-Baym equations offers a systematic approach to formulate the DMFT-MD and higher-order corrections.

3.2.2 Real-space dynamical mean-field theory

The adiabatic expansion discussed above shows that at each instance the electronic system can be treated in quasi-equilibrium. Under this condition, the various Green's functions and self-energies are related. For example, $\mathbf{\Sigma}^A = [\mathbf{\Sigma}^R]^\dagger$. We focus on the retarded self-energy $\mathbf{\Sigma} \equiv \mathbf{\Sigma}^R$ and drop the superscripts for convenience. By introducing the non-interacting Green's function:

$$\mathbf{G}_0^{-1}(\omega, t) = (\omega + \mu \pm i0)\,\mathbf{I} - \mathbf{h}(t), \tag{3.22}$$

where $\pm i0$ is for the retarded and advanced function, respectively, the zeroth-order solution Eq. (3.20) is equivalent to the Dyson's equation parametrized by the central time t:

$$\mathbf{G}^{-1}(\omega, t) = \mathbf{G}_0^{-1}(\omega, t) - \mathbf{\Sigma}(\omega, t). \tag{3.23}$$

To solve the Green's functions, one needs to relate the self-energy to both the bare and full Green's functions, i.e. $\mathbf{\Sigma} = \mathbf{\Sigma}[\mathbf{G}]$, which is often intractable for general many-body interacting systems.

As discussed in the introduction, the central idea of DMFT is the local self-energy approximation, which means that the self-energy matrix $\mathbf{\Sigma}$ in the Dyson equation (3.23) is diagonal in atom-indices

$$\Sigma_{i\sigma,j\sigma'}(\omega,t) = \delta_{ij}\delta_{\sigma\sigma'}\Sigma_{ii}(\omega,t). \tag{3.24}$$

For simplicity, here we have further assumed non-magnetic solutions, i.e. a spin-independent self-energy, for MD simulations. The self-energy matrix is now diagonal in the atom-spin basis. Based on this locality approximation, it is further assumed that the on-site self-energy Σ_{ii} is obtained from solution of an atom-dependent quantum impurity model with the action

$$\begin{aligned} S^{(i)}_{\text{eff}}(t) = U \int_0^\beta n_\uparrow(\tau) n_\downarrow(\tau) \\ -\sum_\sigma \int_0^\beta d\tau \int_0^\beta d\tau' c^\dagger_\sigma(\tau) \left[\mathcal{G}^{(i)}_0(\tau-\tau';\, t)\right]^{-1} c_\sigma(\tau'), \end{aligned} \tag{3.25}$$

Here $\mathcal{G}^{(i)}_0(\omega;t) = \omega+\mu-\Delta_i(\omega;t)$ is an effective single-electron Green's function and $\Delta_i(\omega;t)$ is a time-varying hybridization to a fictitious bath that contains information about other atoms in the system. The subscript '0' here emphasizes that $\mathcal{G}_0$ is a "bare" Green's function in absence of the Hubbard U term. Notably, $\mathcal{G}_0$ plays a role similar to the Weiss field in the conventional "static" mean-field theory. The full imaginary-time Green's function of the quantum impurity model is formally given by the expression

$$G^{(i)}_{\text{imp}}(\tau,t) = \frac{-1}{\mathcal{Z}(t)} \text{Tr}\left[\mathcal{T}_\tau e^{S^{(i)}_{\text{eff}}(t)} c^\dagger_\sigma(\tau) c_\sigma(0)\right], \tag{3.26}$$

where $\mathcal{T}_\tau$ is the time-ordering operator, and $\mathcal{Z}$ is the partition function of the action. The real-frequency retarded Green's function $G^{(i)}_{\text{imp}}(\omega, t)$ can then be obtained through analytical continuation of the corresponding Matsubara Green's function. The self-energy of this local impurity problem is computed from the Dyson equation

$$\Sigma^{(i)}_{\text{imp}}(\omega, t) = \mathcal{G}^{(i)}_0(\omega, t)^{-1} - G^{(i)}_{\text{imp}}(\omega, t)^{-1}. \tag{3.27}$$

This impurity self-energy is to be identified as the local self-energy given by the diagonal elements of the atomic self-energy matrix $\mathbf{\Sigma}$ in Eq. (3.24).

$$\Sigma_{ii}(\omega, t) = \Sigma^{(i)}_{\text{imp}}(\omega, t). \tag{3.28}$$

The self-consistent condition of DMFT requires that the local Green's function coincides with the diagonal part of the system Green's function matrix:

$$G_{i\sigma, i\sigma'}(\omega, t) = \delta_{\sigma\sigma'}\, G^{(i)}_{\text{imp}}(\omega, t). \tag{3.29}$$

It is worth noting that one can also think of the action in Eq. (3.25) as a single fermion c_σ couples to a bath of free fermions, from which the Weiss field $\mathcal{G}_0$ is generated. This is precisely the single-impurity Anderson model (SIAM) of a magnetic impurity hybridized with a conduction band. The two self-consistency equations (3.28), (3.29) along with the two Dyson equations (3.23), (3.27) essentially provide the following functional dependence for the local self-energy

$$\Sigma_{ii}(\omega, t) = \Sigma_{\mathrm{SIAM}}\left[G_{ii}(\omega, t)\right]. \tag{3.30}$$

which is an exact relation in the infinite dimension limit.

In practical implementations of the real-space DFMT, the self-consistency is achieved through iterations; see Fig. 3.1 for details. One of the challenging parts is the solution of the Anderson impurity model, formally given by Eq. (3.26). Several numerical techniques have been developed to solve the quantum impurity problem. One of the most powerful and widely used impurity solvers is the continuous-time quantum Monte-Carlo algorithm, which in principle can provide numerically exact results for the impurity problem. Other numerically exact impurity solvers include exact diagonalization, numerical renormalization group, and density matrix renormalization group. Some of these solvers have been employed in real-space DMFT calculations for inhomogeneous Hubbard models [49, 50]. However, the huge overhead of these computationally sophisticated methods renders them difficult for large-scale dynamical simulations, where the impurity problems have to be solved for every atom at every time step.

As a proof of principle, as well as to explore qualitatively novel Mott physics in a liquid system, we adopt a modified version of the iterative perturbation theory (IPT) [61, 63, 156] as the local impurity solver, which allows for electron density away from the half-filling. Moreover, the calculation can also be directly performed on the real-time/frequency axes without the need for analytical continuation. Although IPT is an approximate impurity solver, it often gives qualitatively correct results. As introduced in the previous chapter, within IPT, the impurity self-energy can be written in closed form [61]

$$\Sigma^{(i)}_{\rm imp}(\omega, t) = U n_i(t) + \frac{A_i(t)\, \Sigma^{(2)}_i(\omega, t)}{1 - B_i(t)\, \Sigma^{(2)}_i(\omega, t)} \tag{3.31}$$

where $\Sigma^{(2)}_i(\omega, t)$ is the second-order perturbation contribution to the self-energy [131], and the coefficients A_i and B_i are determined in order to reproduce the correct moments of local density of states and the large-U limit. Importantly, despite its appearance as a perturbation expansion, the IPT should be understood as an interpolation scheme as it gives the correct results both in the itinerant and atomic limit. A detailed description of the IPT solver can be found in section 2.2.1. It is also worth noting that when being adopted to the inhomogeneous DMFT scheme, the IPT solver introduced in the previous chapter requires no extra modifications because the information of inhomogeneity is encoded in the bare Green's function $\mathcal{G}^{(i)}_0$ of each impurity.

3.3 Molecular dynamics simulations of Mott transition

Here we consider MD simulations with constant number of atoms ($N_a = 40 \sim 100$) in a fixed volume (V). We assume the system is immersed in a thermal bath of temperature T and adopt the Langevin dynamics to account for the thermal noise and dissipation.

The major difficulty of inhomogeneous DMFT implementation is that the impurity problems on every atom have to be solved individually, and the matrix Dyson's equations Eq. (3.23) have to be solved on all frequencies ($N_\omega \sim 5000$). The computational cost grows extremely fast when the number of site increase, even with fast impurity solvers, such as IPT. Fortunately, both steps can be accelerated using parallel computation techniques. The local impurity problems can be parallelized over sites and Dyson's equations can be parallelized over frequencies.

In particular, the N_a impurity problems will be assigned to multiple computational cores, with each core handles a fewer number of impurity problems so that multiple impurity problems can be solved simultaneously. Likewise, the tasks of solving Dyson's equation defined on N_ω frequencies will be distributed to multiple computational cores. This parallelization is valid because the impurity problems are strictly local, and there is no coupling between different frequencies. Therefore, within this parallelization framework, the inhomogeneous DMFT solver integrates out the electronic degrees of freedom in a time that is adequately short for the molecular dynamics simulation.

Here we explain the overall flow of our DMFT-MD scheme. As stated above, our scheme is based on the adiabatic QMD, and the Born-Oppenheimer approximation is adopted, in which the electron degrees of freedom and ion degrees of freedom are separated so that the electrons can be assumed in equilibrium at any MD time step. Starting with an atomic configuration of the system at time step t_n,

$$C(t_n) = \{\mathbf{R}_1, \mathbf{R}_2, ..., \mathbf{R}_i\} \tag{3.32}$$

From the atomic configuration, an unique hopping matrix $h_{ij} = h\left(|\mathbf{R}_i - \mathbf{R}_j|\right)$ is defined. Together with the on-site Coulomb interaction U, we arrive at a tight-binding Hamiltonian of the inhomogeneous Hubbard model for the electron degrees of freedom,

$$H = \sum_{i \neq j} \sum_{\sigma} h_{ij} c^{\dagger}_{i,\sigma} c_{j,\sigma} + U \sum_{i} n_{i,\uparrow} n_{i,\downarrow} \tag{3.33}$$

This Hamiltonian is then solved using the DMFT solver and the IPT solver and on-site self-energies $\mathbf{\Sigma}\left(\omega\right) = \delta_{ij} \Sigma_{ij}\left(\omega\right)$ are obtained. The system Green's function $\mathbf{G}\left(\omega\right)$ can be then calculated and the spectral function of electrons on each site is given by:

$$A_i(\omega) = -\frac{1}{\pi} \mathrm{Im} G_{ii}(\omega) \tag{3.34}$$

Furthermore, the averaged spectral function of the system is

$$A(\omega) = \frac{1}{N_a} \sum_{i} A_i(\omega) \tag{3.35}$$

The spectral function contains the information of non-quasi-particle excitations of electrons, which is not obtainable in previous methods.

The total force acting on an atom consists of two components, the contributions from both correlated electrons $\mathbf{F}_i^e$ and classical pairwise potentials between ions $\mathbf{F}_i^p$.

$$\mathbf{F}_i = \mathbf{F}_i^e + \mathbf{F}_i^p \tag{3.36}$$

The contributions of correlated electrons to the inter-atomics forces can be calculated from the system Green's function obtained from the DMFT calculation,

$$\mathbf{F}_i^e = -\frac{1}{\pi} \sum_{ij,\sigma} \frac{\partial h_{ij}}{\partial \mathbf{R}_i} \int d\omega f\left(\omega\right) \operatorname{Im} G_{ij}\left(\omega\right) \tag{3.37}$$

The summation over σ is a sum over two spins. In absence of magnetic field, it is a factor of 2. The classical pairwise potential ϕ introduces classical forces between the atoms,

$$\mathbf{F}_i^p = -\sum_j \frac{\partial \phi_{ij}}{\partial \mathbf{R_i}} \tag{3.38}$$

The atomic configuration is updated using Langevin Dynamics with the standard velocity-Verlet method, and the new atomic configuration is obtained.

In this scheme, solving the Hubbard model with the DMFT solver is the most time-consuming step; hence the parallelization technique is crucial in large-scale simulations. Our DMFT solver is parallelized over both sites when solving impurity problems and frequencies when solving Dyson's equation. This allows us to solve a system consisting of 40 atoms in less than a minute. Indeed, it is slower than previously developed GA-MD scheme [44], but it provides access to information of the incoherent non-quasi-particle electronic excitations, which is previously inaccessible. In addition to that, GA and DMFT solver can give qualitatively different results on some observables of the Hubbard model, such as the behaviors of the double occupancy and the quasi-particle weight near MIT [13].

3.4 Mott transition in correlated liquid

We applied our method to the Hubbard liquid model defined by Eq. (3.1). The simulation is perform on a system of $N_a = 40$ atoms with constant system size V that is determined by the average atom distance $r_s = (3V/4\pi N_a)^{1/3} \approx 1.2$. In the absence of the Coulomb potential $U = 0$, the average band energy is $\overline{W}_0 = 4.81$, and we shall normalize all the energy scale to this value for clarity. The temperature is at $T \approx 0.03W_0$, and the total electron filling is kept at half-filling $N_e = N_a$ by tuning the chemical potential μ. The system is first allowed to fully relax and converge to equilibrium before the measurement. We performed a series of simulations at various interaction strengths U. A previous study of this model indicates a U-driven phase transition [44].

It is important to first look into the energies of the system. Fig. 3.2 shows several energies of the system versus on-site Coulomb interaction U. The total kinetic energy of the atoms dependents only on temperature $E_{\text{kin}} = 3/2k_BT$ due to the Langevin dynamics. In fact, E_{kin} is considered as a criterion to check if the MD simulation converge to equilibrium The pair-wise potential energies is given by, $E_{\text{pot}} = \sum_{i\neq j} \frac{1}{2}\phi\left(|\mathbf{R}_i - \mathbf{R}_j|\right)$.

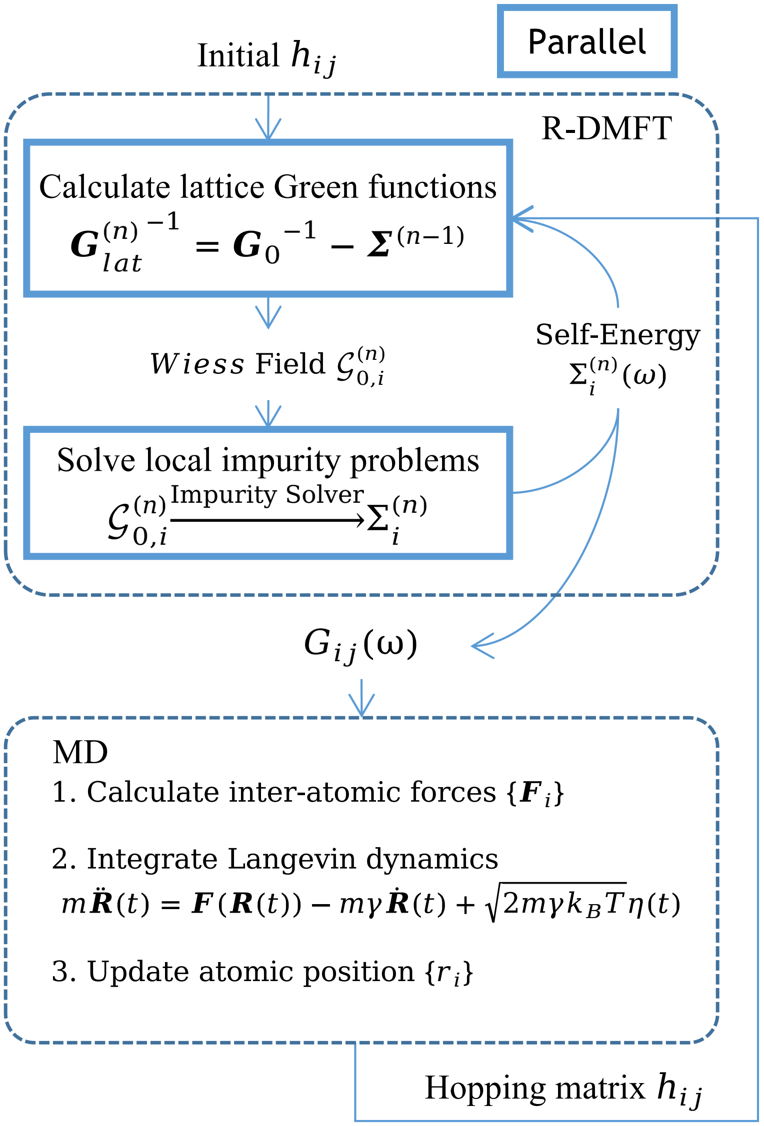

Figure 3.1: DMFT-MD Flowchart. Parallelization is implemented in the DMFT solver on both solving local impurity solver and solver Dyson's equation. Due to the lack of symmetry in liquid, every atom have to be solved individually, this can not be done with proper parallelization.

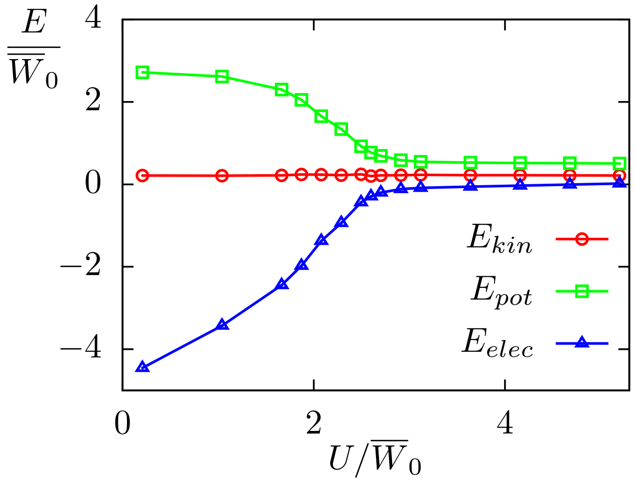

Figure 3.2: The averaged energies of the system as a function of on-site Coulomb interaction U. The energies are normalized by $\overline{W}_0$.

The electronic energies $E_{\rm elec}$ is calculated from the Galitski-Migdal formula; it includes both the electron kinetic and the electron potential energy. The electronic energy on atom i is given by,

$$E_i^{\rm pot} = T \sum_m e^{-i\omega_m 0^+} \Sigma_i(i\omega_m) G_i(i\omega_m), \tag{3.39}$$

where $\Sigma_i(i\omega_m)$ and $G_i(i\omega_m)$ are the local self-energy and local Green's function on the Matsubara frequencies $\omega_m = (2m+1)\pi/\beta$; T is the temperature and $\beta = 1/T$. The Matsubara Green's functions $G(i\omega_m)$ can be very useful when calculating various observables, which can be obtained from the spectral function $A(\omega)$,

$$G(i\omega_m) = \int d\omega \frac{A(\omega)}{i\omega_m - \omega} = -\frac{1}{\pi} \int d\omega \frac{\operatorname{Im} G(\omega)}{i\omega_m - \omega} \tag{3.40}$$

Such relation also holds for self-energies,

$$\Sigma(i\omega_m) = -\frac{1}{\pi}\int d\omega \frac{\operatorname{Im}\Sigma(\omega)}{i\omega_m - \omega} \tag{3.41}$$

It is worth mentioning that the inverse process, calculating real axis Green's function from Matsubara Green's function, is much more complicated, where analytic continuation technique is involved. The choice of specific analytic continuation method dependents on the characteristics of the input function. If the input Matsubara Green's function or self-energy is smooth, simple Padé algorithm can be used; if the input function has statistical noises, for example the Green function obtained from CTQMC, maximum entropy method is preferred.

The dramatic change of both E_{elec} and E_{pot} after a critical $U_c \approx 2.1\overline{W}_0$ indicates that at large U the system exhibiting different atomic and electron properties than that of the small U case. This smooth change of energies suggests a potential crossover driven by U instead of a first-order transition. A similar result has been reported in the previous GA-MD study [44] where an abrupt jump in electronic energy E_{elec} near $U \approx 2.1\overline{W}_0$ is observed instead of a smooth curve. The energies smoothly varying as a function of U of this system was later also observed [45], where updated GA solver and machine learning techniques were used. In the updated GA-MD scheme, electron hysteresis is eliminated by reinitializing the Gutzwiller parameters at every time step, which is more consistent with the assumption that the electrons are in equilibrium at each time step. In our study, the self-energy in the previous

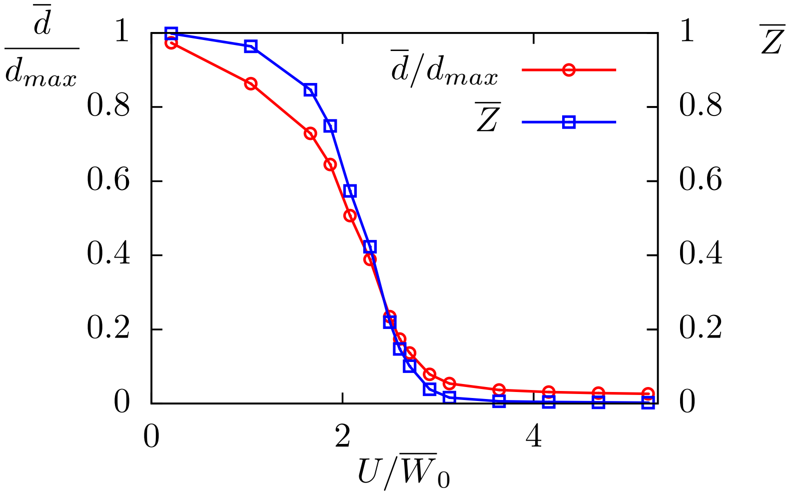

Figure 3.3: The averaged double occupancy $\overline{d}/d_{max}$ and averaged quasi-particle weight $\overline{Z}$ as a function of on-site Coulomb interaction U. $d_{max} = \langle n_\uparrow \rangle \langle n_\downarrow \rangle = 0.25$ is the maximum double-occupancy at half-filling.

time step is used as the initial guess for the next time step to accelerate the convergence of the DMFT calculation; nevertheless, a similar smooth curve is obtained even without explicitly eliminated the hysteresis. Hence the DMFT solver is more robust in this case than the GA solver. Previously, the inhomogeneous DMFT method was used mostly in lattice systems with disorders or in optical traps [49, 50]; however, how a highly disordered atomic configuration affects the performance or the convergence of DMFT solver is yet to be investigated systematically. Indeed, Sachdev's study of MIT in disordered metal sheds important insights on the importance of local moments near metal-insulator transition [60], but how the bond randomness affects the nature of Mott transition remains unknown.

In order to understand the nature of this change of electronic properties, it is instructive to study how the double occupancy and quasi-particle weight change as a function of U. The double occupancy on the i-th atom is defined as $d_i = \langle n_{i\uparrow} n_{i\downarrow} \rangle$, which is the possibility of i-th site been occupied by two electrons. The local double occupancy is given by,

$$d_i = \frac{T}{U} \sum_m e^{-i\omega_m 0^+} \Sigma_i(i\omega_m) G_i(i\omega_m) \tag{3.42}$$

The averaged double occupancy in a metallic state is expected to be larger than that in an insulator state since the electrons freely hopping across atoms indicates a larger possibility of an atom being occupied by two electrons. The local quasi-particle weight Z_i can be obtained from the local self-energy

$$Z_i^{-1} = 1 - \left. \frac{\partial \mathrm{Re} \Sigma_i(\omega + i0^+)}{\partial \omega} \right|_{\omega=0} \tag{3.43}$$

It describes the spectral weight of quasi-particles. In the Mott phase, the quasi-particle weight vanishes, indicating that no quasi-particle excitations exist.

Fig. 3.3 shows the averaged double occupancy $\overline{d}$ and averaged quasi-particle weight $\overline{Z}$ as function of on-site Coulomb interaction U. The average is performed over both atoms and equilibrium states. As the U increase, the $\overline{d}$ and $\overline{Z}$ decreases and quickly drops to very small values after a critical interaction strength $U_c \approx 2.1\overline{W}_0$. Unlike previous studies using GA-MD [44] where the double occupancy goes to zero immediately after U_c, the double occupancy obtained by DMFT remains at a small but non-zero value. This difference is also observed in the lattice case, and it is suggested that double occupancy cannot be used as an order parameter for the Mott transition. The order parameter for the MIT is quite an ambiguous problem, and there is no well-accepted order parameter for it [13]. The non-zero double occupancy is actually expected due to the virtual hopping in the insulating state [13]. This virtual hopping is the source of the exchange interactions between local moments in the large U limit. The quasi-particle weight is almost zero in the large U regime, indicating the vanishing of Fermi liquid in that regime. This phenomenon suggests a transition marked by the electron localization on each atom. In the GA-MD simulations, the sudden vanishing of double occupancy above U_c can result in the sudden change of E_{elec} and lead to a jump of energy in the GA-MD case [44].

It is known that the Mott transition is a first-order transition on lattice system even with short-range quantum fluctuations included [47], and hysteresis in d and Z can be observed (as shown in the numerical results in the previous chapter); however, what we see here is rather a smooth change without obvious discontinuity. We shall see later, the nature of this transition is still first order but, however, not a simple transition from a metallic state to an insulating one due to the distinct properties of the liquid.

In MD simulations, the properties of the atomic configuration are also of great significance. The radial pair distribution function $g(r)$ represents the possibility of finding another atom at the distance r of an certain atom, it is given by

$$g\left(r\right)=\frac{1}{4\pi r^{2}N\rho}\left\langle\sum_{i=1}^{N}\sum_{j\neq i}^{N}\delta\left(r-r_{ij}\right)\right\rangle \tag{3.44}$$

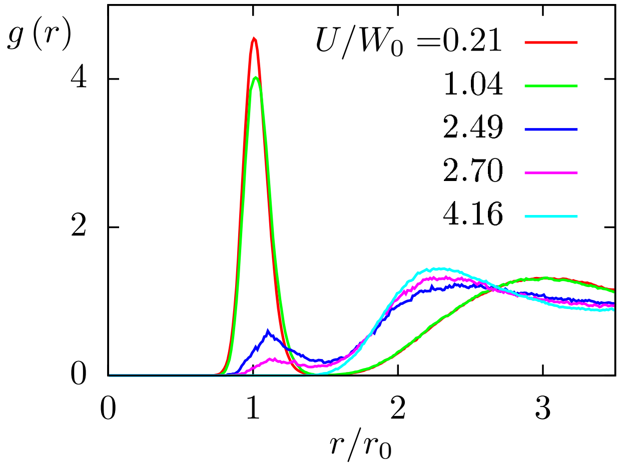

Figure 3.4: Pair distribution functions $g(r)$ obtained from DMFT-MD for varying values of U.Here r_0 is the equilibrium distance between atoms in a molecule.

The radial pair distribution function $g(r)$ at various U are shown in Fig. 3.4. In the absence of the Coulombic repulsion, at $U = 0$, atoms tend to couple in pairs forming H_2-like molecules, and the equilibrium distance between the two atoms is $r_0 \approx 0.83$. The value of the equilibrium distance r_0 is determined by the minimum of the energy curve $e(r) = -2t(r) + \phi(r)$. In the small U regime, a clear peak forms at r_0, indicating the presence of atomic dimers. In this regime, the electrons hop within the pairs and binding them together; thus, the system is not metallic, and a gap exists at the Fermi level. As the on-site Coulomb U increases to the strong coupling regime, the dimer peak vanishes; moreover, a broad peak forms at $r \approx 2.2r_0$, which suggests that atoms are separated further apart from each other. This trend is consistent with the expectation that the formation of covalent bonds is suppressed by the increasing Coulomb repulsion as electrons become localized. In this regime, the electrons are mostly localized, and thus the inter-atomic force is dominated by the classical potential $\phi(r)$, which is mostly repulsive in this case.

The vanishing of the molecular peak describes the well-known molecular dissociation phenomenon. It has been reported in the hot dense hydrogen simulations, which is similar to the system we studied here and has been simulated using the VMC-MD method and path-integral MC methods [157, 158]. The dense hydrogen goes through a molecular dissociation as the temperature increase. The system changes from molecular liquid to monoatomic liquid. It is reported that the molecular peak almost disappears at high temperature with only a few features left. Similar results have been seen in the original GA-MD method simulations [44]. Note that the change of peaks is rather smooth, and no strong hysteresis effect is observed in our simulations, which is similar to the later simulations of the Hubbard liquid model [45].

One important question is that does the continuous change of energy suggest a continuous Mott transition [159, 160, 161]? The presence of phase coexistence in later results suggests that this is not a continuous transition. The coexistence also indicates that it is not a first-order transition rounded by disorders where the coexistence disappears due to the formation of finite-size domains that is favored by disorder [162]. The bond randomness indeed has effects on the first ordered transition, but in 3-dimension, the first-order transition is suppressed by temperature instead of being eliminated [163, 164]. The hysteresis might be harder to identify in this case but could still survive. Therefore, "crossover" at low temperature is merely a kinetic result, and it is intrinsically a first-order transition.

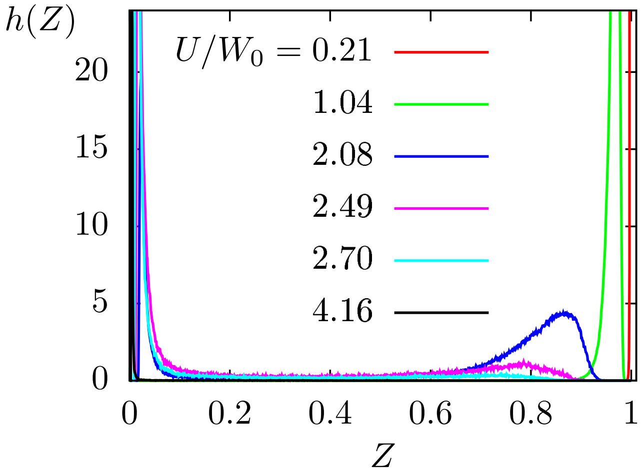

Figure 3.5: The probability distribution of quasi-particle weight $h(Z)$ for different U values.

Histogram studies of both local quasi-particle weight $h(Z)$ and local double occupancy $h(d)$ are performed further to analyze the electronic properties of the liquid system. Note that h here is the probability distribution. In Figs. 3.6 and 3.5, the clear bimodal distributions of both Z and d indicate that two types of atoms coexist near U_c: on one type of atoms, electrons behave like a Fermi liquid with finite quasi-particle weight, and the electrons are allowed to hopping between them giving finite double occupancy; one the other type of atoms electrons are highly localized with small Z and d values. This coexistence of two types of atoms indicates that the nature of this transition is still first-order. The higher peaks of $h(d)$ and $h(Z)$ are broader than the lower peaks because of the formation of metallic clusters. In this regime, the atoms are no longer tightly bonded in pairs but forming clusters. This argument is supported by the fact that the first peak in $g\left(r\right)$ is shifting and broadening as U increases. The average hopping amplitude within these clusters is large,

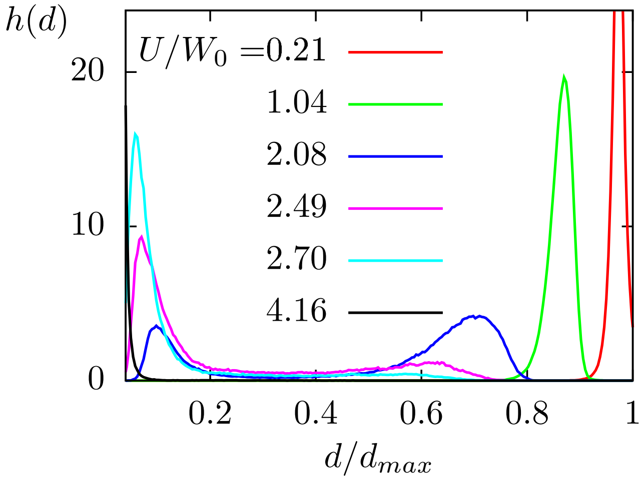

Figure 3.6: The probability distribution of double occupancy $h(d)$ for different U values.

and the variation is significant due to the broad distribution of interatomic distances within the clusters. On the other hand, the localized atoms are less attractive and tend to move away from other atoms making the electron localization robust, which results in the shaper peaks of $h(d)$ and $h(Z)$ on the left. In the GA-MD simulations, a bimodal distribution of double occupancy is also observed where the left peak is, however, much broader[44]. This difference might be because of the artifact of the Gutzwiller solver, where atoms with small double occupancy are not fully resolved. This coexistence of two types of atoms might be evidence of a first-order transition.

The spectral function is one of the most important observables in DMFT simulations. It provides important information about the electronic excitations in the system. Fig. 3.7 shows the time-averaged total spectral function of the liquid. A reentrant type transition driven by U can be clearly observed.

It is widely known that in the single-site DMFT calculations, as the U

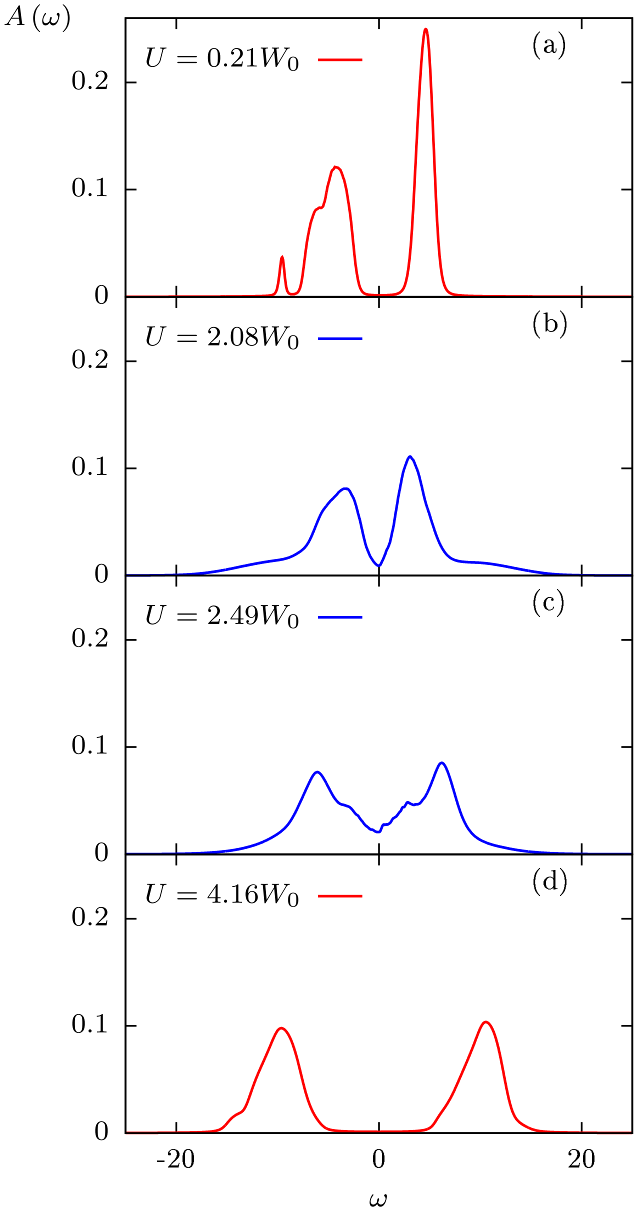

Figure 3.7: Time averaged spectral functions for different U values. Near $U_c \approx 2.1\overline{W}_0$, the gap is closed and the system is metallic. The red curve indicates that the system is insulating, while the blue curve represents a metallic solution.

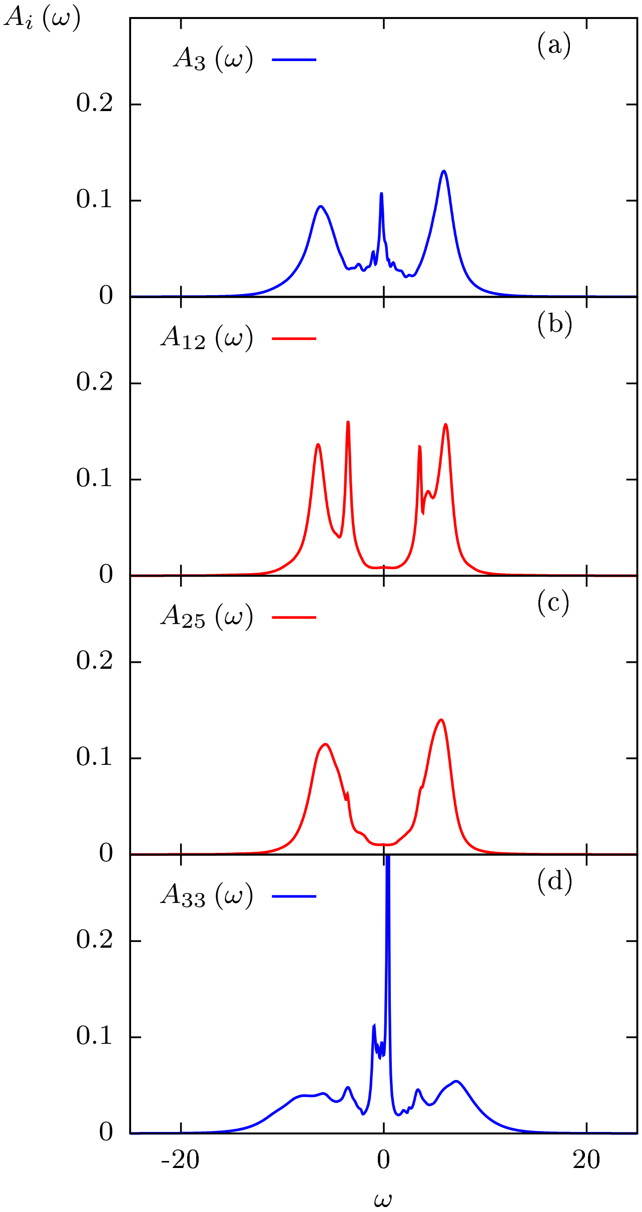

Figure 3.8: Local spectral functions $A_i\,(\omega)$ at various sites i, simulated at $U = 2.29\bar{W}_0$. The strong spatial inhomogeneity in the liquid system results in different behaviors of spectral functions on each site. The system consists of both (a)(d) metallic local solutions, and (b)(c) insulating local solutions. The existence of quasi-particle peaks in the metallic solutions marks the formation of Fermi liquid in the metallic clusters.

increases and in the vicinity of the critical U, two Hubbard bands at $\pm U/2$ grow out of the quasi-particles peak at the Fermi level, while the height of the central peak remains unchanged. When the system is near the critical U_c, a phase coexistence regime exists where both metallic solution and insulating solution are both. The final state in this regime depends on the initial condition. In this intermediate regime, the metallic solution is a usually bad metal whose spectral function has two wide Hubbard bands and a very sharp quasi-particle peak. As the system enters the strong coupling regime, a gap is opened at the Fermi level, and the system becomes a Mott insulator with only two Hubbard bands in its spectral function. This picture of Mott transition is clear and monotonically driven by U. However, in the liquid system, the transition does not have the luxury of simplicity; it shows an intriguing reentrant type transition.

As can be seen, at the small U regime, the spectral function has a gap at the Fermi level; the system is insulating. The gap width is approximately the binding energy of the molecule. This is as expected since the system is now a molecular liquid where electron excitations at the Fermi level are not allowed since they are limited in the covalent bond. Note that in this regime, both averaged double occupancy and average quasi-particle weight is finite, which is conventionally a sign of metallic state in lattice systems. In a molecular liquid, electrons are allowed to hop between the atoms within the molecule, giving finite double occupancy and quasi-particle weight. However, they are localized and bounded to their corresponding molecule; thus, they cannot behave like free electrons in actual metals. Although the formation of dimer can be observed from $g(r)$, one has to check the spectral functions $A(\omega)$ of the system to confirm the formation of molecules and covalent bonds.

As the U increase, the spectral functions gain finite spectral weight at the Fermi level, and the gap is gradually closed. The molecule starts to dissociate, and atoms form metallic clusters, where electrons can move across the system and behave like Fermi liquid. Fig. 3.8 shows the local spectral function in a snapshot during the simulation at $U = 2.29\bar{W}_0$. The spatial inhomogeneity in the liquid system results in distinctive spectral functions on each site. Both local metallic solutions and local insulating solutions coexist in the system. The existence of quasi-particle peaks in the metallic solutions marks the formation of the metallic clusters in which electrons can behave like Fermi liquid. There are sites with localized electrons with the Hubbard bands at $\pm U/2$ in their spectral functions.

In the strong coupling regime, the spectral functions reopened a gap at the Fermi level, and the system becomes a monoatomic liquid that is insulating again. The spectral function has two clear Hubbard bands at $\pm U/2$. This is previously unavailable in *ab initio* MD simulations and GA-MD simulations. The spectral function behavior acts as proof for the reentrant transition.

For a liquid system, the diffusion coefficient is also important, which describes how fast particles can diffuse in the liquid. It can be obtained by an integral of the velocity autocorrelation function,

$$D = \frac{1}{3N} \int_0^\infty \sum_{i=0}^{N} \langle \mathbf{v}_i(t_0) \cdot \mathbf{v}_i(t_0 + t) \rangle \, dt, \tag{3.45}$$

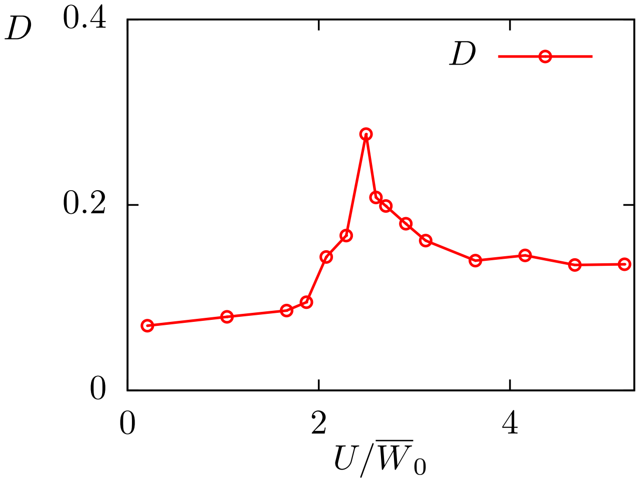

Figure 3.9: Diffusion coefficient D as a function of U. The diffusion coefficient has a maximum near $U_c \approx 2.1\overline{W}_0$.

The time correlation function measures the correlation between two time-dependent quantities,

$$C\left(t\right) = \left\langle A(t_0)B(t_0+t)\right\rangle , \tag{3.46}$$

where $< ... >$ indicates an averaging over time origins t_0 in an equilibrium ensemble. If A and B are same, then C is an auto-correlation function; otherwise, C is a cross-correlation function. In molecular dynamics simulation, we are interested in auto-correlation functions which can describe important dynamics of a system.

In our implementation, a block averaging method is used to compute the autocorrelation function,

$$C\left(t\right) = \langle f(t_0) f(t_0 + t) \rangle = \frac{1}{k} \sum_{n=0}^{k-1} C_n\left(t\right), \tag{3.47}$$

where $C_n\left(t\right) = f(t_n) f(t_n + t)$. After equilibrium is reached, we evaluate $C_n\left(t\right)$ in k time blocks of size $t \in [0, t_{\mathrm{measure}}]$ with various time origins t_n and the autocorrelation function $C\left(t\right)$ is obtained by averaging over k blocks. In general, the separation between time origins should be larger than the measurement time t_{measure}, and the time blocks do not overlap with each other so that the statistical bias introduced by self-correlation can be minimized. However, such measurement takes extremely long simulations to obtain good accuracy.

In the MD simulation of liquid, to fast accumulate data, time blocks are allowed to overlap as long as time origins are well separated, such that the molecular configurations at each starting time are independent. This is valid because the auto-correlation function of the liquid phase quickly vanishes to zero as time increases; thus, the separation between the starting point of adjoint time blocks needs to be larger than the correlation time $\tau_c = 1/C(0) \int_0^\infty C\left(t\right) dt$. This approach, though faster than the original one, yet still requires long simulations.

The self-diffusion coefficient (diffusion constant) D can be calculated from the velocity auto-correlation function using the standard Green-Kubo relation,

$$D = \frac{1}{3N} \int_0^\infty \sum_{i=0}^{N} \langle \mathbf{v}_i(t_0) \cdot \mathbf{v}_i(t_0 + t) \rangle \, dt, \tag{3.48}$$

where the velocity auto-correlation function is

$$C_v\left(t\right)=\frac{1}{N}\sum_{i=0}^{N}\left\langle \mathbf{v}_i(t_0)\cdot\mathbf{v}_i(t_0+t)\right\rangle \tag{3.49}$$

Since we cannot measure the auto-correlation function for infinite time, thus it is useful to introduce a time cutoff τ and define the accumulative diffusion coefficient as,

$$D(\tau)=\frac{1}{3N}\int_0^{\tau}\sum_{i=0}^{N}\left\langle \mathbf{v}_i(t_0)\cdot\mathbf{v}_i(t_0+t)\right\rangle dt \tag{3.50}$$

The accumulative diffusion coefficient converges to the diffusion coefficient in the infinite time limit, $D=\lim_{\tau\to\infty}D(\tau)$. In the liquid phase, velocity auto-correlation function converges to zero very fast, the long-time contribution to velocity auto-correlation function is relatively small. Therefore, it is appropriate to estimate the self-diffusion coefficient using the accumulative diffusion coefficient at a large enough time cutoff $\tau=t_{\text{measure}}$. In practice, we should monitor the convergence of $D(\tau)$ to check the quality of final result.

The diffusion coefficient as a function of U is shown in Fig. 3.9. The diffusion coefficient exhibits a non-monotonic dependence on U, and a peak near U_c is observed. Such behavior of diffusion coefficient is also reported in the previous study using GA-MD [44]. Its increase in the small U regime is due to the dimer dissociation, which decreases the effective mass of atoms, and the particles are can diffuse in the liquid much easier. In the $U>Uc$ regime, the interaction between atoms is dominated by the classical pairing potential, which leads to a larger transport cross-section; thus, the system shows a decrease of diffusion coefficient.

The frequency resolved optical conductivity $\sigma_{\alpha\beta}(\Omega)$ can be obtained using the Greenwood-Kubo formula,

$$\sigma_{\alpha\beta}(\Omega) = \pi e^2 \hbar \int d\omega \Gamma_{\alpha\beta}(\omega + \Omega, \omega) \frac{f(\omega) - f(\omega + \Omega)}{\Omega}, \tag{3.51}$$

where $\Gamma_{\alpha\beta}(\omega_1, \omega_2)$ is the transport distribution function, which is given by,

$$\Gamma_{\alpha\beta}(\omega_1, \omega_2) = \frac{1}{V} \mathrm{Tr}\left(\mathbf{v}_\alpha \mathbf{A}(\omega_1) \mathbf{v}_\beta \mathbf{A}(\omega_2)\right). \tag{3.52}$$

The velocity matrix in $\alpha = x, y, z$ direction is given by,

$$v_{ij}^{\alpha} = -\frac{i}{\hbar} H_{ij}(R_i^\alpha - R_j^\alpha) \tag{3.53}$$

The system Green function $\mathbf{G}(\omega)$ is obtained from Dyson's equation and the spectral function matrix is given by $\mathbf{A}(\omega) = -1/\pi Im\mathbf{G}(\omega)$. The kinetic coefficient is defined as,

$$A_{n,\alpha\beta} = \pi \hbar \int d\omega \, (\beta\omega)^n \, f(\omega) \, f(-\omega) \, \Gamma_{\alpha\beta}(\omega, \omega). \tag{3.54}$$

Finally, conductivity can be written in terms of the kinetic coefficient ,

$$\sigma_{\alpha\beta} = \beta e^2 A_{0,\alpha\beta} \tag{3.55}$$

In the numerical simulation, the main task of transport calculation is to obtain the transport distribution function $\Gamma_{\alpha\beta}(\omega + \Omega, \omega)$. Because the spectral

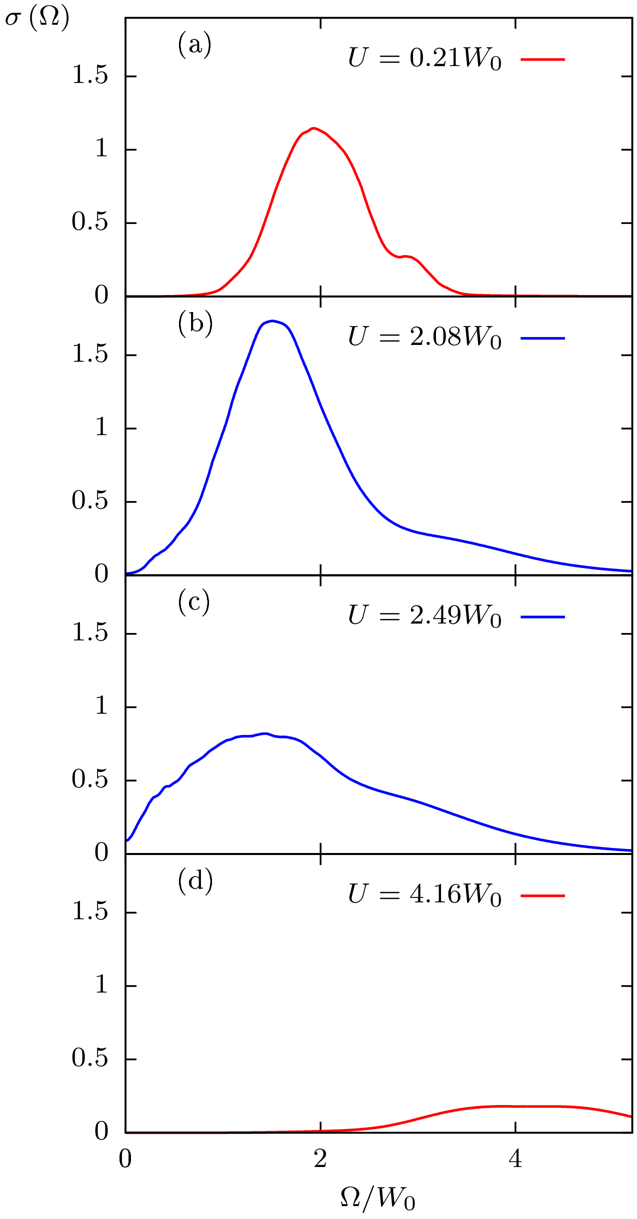

Figure 3.10: Time averaged optical conductivity for different U values. The DC conductivity can be obtained from the optical conductivity at $\Omega = 0$ Near $U_c \approx 2.1\overline{W}_0$, the dc conductivity increases.

functions are calculated on a discrete frequency grid, we need to be careful with the frequency grid for $\Omega > 0$. Assuming that the frequency grid of spectral functions is ranged from $[-\omega_{max}, \omega_{max}]$, then the range of Ω should be $[0, \Omega_{max}]$ with $\Omega_{max} < \omega_{max}$. The numerical integration window is therefore $[-\omega_{max}, \omega_{max} - \Omega_{max}]$. For each Ω, we evaluate the transport distribution function $\Gamma_{\alpha\beta}(\omega + \Omega, \omega)$ within $[-\omega_{max}, \omega_{max} - \Omega_{max}]$, and perform the integration. The choice of Ω_{max} should not be too large; otherwise, the integration for large Ω can be inaccurate due to truncation of spectral functions.

In the MD case, we only consider the Γ point due to the spatial inhomogeneity. The actual transport properties should be averaged over a thermal equilibrium ensemble, i.e., average over multiple independent molecular configurations, $\sigma_{\alpha\beta}(\Omega) =< \sigma_{\alpha\beta}(\Omega) >$. Additionally, only diagonal terms of the conductivity tensor is considered (xx,yy,zz), and the overall conductivity is $\sigma(\Omega) = \mathrm{Tr}\boldsymbol{\sigma}(\Omega) = \sum_{\alpha} \sigma_{\alpha\alpha}(\Omega)$. Moreover, the complex optical conductivity can be obtained using KK transformation.

In contrast to the Bethe lattice optical conductivity [13], the sharp Drude peak the $\Omega = 0$ is absent. It is likely because of lacking a pronounced quasiparticle peak at the Fermi level. Indeed, the gap in the spectral Functions being closed near U_c increases the dc conductivity of the system to almost 80 time larger than that of the small U case. The calculation is very computational demanding; therefore, it is difficult to calculate the optical conductivity for all U. The current results confirm the reentrant transition, where the dc conductivity of the system is enhanced near the U_c and decreases backing to the insulating phase after the transition.

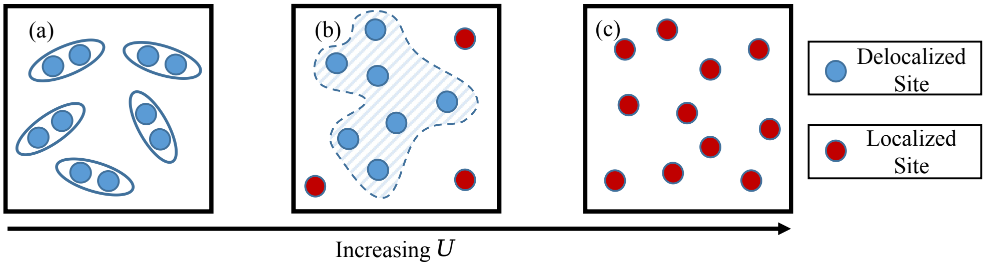

Figure 3.11: Schematic diagram of atomic configuration of the U-driven reentrant transition. (a) In the weak interaction regime, the system is a molecular fluid consisting of atomic dimers. Electrons are not fully localized on individual atoms but are still bounded in the bond within the dimers, which opens a gap at the Fermi level. (b) In the intermediate regime, there are atoms with localized electrons and atomic clusters with electrons that can hop between multiple atoms. The formation of atomic clusters closes the gap, making the system metallic. (c) In the strong interaction regime, the electrons are fully localized at each atom and forms local moments. The system is insulating, and the gap is reopened.

3.5 Conclusion

To summarize, we propose a novel MD scheme that uses the DMFT method to treat the effect of electron correlations exactly. Applying our new method to the Hubbard liquid model, the picture of this U driven reentrant transition is unveiled. Of course, there are still some open questions about this model. For example, exchange interaction is ignored in the Mott phase. In the strong regime, the spin-exchange interaction h_{ij}^2/U between moments should also be considered. The physics in this regime will be discussed in the following chapter.

As suggested by Sachdev [60], the effects of local moments play a vital role in the complete picture of MIT. The interplay between disorders and the first-order transition is essential to understand the MIT in this system. Disorders in the off-diagonal terms of the hopping matrix can create local environments that favor the formation of local moments, where the local double occupancy is close to zero. The interaction between local moments might be important to describe the dynamics of the Hubbard liquid. Our current DMFT solver or previously developed GA solver does not consider spin-exchange interactions, thus cannot describe the frustrated state in the Mott phase. It might be possible to utilize more advanced DMFT methods in our DMFT-MD scheme to incorporate the effect of both spacial fluctuation and short-range quantum fluctuation. However, it is beyond the scope of this study.

Another promising direction is to incorporate *ab initio* calculations at every time step to update h_{ij} and U, which will allow us to simulate real materials and to connect with experiments such as alkali metal and liquid hydrogen. However, this will be highly computationally expensive and almost impossible to simulate large enough systems to provide useful insight. However, machine learning can be a potential solution to the substantial computational cost, which could be the key to future QMD simulations. As the machine learning technique has been more and more utilized by the physics community, it helps researchers in various areas, such as phase classifications, pattern identifications. In recent studies, it is proven that the neural network can be a robust solver to calculate the electron contribution of forces in MD simulations with strongly correlated electrons and disordered systems [45, 165]. A properly trained neural network is both fast and accurate and can push the system size to a much large value.

Chapter 4

Spin Liquid Molecular Dynamics

In this chapter, we discuss the Hubbard liquid in the large U limit where the local moments and their interactions are dominant. We propose a scheme that combines the molecular dynamics and the exact diagonalization method to study the Hubbard liquid in this limit.

4.1 Local moments during MIT

It is widely accepted that as the Coulomb repulsion U increases, the electron double occupied states are further suppressed, and the electrons are strongly localized on each atom. Remarkably, at half-filling, all atoms are singly occupied in the ground state, and any electron hopping will lead to an energy cost of order U. In this case, the strongly localized electrons act as spin-1/2 local magnetic moments located on each atom [66].

These magnetic moments are created due to electron localization; thus, their existence is not limited to clean Hubbard systems but can also be found in highly disordered Hubbard systems. Additionally, they are not even limited to Mott insulating phase. In fact, the local magnetic moments can have finite localization length even in metallic states, in which extended single quasi-particle states can be found near the Fermi level. The formation of local moments is favored and stabilized by local environments created by hopping factors with off-diagonal disorders [60]. During the Mott transition, both the local moments and the itinerant electrons can coexist and form a two-fluid system [60]. It is suggested that to understand the full picture of metal-insulator transition, the presence of local moments and their interaction with itinerant electrons should be carefully considered [60]. Although the mean-field level analysis was performed to study a fully disordered Hubbard model where sites are randomly placed in space and have random on-site potentials [60], there is currently no research on how the presence of local moments and their interactions affect the dynamics of these sites. To better describe the Mott transition in the highly inhomogeneous Hubbard liquid system, we should consider the effect of the local moments. In particular, in the Hubbard liquid model, the interactions between local moments can be important to describe the dynamics of the system near the Mott transition regime and in the large U limit.

It is known that homogenous single-site DMFT solvers cannot take the short-range quantum fluctuations into account; thus, they fail to reproduce the antiferromagnetic state in the Mott phase. This phase can be correctly obtained through cluster DMFT methods, in which shot range quantum fluctuations are included to capture the effect of localized spins [47] fully. The current DMFT-MD algorithm or previously developed GA-MD scheme do not include the short-range quantum fluctuations, thus cannot describe the frustrating states in the disordered Mott insulating phase. To simultaneously consider the effects of both spacial inhomogeneity and short-range quantum fluctuation in molecular dynamics, a combination of inhomogeneous DMFT and cluster DMFT methods might be required. Inhomogeneous cluster DMFT method for lattice system has been proposed recently [166], but it has not yet been widely utilized. Moreover, the proposed inhomogeneous cluster DMFT method is not suitable to study a fully disordered Hubbard model. The cluster DMFT part of this method requires combining well-defined small clusters to form a super-cluster, which can be systematically performed on a well-defined lattice system with translational invariant atomic configuration. Unfortunately, this can be problematic in the fully disordered Hubbard model case because it is currently impossible to systematically expand the clusters or define small clusters for a fully disordered atomic configuration. It might be possible to treat the entire system as a single super-cluster, but in that case, the dimension of the multiple-site impurity problem is too large to handle. Developing a method that can consistently treat both spatial inhomogeneity and short-range quantum fluctuation on an equal footing could be the next direction of the development of the DMFT method and can help the community to fully understand the dynamics of Mott transition and the effect local moments during the MIT, yet it is beyond the scope of our current research.

In this chapter, the Hubbard liquid system in the deep Mott phase is studied, namely in the strong coupling limit $U \gg U_c$. We further limit our study to the half-filling case, the presence of extended quasi-particle states in the Mott insulating phase can be neglected, and the system is a liquid consisting of only spin-1/2 local magnetic moments,

$$H_{\text{Mott}} = H_{\text{spin}} + H_{\text{ion}} \tag{4.1}$$

Similarly, the system has two degrees of freedom, H_{spin} describes the spin-1/2 local moments interacting with each other via short-range quantum fluctuations, and the other one H_{ion} is the ion degree of freedom, governed by classical repulsive potentials. Because the effect of itinerant electrons and their interaction can be ignored in the deep Mott phase, the problem is simplified, and the spin degree of freedom H_{spin} can be solved directly.

Studying this system can shed light on the physical picture of MIT in a fluid system and help us understand the effect of local magnetic moments interactions on the dynamics of the atoms. Real fluid systems, such as liquid mercury and alkali metals, are very important in the studies of MIT in disordered medium [76, 77, 78, 80]. Although it is currently not possible to consistently treat both the local magnetic moments and the itinerant electrons on the same footing, our results in the deep Mott phase, combined with the result in the previous chapter, can provide us valuable information on both sides of the Mott transition in a strongly correlated liquid.

4.2 Interactions between local moments

Before studying the dynamics of the fluid system, it is crucial first to identify the interactions between the local moments. There are a few candidates to consider.

A naive choice of the interaction between two local moments is the magnetic dipole-dipole interaction,

$$H_{\text{dipolar}} = \frac{\mu_0}{4\pi r^3}\left[\mathbf{m_1}\cdot\mathbf{m_2} - \frac{3\left(\mathbf{m_1}\cdot\mathbf{r}\right)\left(\mathbf{m_2}\cdot\mathbf{R}\right)}{r^2}\right], \tag{4.2}$$

where $\mathbf{m_1}$ and $\mathbf{m_2}$ are the magnetic moments of the localized spin, μ_0 is the magnetic constant and r is the displacement vector between the two magnetic moments. However, the dipolar interaction is too weak comparing to other possible interactions, thus it can hardly have any significant effect on the dynamics of atoms in the Mott phase.

Another class of interaction between the local moments is the exchange interaction, which results in an effective Heisenberg model for the local moments,

$$H = J\hat{\mathbf{S}}_1\cdot\hat{\mathbf{S}}_2, \tag{4.3}$$

where J is the exchange constant and $\hat{\mathbf{S}}$ is the spin operator,

$$\hat{\mathbf{S}} = \begin{pmatrix} \hat{S}^x \\ \hat{S}^y \\ \hat{S}^z \end{pmatrix} \tag{4.4}$$

The spin components on the same atom followed the standard commutation relations of angular momentum,

$$\left[S^\alpha, S^\beta\right] = i\hbar\varepsilon_{\alpha\beta\gamma}S^\gamma, \tag{4.5}$$

where $\varepsilon_{\alpha\beta\gamma}$ is the Levi-Civita symbol and $\alpha, \beta, \gamma = x, y, z$. In fact, it is well-known that in the Hubbard model in the strong coupling limit can be mapped to an effective antiferromagnetic Heisenberg model [167].

There exist several types of exchange interaction with different physical origins. Among them, the simplest one is the direct exchange interaction. Through a virtual intermediary double occupied state that does not violate the Pauli exclusion principle of fermions, the two nearby atoms are coupled. This intermediary state can be created through the virtual hopping of spins between two sites with antiparallel spins. The virtual hopping can result in a non-vanishing double occupancy in the Mott phase, which has been observed in the Hubbard liquid model. The direct exchange interaction leads to an antiferromagnetic Heisenberg model for the local moments. By treating the hopping h_{ij} as a perturbation, one can found that the strength of the interaction is $J_{ij} \sim h_{ij}^2/U$. Because the hopping strength exponentially decays with distance, the exchange interaction is stronger than the hopping but has a shorter range.

Another type of exchange interaction is the super-exchange interaction. In real materials, magnetic moments in lattices can interact through the magnetic super-exchange interaction, where next-to-nearest neighbor atoms are coupled with each other through an intermediary nonmagnetic atoms [168, 169]. This type of interaction can often be found in the oxides of transition metal, for example, in MnO crystal, through the nonmagnetic O^{2-} anions between Mn^{2+} cations, the Mn^{2+} atoms can interact with each other. Instead of a direct overlap between the *d*-orbital wave-functions of two Mn^{2+} atoms, one *p*-orbital electron on the intermediary O^{2-} anions can hop to one of the two cations; the remaining *p* electron on the O^{2-} can have a direct exchange with the other cation, resulting in a coupling between the two cations [169]. Depending on the orientation of the atoms and the electron configurations, the super-exchange mechanism can not only leads to antiferromagnetic interaction between the cations but also can create ferromagnetic couplings [170].

There is also an exchange mechanism called double-exchange, where two ions of different oxidation states interact through an in-between ion. This type of interaction looks similar to the super-exchange but can only occur between atoms when one of the two atoms has more one electron than the other [171].

To summarize, the dipolar interaction is too weak comparing to the exchange interactions; thus, its influence is negligible. Moreover, super-exchange and double-exchange mechanisms are also not possible because there are no intermediary nonmagnetic atoms. We limit all atoms to be hydrogen-like with only s-orbital. Thus there are only one species of atoms in the system. Therefore, it is reasonable to assume that the dominant interaction between local moments is the direct exchange, and the Hamiltonian of the local moments is given by,

$$H_{\text{spin}} = \sum_{\langle i,j \rangle} J\left(|\mathbf{R}_i - \mathbf{R}_j|\right) \hat{\mathbf{S}}_i \cdot \hat{\mathbf{S}}_j \tag{4.6}$$

$$\text{where} \quad J\left(|\mathbf{R}_i - \mathbf{R}_j|\right) = \frac{4\left[h\left(|\mathbf{R}_i - \mathbf{R}_j|\right)\right]^2}{U} = \frac{4h_0^2 \exp(-2r/\xi_1)}{U} \tag{4.7}$$

Here $h\left(r\right) = h_0 \exp(-r/\xi_1)$ is the hopping factor of the original Hubbard model where h_0 and ξ_1 are constant. From the above expression, it is easy to see that the strength of exchange interaction is stronger than the hopping, but it decays much faster. In applications to real materials, these parameters can be obtained by fitting to bulk band-structure *ab initio* calculations or to experimental results.

Although the direct exchange is dominant here, it might still be possible to achieve a more complex exchange mechanism in a Mott liquid system. For example, if another species of a nonmagnetic atom is added and complex atoms with *d*-orbitals are considered, super-exchange might be possible. It is interesting to see how the super-exchange or the double-exchange interaction can affect the dynamics of the system. Again, this is far beyond the scope of our work, where we focus on the direct exchange interaction between local moments.

4.3 The Mott liquid model

In this system, we consider the half-filling case, which means there are only one spins on each atoms. The system consists of two degrees of freedom, one for spin 1/2 local moments with exchange interaction and the other one is the ion degree of freedom and the Hamiltonian is given by,

$$
\begin{aligned}
H_{\text{Mott}} =& H_{\text{spin}} + H_{\text{ion}} && (4.8)\\
H_{\text{spin}} =& \sum_{\langle i,j\rangle} J\left(\left|\mathbf{R}_i - \mathbf{R}_j\right|\right) \hat{\mathbf{S}}_i \cdot \hat{\mathbf{S}}_j && (4.9)\\
H_{\text{ion}} =& \frac{1}{2}\sum_{i\neq j} \phi\left(\left|\mathbf{R}_i - \mathbf{R}_j\right|\right) + \sum_i \frac{\left|\mathbf{P}_i\right|^2}{2m}. && (4.10)
\end{aligned}
$$

Here H_{spin} describes the local spin moments on a disordered Heisenberg model, where $J\left(\left|\mathbf{R}_i - \mathbf{R}_j\right|\right)$ is the distance-dependent exchange constant between two local moments which also depends on the on-site Coulomb repulsion U. The operator $\hat{\mathbf{S}}_i$ is the spin operator of a localized spin on the i-th atom. $\mathbf{R}_i$ is the position of the i-th atoms. H_{ion} describe the ion degree of freedom, where ϕ is the pairwise repulsive inter-atomic potential. The last term is the kinetic energy of atoms. As discussed in the above sections, the previously developed inhomogeneous DMFT method does not take into account the spin-exchange interaction between local moments. Fortunately, the Heisenberg Hamiltonian can be solved straightforwardly using the exact diagonalization method.

In the numerical simulation, it is crucial to correctly generate the matrix representation of H_{spin}, whose size of the Hilbert space grows exponentially, $D = 2_s^N$, where D is the dimension of the matrix and N_s is a total number of atoms. However, in practice, it is difficult to simulate a large system due to the exponential growing Hilbert space; the technical details will be discussed in a later section.

For spin 1/2, the components of the spin operators can be written using Pauli matrices,

$$\hat{S}_i^\alpha = \frac{1}{2}\sigma_\alpha, \text{ where } \alpha = x, y, z \tag{4.11}$$

σ_α are Pauli matrices,

$$\sigma_x = \begin{pmatrix} 0 & 1 \\ 1 & 0 \end{pmatrix}, \quad \sigma_y = \begin{pmatrix} 0 & -i \\ i & 0 \end{pmatrix}, \quad \sigma_z = \begin{pmatrix} 1 & 0 \\ 0 & -1 \end{pmatrix} \tag{4.12}$$

To construct the matrix representation of H_{spin}, the eigenvectors of $\hat{S}^z$ are chosen as the basis of the Hamiltonian.

$$|\uparrow\rangle = \begin{pmatrix} 1 \\ 0 \end{pmatrix}, \quad |\downarrow\rangle = \begin{pmatrix} 0 \\ 1 \end{pmatrix} \tag{4.13}$$

The spin-up state $|\downarrow\rangle$ and the spin-down state $|\uparrow\rangle$ are eigenvectors of $\hat{S}^z$, The eigenvalues of $\hat{S}^z$ are,

$$\hat{S}^z |\uparrow\rangle = +\frac{1}{2} |\uparrow\rangle, \tag{4.14}$$

$$\hat{S}^z |\downarrow\rangle = -\frac{1}{2} |\downarrow\rangle \tag{4.15}$$

A many-body state of N_s spins in this basis can be easily written as,

$$|m\rangle = \underbrace{|\uparrow\downarrow\uparrow\uparrow\uparrow\cdots\rangle}_{N_s \text{ spins}} \tag{4.16}$$

These states forms an orthogonal basis,

$$\langle m|n\rangle = \delta_{mn} \tag{4.17}$$

$\hat{S}_i^z$ is the spin-z operator defined on the site i, and it effects on a many-body state are given by,

$$\hat{S}_i^z|\cdots\underset{\text{i-th site}}{\uparrow}\cdots\rangle = +\frac{1}{2}|\cdots\underset{\text{i-th site}}{\uparrow}\cdots\rangle, \tag{4.18}$$

$$\hat{S}_i^z|\cdots\underset{\text{i-th site}}{\downarrow}\cdots\rangle = -\frac{1}{2}|\cdots\underset{\text{i-th site}}{\downarrow}\cdots\rangle, \tag{4.19}$$

Note that, spin operators defined on different sites commutes with each other,

$$\left[\hat{S}_i^\alpha, \hat{S}_j^\alpha\right] = 0 \quad \text{when} \quad i \neq j \tag{4.20}$$

It is also very helpful to defined the spin ladder operators in this basis,

$$\hat{S}_i^+ = \hat{S}_i^x + \mathrm{i}\hat{S}_i^y, \tag{4.21}$$

$$\hat{S}_i^- = \hat{S}_i^x - \mathrm{i}\hat{S}_i^y \tag{4.22}$$

When acting on a spin state, the spin raising operator $\hat{S}^+$ can change a spin-down state to a spin-up state and the spin lowering operator $\hat{S}^+$ can change a spin-up state to a spin-down state.

$$\hat{S}^{+}\left|\downarrow\right\rangle = \left|\uparrow\right\rangle, \quad \hat{S}^{+}\left|\uparrow\right\rangle = 0 \tag{4.23}$$

$$\hat{S}^{-}\left|\uparrow\right\rangle = \left|\downarrow\right\rangle, \quad \hat{S}^{-}\left|\downarrow\right\rangle = 0 \tag{4.24}$$

It is easy to identify the following relation,

$$\hat{S}_i^x\hat{S}_j^x + \hat{S}_i^y\hat{S}_j^y = \frac{1}{2}\left(\hat{S}_i^+\hat{S}_j^- + \hat{S}_j^+\hat{S}_i^-\right), \quad \text{when} \quad i \neq j \tag{4.25}$$

With this relation, we can rewrite the Hamiltonian using the spin ladder operators,

$$\begin{aligned}
H_{\text{spin}} &= \sum_{\langle i,j\rangle} J\left(\left|\mathbf{R}_i - \mathbf{R}_j\right|\right)\hat{\mathbf{S}}_i \cdot \hat{\mathbf{S}}_j && (4.26)\\
&= \sum_{\langle i,j\rangle} J\left(\left|\mathbf{R}_i - \mathbf{R}_j\right|\right)\left(\hat{S}_i^x\hat{S}_j^x + \hat{S}_i^y\hat{S}_j^y + \hat{S}_i^z\hat{S}_j^z\right) && (4.27)\\
&= \sum_{\langle i,j\rangle} J\left(\left|\mathbf{R}_i - \mathbf{R}_j\right|\right)\left[\frac{1}{2}\left(\hat{S}_i^+\hat{S}_j^- + \hat{S}_j^+\hat{S}_i^-\right) + \hat{S}_i^z\hat{S}_j^z\right] && (4.28)\\
&= H_{\text{off}} + H_{\text{diag}} && (4.29)
\end{aligned}$$

In the final step, we separate the Hamiltonian operator into two terms: the diagonal term H_{diag} and the off-diagonal term H_{off},

$$H_{\text{off}} = \sum_{\langle i,j\rangle} J\left(\left|\mathbf{R}_i - \mathbf{R}_j\right|\right)\frac{1}{2}\left(\hat{S}_i^+\hat{S}_j^- + \hat{S}_j^+\hat{S}_i^-\right) \tag{4.30}$$

$$H_{\text{diag}} = \sum_{\langle i,j\rangle} J\left(\left|\mathbf{R}_i - \mathbf{R}_j\right|\right)\hat{S}_i^z\hat{S}_j^z \tag{4.31}$$

It is important to see that, when acting on a state, the diagonal term will not change the original state, but the off-diagonal will leads to a new state. The matrix representation of the Hamiltonian will be constructed based on the above expressions. The matrix element of the Hamiltonian is then given by,

$$H_{mn} = \langle m| \, H_{\text{off}} + H_{\text{diag}} \, |n\rangle \tag{4.32}$$

where $\langle m|$ and $|n\rangle$ are the possible many-body states of the system.

How a matrix element of the Hamiltonian is calculated in practice is briefly introduced here. Consider a many-body state of N_s spins,

$$|n\rangle = |\sigma_1 \sigma_2 \cdots \sigma_{N_s}\rangle \,, \tag{4.33}$$

where $\sigma_i =\uparrow, \downarrow$ is the spin state on the i-th atom. Due to the presence of off-diagonal terms in the matrix representation, it is beneficial to have an efficient indexing system to index all the possible many-body states of the system, so that we can quickly navigate through these matrix elements. In an other word, we have to systematically assign an integer $n \in \left[0, 2^{N_s}\right]$ to all possible states $|n\rangle$.

It turns out that a binary representation of state can be very helpful in this case. Because there are only two possible states $\uparrow$ or $\downarrow$ on each atom, we can consider the following mapping rules,

$$\uparrow \rightarrow 1, \quad \downarrow \rightarrow 0 \tag{4.34}$$

Using these rules, any given spin state can be represented using a binary number,

$$|\sigma_1\sigma_2\cdots\sigma_{N_s}\rangle \rightarrow d_1d_2\cdots d_{N_s} \tag{4.35}$$

This binary number can be then converted to a decimal number which is the index of the state,

$$n = d_1 2^0 + d_2 2^1 + d_3 2^2 + \cdots d_{N_s} 2^{N_s-1} \tag{4.36}$$

It is easy to see that the dimension of the matrix representation of operators in this system is 2_s^N, where N_s is total number of spins. Therefore, we have the one-to-one correspondence between a spin state and an index,

$$|\sigma_1\sigma_2\cdots\sigma_{N_s}\rangle \rightleftarrows |n\rangle\,, \tag{4.37}$$

where $|n\rangle$ is the state with index n. By applying the spin operators on the original state, we can quickly identify the new state by manipulating the corresponding spins, and the index of the new state can then be obtained using the above mapping. Note that the matrix representations of useful operators can also be constructed in this way, each as $\hat{S}_i^z$, $\hat{S}_i^+\hat{S}_j^-$.

For example, to compute the matrix representation of S_i^+, one need to go through all possible state $|k\rangle$ and find the finite matrix elements.

$$S_i^+ |k\rangle = S_i^+ \left| \cdots \underset{\text{i-th site}}{0} \cdots \right\rangle \tag{4.38}$$

$$= | \cdots \underset{\text{i-th site}}{1} \cdots \rangle = |l\rangle \tag{4.39}$$

The matrix element $(S_i^+)_{lk}$ is

$$(S_i^+)_{lk} = \langle l| S_i^+ |k\rangle = 1 \tag{4.40}$$

The major advantage of this indexing system is that, when applying a spin operator on a state, we avoid going through all possible states to search for the final state; instead, we can compute its index directly. This can reduce the complexity of matrix construction from $O(2^{2N_s})$ to $O(2_s^N)$ complexity, which can leads to a significant performance improvement when the system is large.

4.4 Molecular dynamics with exact diagonalization

In this section, the exact diagonalization MD (ED-MD) scheme is introduced. We adopt the Born-Oppenheimer approximation, where the electron degrees of freedom and ion degrees of freedom are well separated so that the electrons can be assumed in equilibrium at any MD time step.

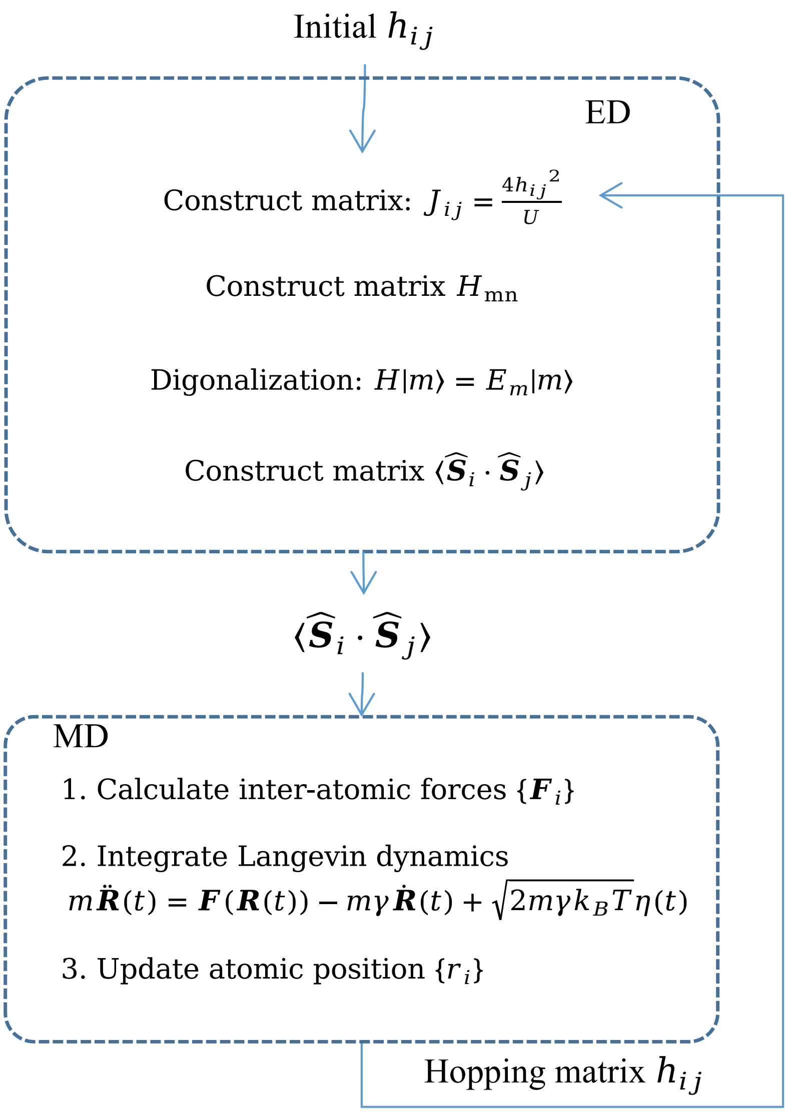

Figure 4.1: The flowchart of ED-MD algorithm. The loop will end after certain numbers of iterations. The measurement should be performed after the system reaches equilibrium.

Consider an initial atomic configuration of the system at time step t_n,

$$C(t) = \{\mathbf{R}_1, \mathbf{R}_2, \cdots, \mathbf{R}_i\} \tag{4.41}$$

A hopping matrix can be uniquely defined from the atomic configuration,

$$h_{ij} = h\left(|\mathbf{R}_i - \mathbf{R}_j|\right) \tag{4.42}$$

Then the exchange constant matrix is calculated,

$$J_{ij} = \frac{4h_{ij}^2}{U} \tag{4.43}$$

The spin Hamiltonian matrix is then constructed using the exchange constant matrix J_{ij},

$$H_{\text{spin}} = \sum_{\langle i,j \rangle} J_{ij} \hat{\mathbf{S}}_i \cdot \hat{\mathbf{S}}_j \tag{4.44}$$

This Hamiltonian is solved using exact diagonalization method. Note that, the Hamiltonian is positive symmetric sparse matrix, and the sparse matrix diagonalization techniques can be utilized to speed up the calculation.

Similar to the DMFT-MD, the total force on an atom consists of the contributions from both exchange interaction of local moments and classical pairwise potentials between ions,

$$\mathbf{F}_i = \mathbf{F}_i^{\text{spin}} + \mathbf{F}_i^{\text{classical}} \tag{4.45}$$

With the information of the eigenstates of the Hamiltonian, we are able to calculate the contribution of local moments to the interatomic force. This force can be derived using the Feynman Hellman theorem,

$$\begin{aligned}\mathbf{F}_i^{spin} &= -\frac{\partial \langle H_{\mathrm{spin}} \rangle}{\partial \mathbf{R}_i} && (4.46)\\ &= -\left\langle \sum_j \frac{\partial J_{ij} \hat{\mathbf{S}}_i \cdot \hat{\mathbf{S}}_j}{\partial \mathbf{R}_j} \right\rangle && (4.47)\end{aligned}$$

Therefore, the final expression is given by,

$$\mathbf{F}_i^{spin} = -\sum_j \frac{\partial J_{ij}}{\partial \mathbf{R}_j} \langle \hat{\mathbf{S}}_i \cdot \hat{\mathbf{S}}_j \rangle \tag{4.48}$$

Note that the largest possible value of $\langle \hat{\mathbf{S}}_i \cdot \hat{\mathbf{S}}_j \rangle$ is $1/2(1/2+1) = 3/4$. The expectation value of the operator is given by,

$$\langle \hat{\mathbf{S}}_i \cdot \hat{\mathbf{S}}_j \rangle = \sum_m \langle m | \hat{\mathbf{S}}_i \cdot \hat{\mathbf{S}}_j | m \rangle e^{-\beta E_m} / \mathcal{Z}, \tag{4.49}$$

where E_m are the energy levels and $|m\rangle$ are the corresponding eigenvectors; $\mathcal{Z}$ is the total partition function,

$$\mathcal{Z} = \sum_m e^{-\beta E_m} \tag{4.50}$$

In practice, the Boltzmann weight $e^{-\beta E_m}$ can be very large in low temperature, $\beta >> 0$, which may even exceed the maximum limit of the computer data type and cause runtime errors. Thus, it is wise to measure the eigenenergies relative to the ground state energy E_0,

$$\langle \hat{\mathbf{S}}_i \cdot \hat{\mathbf{S}}_j \rangle = \frac{\sum_m \langle m | \hat{\mathbf{S}}_i \cdot \hat{\mathbf{S}}_j | m \rangle e^{-\beta(E_m - E_0)}}{\sum_m e^{-\beta(E_m - E_0)}} \tag{4.51}$$

In the simulation, we found that the ground state has the largest contribution to the expectation value calculation, whose weight is several orders of magnitude larger than other states. Therefore, it is reasonable to use only a few low energy states to calculate the expectation values,

$$\langle \hat{\mathbf{S}}_i \cdot \hat{\mathbf{S}}_j \rangle = \frac{\sum_m^{N_k} \langle m | \hat{\mathbf{S}}_i \cdot \hat{\mathbf{S}}_j | m \rangle e^{-\beta(E_m - E_0)}}{\sum_m^{N_k} e^{-\beta(E_m - E_0)}} \tag{4.52}$$

where N_k is the number of lowest energy states kept when solving the Hamiltonian. Without any noticeable influence on the full results, this approximation can dramatically improve the performance of the simulation, since not all - states are calculated.The classical pairwise potential $\phi(r)$ introduces classical forces between the atoms,

$$\mathbf{F}_i^{\text{classical}} = -\sum_j \frac{\partial \phi_{ij}}{\partial \mathbf{R_i}} \tag{4.53}$$

The atomic configuration is then updated using Langevin dynamics with the standard velocity-Verlet method.

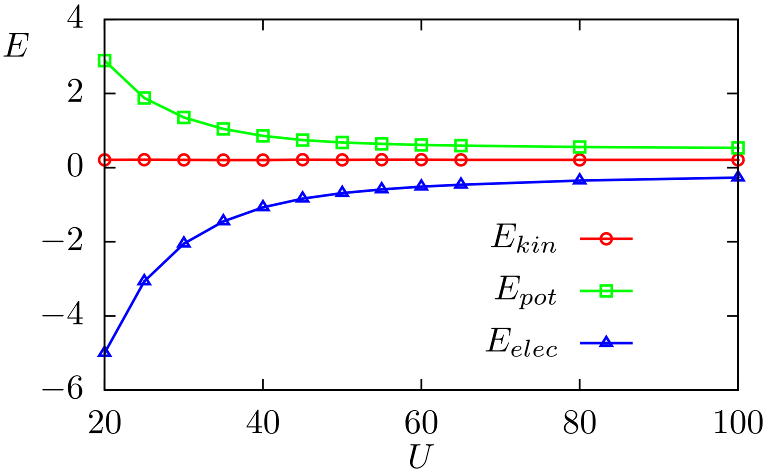

Figure 4.2: Energies as function of U. Simulation is performed at $N_s = 12$, $r_s = 1.2$, $T = 0.15$.

4.5 Dimers in Mott liquid

We applied the ED-MD method to the Mott liquid model defined by Eq. (4.8). The simulation is perform on systems of $N_s = 14$ atoms with constant system size V that is determined by the average atom distance $r_s = (3V/4\pi N)^{1/3}$. The system is first allowed to fully relax and converge to equilibrium before the measurement. One of the criteria for equilibrium is the check the atomic kinetic energy of the system,

$$E_{\text{kin}} = \sum_i \frac{1}{2} m \mathbf{v}_i^2 \tag{4.54}$$

Due to the Langevin dynamics, $E_{kin} = 3/2 k_B T$ when the system is in equilibrium.

Fig. 4.5 shows the three major types of energies of the system as a function of on-site Coulomb interaction U. As mentioned above, the total kinetic energy of the atoms dependents only on temperature $E_{kin} = 3/2k_B$ should be a constant for fixed temperature simulations. The pairwise potential energies are given by,

$$E_{\text{pot}} = \sum_{i \neq j} \frac{1}{2} \phi \left(|\mathbf{R}_i - \mathbf{R}_j| \right) \tag{4.55}$$

The electronic energies E_{elec} is the expectation value of H_{spin}.

$$E_{\text{elec}} = \langle E \rangle = \frac{\sum_m^{N_k} E_m e^{-\beta(E_m - E_0)}}{\sum_m^{N_k} e^{-\beta(E_m - E_0)}} \tag{4.56}$$

The magnitude of both E_{elec} and E_{pot} decrease as U increases. Unlike the dramatic change of energies in the previous simulation of Hubbard liquid, this change of energies is very smooth suggesting that the system exhibits a crossover driven by U. Later one will see that this crossover is related to the molecular dissociations.

The pair distribution functions $g(r)$ are measured during the simulations and shown in Fig. 4.5, which gives us information on the atomic configuration in the system.

When $U \sim U_c$, the presence of a dimer peak is observed; in this regime, the exchange interactions between local moments bind their corresponding atoms together and form dimers. As U further increases, the exchange interaction is weaker, and the equilibrium length r_0 is of a similar order with the averaged atomic distance r_s, the dimers start to dissociates, and the dimer peak merges to a broad peak at large r. Note that this does not indicate that there are

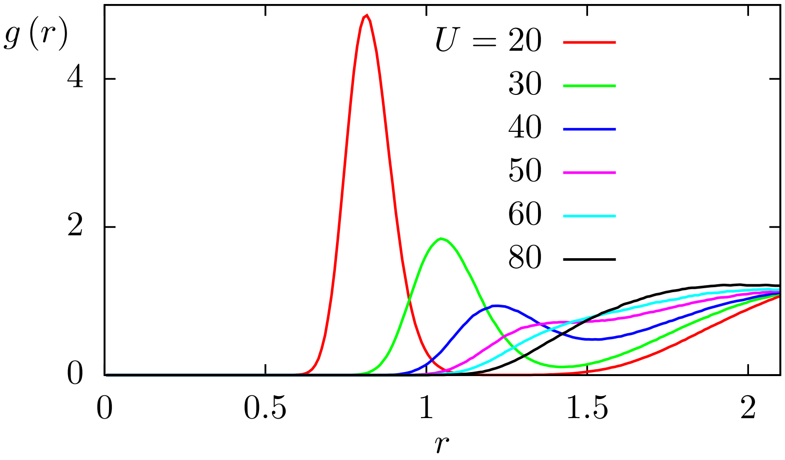

Figure 4.3: Pair distribution function $g(r)$ obtained from ED-MD for varying values of U. The dimers form in the Mott liquid. As the U increases, the exchange interaction is weaker and dimers starts to dissociate.

no attractive forces between atoms, but the attractive force due to exchange interaction is too weak to have significant effects.

The partial pair distribution function $g_{AB}(r)$ is the possibility of finding another atom of species A at a distance r of atoms of species B. One can see that even though there are no clear dimer peaks in the $g(r)$, the partial pair distribution function $g_{\uparrow\downarrow}(r)$, between atoms whose expectation value of $\left\langle \hat{S}_i^z \right\rangle$ are different, exhibits a peak. This indicates that the atoms with different expectation values of $\left\langle \hat{S}_i^z \right\rangle$ are still attracting each other, though this effect cannot be clearly distinguished in the total $g(r)$.

The formation of dimers and the dissociation process are intuitive yet have never been reported before. Combined with previous results, one may expect a rich phase diagram for the Hubbard liquid. As U increases from the non-interacting limit, the molecular dimer starts to dissociate near the transition.

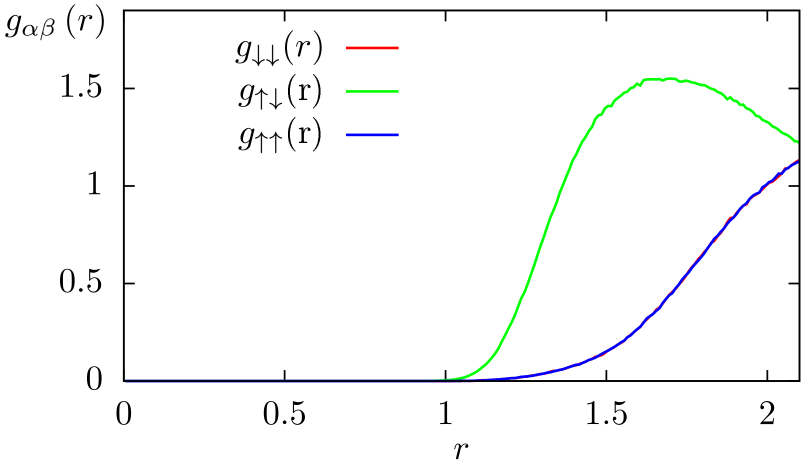

Figure 4.4: Partial pair distribution functions. The peak at $r \sim 1.6$ indicates there is an effective attraction between spin up and spin down atoms.

In contrast, after the Mott transition, the presence of local moment and their exchange interaction binds the atoms again and forms dimers who will eventually vanish in the strongly interacting limit. If the box size decreases, one might expect that the molecular dimer in the small U vanishes far before the Mott transition. In this case, the dimer will form at the Mott transition and vanish in the large U limit.

It is well-known that ground state of Heisenberg Model with 2 spins is a singlet states with total spin $S = 0$. For a system with N_s atoms, we can define the total spin operator,

$$\hat{\mathbf{S}} = \sum_i \hat{\mathbf{S}}_i \tag{4.57}$$

We cannot calculate the expectation value of this operator directly, but we can write the square of the total spin operator, whose expectation can be

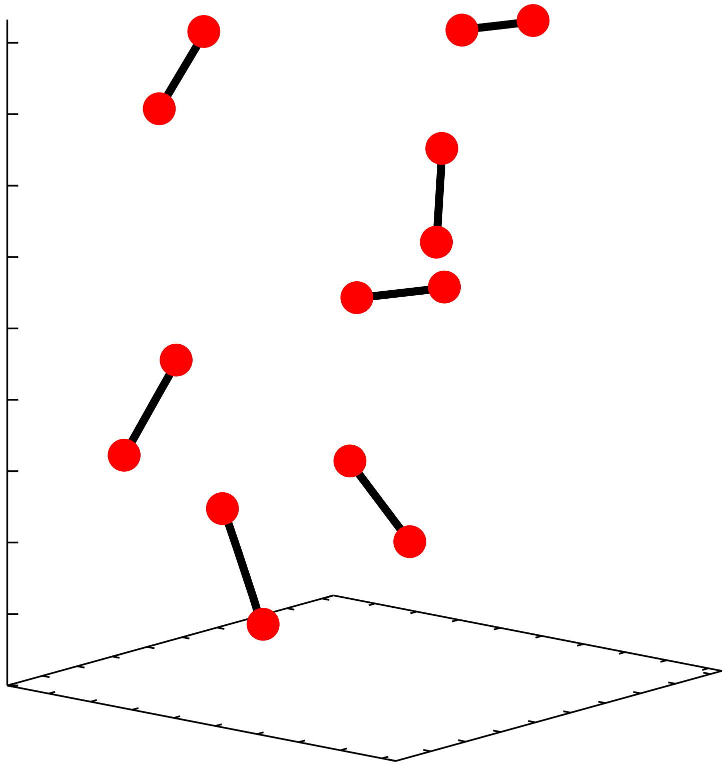

Figure 4.5: Atomic configurations of a snapshot at $U = 20$. The red dots are the atoms, the bond between atoms are labeled using a black line.

computed easily,

$$\hat{\mathbf{S}}^2 = \sum_i \hat{\mathbf{S}}_i + \sum_{i \neq j} \hat{\mathbf{S}}_i \cdot \hat{\mathbf{S}}_j \tag{4.58}$$

The total spin S of a state $|m\rangle$ is then given by,

$$S(S+1) = \langle m| \hat{\mathbf{S}}^2 |m\rangle \tag{4.59}$$

$$= \sum_i \langle m| \hat{\mathbf{S}}_i^2 |m\rangle + \sum_{i \neq j} \langle m| \hat{\mathbf{S}}_i \cdot \hat{\mathbf{S}}_j |m\rangle \tag{4.60}$$

In the simulation, we find that, for systems consisting even number of atoms, the ground state is almost always a singlet state $S = 0$ with no degeneracy when U is relatively small; however, when U is very large, triplet states with $S = 1$ might occur due to the spatial inhomogeneity. When molecules dissociate, atoms can form local clusters consisting odd number of atoms, which can result in ground states with finite total spin S.

One can estimate the dimer length by examining the binding energy. Consider the binding energy as a function of distance,

$$E_b = \alpha_1 \exp(-\beta_1 r) - \alpha_2 \exp(-\beta_2 r) \tag{4.61}$$

An extreme exists at,

$$r_{\text{ex}} = \frac{\ln \frac{\alpha_1 \beta_1}{\alpha_2 \beta_2}}{\beta_1 - \beta_2} \tag{4.62}$$

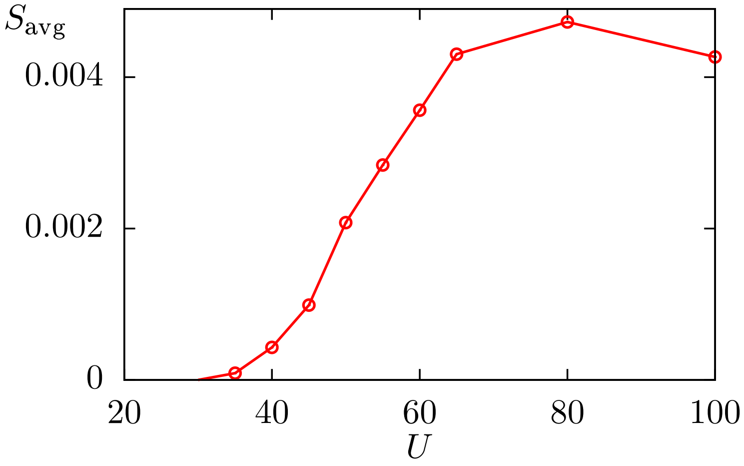

Figure 4.6: Averaged total spin S_{avg} of the ground state as a function of U. As U increases, the S_{avg} increases, indicating the presence of triplet states.

For this extreme to be physical, we require $r_{\mathrm{ex}} > 0$,

$$\beta_1 > \beta_2, \quad \text{and} \quad \alpha_1\beta_1 > \alpha_2\beta_2 \tag{4.63}$$

$$\beta_1 < \beta_2, \quad \text{and} \quad \alpha_1\beta_1 < \alpha_2\beta_2 \tag{4.64}$$

The second derivatives of the binding energy at the extreme r_{ex},

$$\frac{d^2}{dr^2}E_b(r_{ex}) = \alpha_1\beta_1^2\exp(-\beta_1 r_{ex}) - \alpha_2\beta_2^2\exp(-\beta_2 r_{ex}), \tag{4.65}$$

$$= \alpha_1\beta_1^2\left(\frac{\alpha_1\beta_1}{\alpha_2\beta_2}\right)^{-\frac{\beta_1}{\beta_1-\beta_2}} - \alpha_2\beta_2^2\left(\frac{\alpha_1\beta_1}{\alpha_2\beta_2}\right)^{-\frac{\beta_2}{\beta_1-\beta_2}} \tag{4.66}$$

$$= \alpha_1\beta_1\left(\beta_1-\beta_2\right)\left(\frac{\alpha_2\beta_2}{\alpha_1\beta_1}\right)^{-\frac{\beta_1}{\beta_2-\beta_1}} \tag{4.67}$$

The binding energy has a minimum when $\frac{d^2}{dr^2}E_b(r_{ex}) > 0$ or a maximum when $\frac{d^2}{dr^2}E_b(r_{ex}) < 0$. Therefore, to form stable dimers, the binding energy must have a minimum and the parameters of the potentials have to satisfy,

$$\beta_1 > \beta_2, \quad \text{and} \quad \alpha_1\beta_1 > \alpha_2\beta_2 \tag{4.68}$$

One can define the ratios between the strength and the decay length of the repulsive and the attractive potential,

$$\alpha = \frac{\alpha_1}{\alpha_2}, \quad \beta = \frac{\beta_1}{\beta_2} \tag{4.69}$$

Therefore requirements of forming stable dimers become,

$$\beta > 1 \quad \text{and} \quad \alpha\beta > 1 \tag{4.70}$$

On the other hand, if the position extrema is negative, $r_{\text{ex}} < 0$, the inter-atomic force is either purely attractive or repulsive. Note that a purely attractive force case is usually very unstable and have collisions. A purely attractive force case results in a simple atomic liquid.

The diffusion coefficient as a function of U is shown in Fig. 4.5. The diffusion coefficient is obtained by using the same method discussed in the previous chapter. A dramatic increase of diffusion coefficient is observed near $U \sim 40$. This is due to the fact that the effective mass of atoms decreases when the atomic dimers dissociate.The atoms become more mobile after the dissociation.

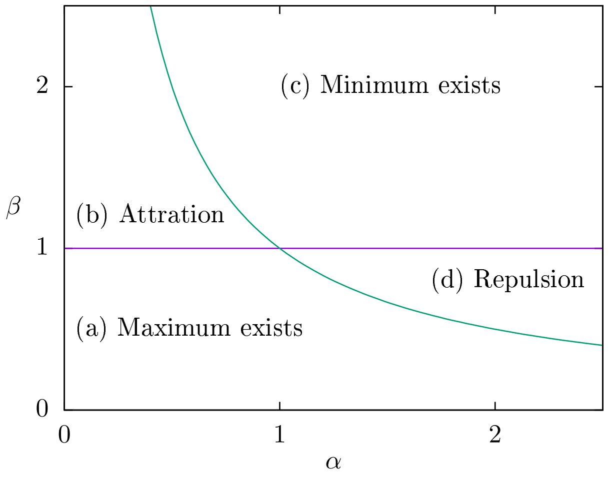

Figure 4.7: Schematic diagram of binding energy. There are four possible situations for the inter-atomic forces in the liquid system.

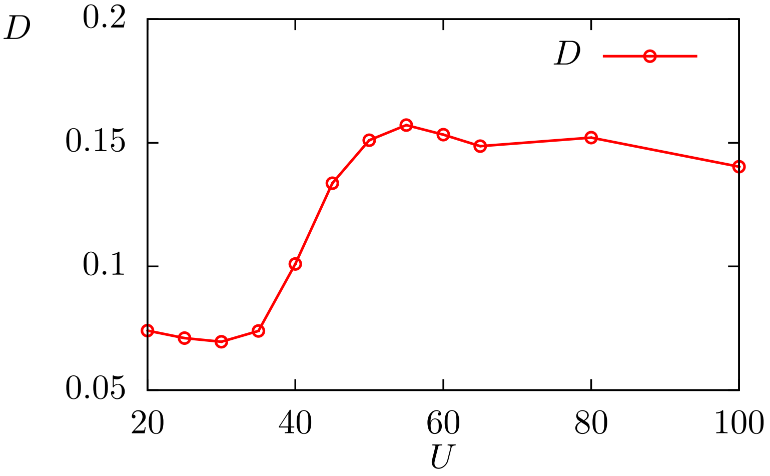

Figure 4.8: Diffusion constant as function of U.

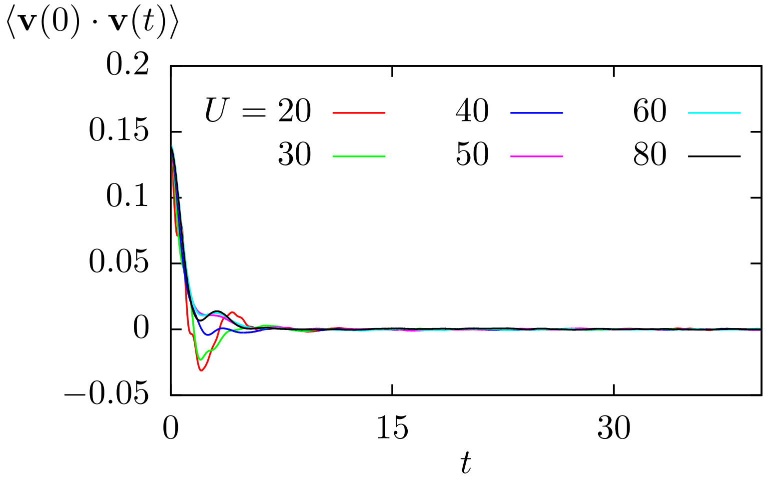

Figure 4.9: Velocity autocorrelation functions $\langle \mathbf{v}(0) \cdot \mathbf{v}(t) \rangle$ as a function of time. These functions are sampled in time windows of 40. During a single simulation, multiple time windows are sampled and averaged for better data quality.

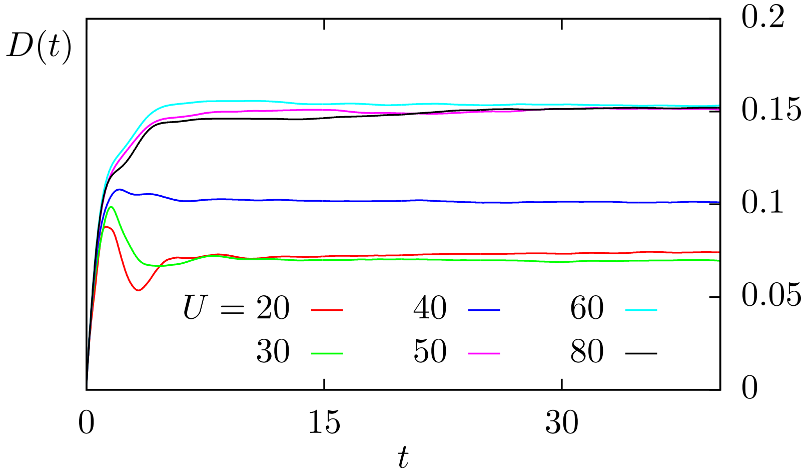

Figure 4.10: Accumulative diffusion coefficients $D(t)$ at various U. They are calculated by integrating the sampled velocity autocorrelation functions. Note that we use the large time $D(t)$ to approximate the actual diffusion constant.

4.6 Simulation details

In this section, some important technical details of ED-MD simulation are discussed. First, the implementation of the index system is worth mentioning. A many-body spin state can be stored as a string of 0 or 1. The C++ built-in class, bitset, can convert the string to an integer and visa-versa. Therefore, the effect of a spin operator on an Ising state can be achieved by manipulating the corresponding string, and the index of the new state can be obtained using the bitset class.

Second, we discuss some methods we adopted in the exact diagonalization to make the problem feasible. In our study, the simulation is performed on systems with up to 14 atoms, and the corresponding size of the Hamiltonian matrix is 16384×16384. When solving static systems with exact diagonalization, this size is not large and should not be difficult to solve. However, in our case, we are studying a dynamic problem, and the Hamiltonian should be constructed and solved at every time step. In order to have good diffusion or radial distribution function measurements, enough MD iterations are required. Therefore, the matrix construction and matrix diagonalization time will be the major computational bottleneck.

In this study, we implemented several methods to improve the performance and make the simulation feasible. Firstly, we store the Hamiltonian as a sparse matrix and use the sparse matrix diagonalization method to extract only the important eigenvalues instead of all of them. A matrix is considered to be sparse if most of its elements are zero. We can define the sparsity of a matrix as the ratio between the number of zero elements and the total number of matrix elements $s = N_{\text{zero}}/N_{\text{total}}$. We can see that each off-diagonal terms $\frac{1}{2}\left(\hat{S}_i^+\hat{S}_j^- + \hat{S}_j^+\hat{S}_i^-\right)$ can lead to $2 \times 2^{N_s-2}$ nonzero terms, provided that there are finite interaction between i-th atom and j-th atom. Therefore, the total number of non-zeros terms for Hamiltonian of N_s atoms, is

$$N_{\text{nonzero}} = 2 \times 2^{N_s-2} \times \frac{N_s(N_s-1)}{2} + 2^{N_s} \tag{4.71}$$

the last term is the number of finite diagonal term. Therefore, the sparsity of the Hamiltonian is,

$$s = 1 - \frac{2 \times 2^{N_s-2} \times \frac{N_s(N_s-1)}{2} + 2^{N_s}}{2^{2N_s}} \tag{4.72}$$

The sparsity of a Hamiltonian in the Mott liquid with $N_s = 14$ is 0.283% if we don't set a cutoff distance $r_{\max}$ for the exchange interaction. The calculated value agrees with the simulation result. Therefore, sparse matrix treatment of the Hamiltonian is valid. There exist several advantages when using a sparse matrix representation. From one aspect, a sparse matrix data type will occupy only a small amount of computer memory space. If one store the Hamiltonian with size 16384 × 16384 as dense matrix where all the elements will be stored, it will takes approximately 2 gigabytes (GB) of memory and this value will increase exponentially as the number of atoms increases. However, if this matrix is stored as a sparse matrix data type, it takes only a few megabytes (MB) of memory, since only the indices and the corresponding

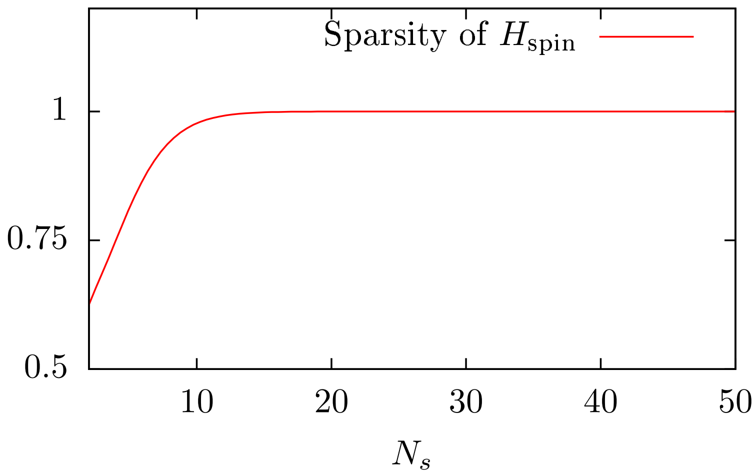

Figure 4.11: The sparsity of H_{spin} matrix. The Hamiltonian matrix is extremely sparse and becomes almost empty as the system size increases.

values of nonzero elements are stored. For example,

$$\begin{pmatrix} 0 & 1 & 0 & 0 \\ 0 & 0 & 0 & 1 \\ 2 & 0 & 0 & 0 \\ 0 & 0 & 0 & 1 \end{pmatrix} \rightarrow \begin{matrix} (0,1,1) \\ (1,3,1) \\ (2,0,2) \\ (3,3,1) \end{matrix} \tag{4.73}$$

The sparse matrix is save as a list of tuples where first two numbers are the indices and the third one is the matrix element. Another advantages is that the sparsity of the matrix can be utilized during the diagonalization. As discuss above, the eigenvalues E_m and eigenvectors $|m\rangle$ of the Hamiltonian are used to compute the expectation values of various observables and only the first few low energy states matters at low temperature. In practice, computing only the first few lowest energy states of a sparse Hamiltonian is much faster than diagonalizing the same Hamiltonian using dense matrix eigen decomposition routines with a computational complexity of $\mathcal{O}(N^3)$. In our code, we use Armadillo package to handle all the matrix operations [172, 173]. Note that one may encounter convergence issue inside the diagonalization routines and it is advised to increase the value of N_k of the algorithm [172, 173]. In our code, a runtime error handling routine is designed to avoid potential errors caused by this decomposition failure.

The other useful method to improve the computational efficiency is to construct and save the matrix representations of all frequently used operators at the beginning of the simulation. In a system with a fixed number of atoms, the spin Hamiltonian H_{spin} at different time steps differs from each other. However, the matrix representation of operator $\hat{\mathbf{S}}_i \cdot \hat{\mathbf{S}}_j$ remains unchanged; the only thing that changes is the exchange constant matrix J_{ij}. Thus, one can construct and save the matrix of $\hat{\mathbf{S}}_i \cdot \hat{\mathbf{S}}_j$ first to avoid reconstructing them at every time step. In our code, the matrices $\left(\hat{\mathbf{S}}_i \cdot \hat{\mathbf{S}}_j\right)_{mn}$ and their indices (i, j) are saved in a map data type for quick access. At each time step, the code sums over all the stored matrices, with their corresponding exchange constants, multiplied to construct the Hamiltonian. These matrices are also needed when calculating the inter-atomic forces. This approach can significantly improve the efficiency of large-scale simulations.

4.7 Conclusion

To summarize, we propose an ED-MD scheme to study the dynamics of the Mott liquid model, i.e., the Hubbard liquid model in the Mott phase. A unique dimer formation and a molecular dissociation, driven by U, are observed. If both spatial inhomogeneity and short-range quantum fluctuation are included, it is possible to have a coexistence of two types of dimers. In one type of dimers, atoms are bounded by electron hopping, while in the other type of dimers, atoms are bounded by exchange interactions. These novel results suggest rich physics and complex dynamics in correlated liquid systems in the Mott phase. Moreover, our study might be closely related to real liquid systems such as Cs and Rb, in which spin paired dimers are reported [174].

Chapter 5

Conclusion

This thesis proposes a novel MD scheme that uses the DMFT method to treat electron correlations exactly. Applying our new method to the Hubbard liquid model, the picture of this U driven reentrant transition is unveiled. Additionally, the effects of exchange interaction at the large U limit are also studied with the new ED-MD scheme simulating the Mott liquid model. The formation of dimers in this limit reveals new phenomena previously never studied in a strongly correlated liquid system. Together, the two sets of simulations can give us a general picture during the correlation-driven transition in liquid by providing us the information of both the kinetics of atoms and the properties of electrons on both sides of the Mott transition. It is believed that such correlation-driven transitions can occur in alkali liquid metals, in which dimers can be observed in the Mott phase [94, 95]. The application of these methods is not limited to the liquid system. However, it can also be extended to solid systems in which kinetic are very important during the MIT transition, such as Plutonium and Cerium exhibiting the volume collapse transitions [175]. Indeed, before being applied to a solid, further performance improvements are mandatory. A system with 40 atoms is adequate for studying the dynamics of a liquid system; however, 40 atoms are too few to construct enough unit cells to study the dynamics of solid systems.

Another promising direction is to use *ab initio* calculations, such as LDA, at every time step to update the hopping matrix t_{ij} and the Coulomb interaction U. This combination allows us to simulate real materials and make direct connections with experiments. From this multi-scale modeling, we can gain a better understanding of the phenomenon observed in actual experiments. However, this process itself will be extremely computationally expensive, let alone being combined with DMFT calculation, because the Wannierization of atomic orbitals on all atoms must be performed at each time step.

To overcome these computational bottlenecks, besides developing a heavily parallelized solver, the technique of machine learning can be a potential solution. It was proven to be a robust solver to calculate the electron contribution of forces in MD simulations with strongly correlated electrons and disordered systems [45, 165]. With a properly designed descriptor that helps to encode the symmetries and other physical characteristics of the system, the trained neural network can generate the total force (with both electron contribution and classical potential contribution) acting on each atom based on the atomic configuration [45, 165]. This method turns out to be fast and adequately accurate, and more importantly, with its help, one can push the system size of the MD simulation to a much large value.

In the candidates of Mott transistors, such as VO_2, heterostructures are playing a vital role during the MIT. Our methods can provide a further understanding of the interplay between the formation of electronic heterostructures and the dynamics of the atoms. Understanding this phenomenon might help the experimentalists improve the Mott transistors' performance and design more complex electronics based on strongly correlated materials.

Bibliography

[1] Yoshinori Tokura. “Correlated-Electron Physics in Transition-Metal Oxides”. In: *Physics Today* 56.7 (2003), pp. 50–55. DOI: `10.1063/1.1603080`. eprint: `https://doi.org/10.1063/1.1603080`. URL: `https://doi.org/10.1063/1.1603080`.

[2] G. Kotliar et al. “Electronic structure calculations with dynamical mean-field theory”. In: *Rev. Mod. Phys.* 78 (3 Aug. 2006), pp. 865–951. DOI: `10.1103/RevModPhys.78.865`. URL: `https://link.aps.org/doi/10.1103/RevModPhys.78.865`.

[3] P. Hohenberg and W. Kohn. “Inhomogeneous Electron Gas”. In: *Phys. Rev.* 136 (3B Nov. 1964), B864–B871. DOI: `10.1103/PhysRev.136.B864`. URL: `https://link.aps.org/doi/10.1103/PhysRev.136.B864`.

[4] W. Kohn and L. J. Sham. “Self-Consistent Equations Including Exchange and Correlation Effects”. In: *Phys. Rev.* 140 (4A Nov. 1965), A1133–A1138. DOI: `10.1103/PhysRev.140.A1133`. URL: `https://link.aps.org/doi/10.1103/PhysRev.140.A1133`.

[5] R. O. Jones and O. Gunnarsson. “The density functional formalism, its applications and prospects”. In: *Rev. Mod. Phys.* 61 (3 July 1989), pp. 689–746. DOI: `10.1103/RevModPhys.61.689`. URL: `https://link.aps.org/doi/10.1103/RevModPhys.61.689`.

[6] John P. Perdew, Kieron Burke, and Matthias Ernzerhof. “Generalized Gradient Approximation Made Simple”. In: *Phys. Rev. Lett.* 77 (18 Oct. 1996), pp. 3865–3868. DOI: `10.1103/PhysRevLett.77.3865`. URL: `https://link.aps.org/doi/10.1103/PhysRevLett.77.3865`.

[7] Vladimir I. Anisimov, Jan Zaanen, and Ole K. Andersen. “Band theory and Mott insulators: Hubbard U instead of Stoner I”. In: *Phys. Rev. B* 44 (3 July 1991), pp. 943–954. DOI: `10.1103/PhysRevB.44.943`. URL: `https://link.aps.org/doi/10.1103/PhysRevB.44.943`.

[8] Stefano Baroni et al. “Phonons and related crystal properties from density-functional perturbation theory”. In: *Rev. Mod. Phys.* 73 (2 July 2001), pp. 515–562. DOI: `10.1103/RevModPhys.73.515`. URL: `https://link.aps.org/doi/10.1103/RevModPhys.73.515`.

[9] Dieter Vollhardt. “Dynamical Mean-Field Theory of Strongly Correlated Electron Systems”. In: *Proceedings of the International Conference on Strongly Correlated Electron Systems (SCES2019)* (Mar. 2020). DOI: `10.7566/jpscp.30.011001`. URL: `http://dx.doi.org/10.7566/JPSCP.30.011001`.

[10] S. A. Kivelson, E. Fradkin, and V. J. Emery. “Electronic liquid-crystal phases of a doped Mott insulator”. In: *Nature* 393.6685 (June 1998),

pp. 550–553. ISSN: 1476-4687. DOI: `10.1038/31177`. URL: `http://dx.doi.org/10.1038/31177`.

[11] Y. Tokura and N. Nagaosa. "Orbital Physics in Transition-Metal Oxides". In: *Science* 288.5465 (2000), pp. 462–468. ISSN: 0036-8075. DOI: `10.1126/science.288.5465.462`. eprint: `https://science.sciencemag.org/content/288/5465/462.full.pdf`. URL: `https://science.sciencemag.org/content/288/5465/462`.

[12] Gabriel Kotliar and Dieter Vollhardt. "Strongly Correlated Materials: Insights From Dynamical Mean-Field Theory". In: *Physics Today* 57.3 (Mar. 2004), pp. 53–59. DOI: `10.1063/1.1712502`.

[13] Antoine Georges et al. "Dynamical mean-field theory of strongly correlated fermion systems and the limit of infinite dimensions". In: *Rev. Mod. Phys.* 68 (1 Jan. 1996), pp. 13–125. DOI: `10.1103/RevModPhys.68.13`. URL: `https://link.aps.org/doi/10.1103/RevModPhys.68.13`.

[14] N. F. Mott. "Metal insulator transitions". In: *Contemporary Physics* 14.5 (1973), pp. 401–413. DOI: `10.1080/00107517308210764`. eprint: `https://doi.org/10.1080/00107517308210764`. URL: `https://doi.org/10.1080/00107517308210764`.

[15] N. F. MOTT. "Metal-Insulator Transition". In: *Rev. Mod. Phys.* 40 (4 Oct. 1968), pp. 677–683. DOI: `10.1103/RevModPhys.40.677`. URL: `https://link.aps.org/doi/10.1103/RevModPhys.40.677`.

[16] Daniel P. Arovas et al. *The Hubbard Model.* 2021. arXiv: `2103.12097 [cond-mat.str-el]`.

[17] Olivier Parcollet et al. “TRIQS: A toolbox for research on interacting quantum systems”. In: *Computer Physics Communications* 196 (2015), pp. 398–415. ISSN: 0010-4655. DOI: `http://dx.doi.org/10.1016/j.cpc.2015.04.023`. URL: `http://www.sciencedirect.com/science/article/pii/S0010465515001666`.

[18] Hiroshi Shinaoka et al. “DCore: Integrated DMFT software for correlated electrons”. In: *SciPost Physics* 10.5 (May 2021). ISSN: 2542-4653. DOI: `10.21468/scipostphys.10.5.117`. URL: `http://dx.doi.org/10.21468/SciPostPhys.10.5.117`.

[19] N F Mott. “The Basis of the Electron Theory of Metals, with Special Reference to the Transition Metals”. In: *Proceedings of the Physical Society. Section A* 62.7 (July 1949), pp. 416–422. DOI: `10.1088/0370-1298/62/7/303`. URL: `https://doi.org/10.1088/0370-1298/62/7/303`.

[20] J. Bednorz and K. Müller. “Possible highTc superconductivity in the Ba-La-Cu-O system”. In: *Zeitschrift für Physik B Condensed Matter* 64 (1986), pp. 189–193.

[21] P. W. ANDERSON. “The Resonating Valence Bond State in La2CuO4 and Superconductivity”. In: *Science* 235.4793 (1987), pp. 1196–1198. ISSN: 0036-8075. DOI: `10.1126/science.235.4793.1196`. eprint: `https://science.sciencemag.org/content/235/4793/1196.full`.

pdf. URL: `https://science.sciencemag.org/content/235/4793/1196`.

[22] V. J. Emery. “Theory of high-T_c superconductivity in oxides”. In: *Phys. Rev. Lett.* 58 (26 June 1987), pp. 2794–2797. DOI: `10.1103/PhysRevLett.58.2794`. URL: `https://link.aps.org/doi/10.1103/PhysRevLett.58.2794`.

[23] A. J. Millis. “Lattice effects in magnetoresistive manganese perovskites”. In: *Nature* 392.6672 (Mar. 1998), pp. 147–150. DOI: `10.1038/32348`.

[24] Yoshinori Tokura. *Colossal magnetoresistive oxides*. CRC Press, 2000.

[25] M. Qazilbash et al. “Mott Transition in VO2 Revealed by Infrared Spectroscopy and Nano-Imaging”. In: *Science (New York, N.Y.)* 318 (Jan. 2008), pp. 1750–3. DOI: `10.1126/science.1150124`.

[26] Mengkun Liu et al. “Phase transition in bulk single crystals and thin films of VO_2 by nanoscale infrared spectroscopy and imaging”. In: *Phys. Rev. B* 91 (24 June 2015), p. 245155. DOI: `10.1103/PhysRevB.91.245155`. URL: `https://link.aps.org/doi/10.1103/PhysRevB.91.245155`.

[27] Daniele Preziosi et al. “Direct Mapping of Phase Separation across the Metal–Insulator Transition of NdNiO3”. In: *Nano Letters* 18.4 (2018). PMID: 29589952, pp. 2226–2232. DOI: `10.1021/acs.nanolett.7b04728`. eprint: `https://doi.org/10.1021/acs.nanolett.7b04728`. URL: `https://doi.org/10.1021/acs.nanolett.7b04728`.

[28] Giordano Mattoni et al. "Striped nanoscale phase separation at the metal-insulator transition of heteroepitaxial nickelates". In: *Nature Communications* 7 (Nov. 2016), p. 13141. DOI: `10.1038/ncomms13141`.

[29] Mehdi Salmani-Jelodar et al. "Design Guidelines for Sub-12 nm Nanowire MOSFETs". In: *IEEE Transactions on Nanotechnology* 14.2 (2015), pp. 210–213. DOI: `10.1109/TNANO.2015.2395441`.

[30] You Zhou et al. "Voltage-Triggered Ultrafast Phase Transition in Vanadium Dioxide Switches". In: *IEEE Electron Device Letters* 34 (2013), pp. 220–222.

[31] Zhensheng Tao et al. "Decoupling of Structural and Electronic Phase Transitions in VO_2". In: *Phys. Rev. Lett.* 109 (16 Oct. 2012), p. 166406. DOI: `10.1103/PhysRevLett.109.166406`. URL: `https://link.aps.org/doi/10.1103/PhysRevLett.109.166406`.

[32] C. Kübler et al. "Coherent Structural Dynamics and Electronic Correlations during an Ultrafast Insulator-to-Metal Phase Transition in VO_2". In: *Phys. Rev. Lett.* 99 (11 Sept. 2007), p. 116401. DOI: `10.1103/PhysRevLett.99.116401`. URL: `https://link.aps.org/doi/10.1103/PhysRevLett.99.116401`.

[33] A. Cavalleri et al. "Femtosecond Structural Dynamics in VO_2 during an Ultrafast Solid-Solid Phase Transition". In: *Phys. Rev. Lett.* 87 (23 Nov. 2001), p. 237401. DOI: `10.1103/PhysRevLett.87.237401`. URL: `https://link.aps.org/doi/10.1103/PhysRevLett.87.237401`.

[34] H. T. Stinson et al. “Imaging the nanoscale phase separation in vanadium dioxide thin films at terahertz frequencies”. In: *Nature Communications* 9.1 (Sept. 2018). ISSN: 2041-1723. DOI: `10.1038/s41467-018-05998-5`. URL: `http://dx.doi.org/10.1038/s41467-018-05998-5`.

[35] Brian T O’Callahan et al. “Inhomogeneity of the ultrafast insulator-to-metal transition dynamics of VO2”. In: *Nature communications* 6 (2015), p. 6849. ISSN: 2041-1723. DOI: `10.1038/ncomms7849`. URL: `https://doi.org/10.1038/ncomms7849`.

[36] F. J. Morin. “Oxides Which Show a Metal-to-Insulator Transition at the Neel Temperature”. In: *Phys. Rev. Lett.* 3 (1 July 1959), pp. 34–36. DOI: `10.1103/PhysRevLett.3.34`. URL: `https://link.aps.org/doi/10.1103/PhysRevLett.3.34`.

[37] C. N. Varney et al. “Quantum Monte Carlo study of the two-dimensional fermion Hubbard model”. In: *Phys. Rev. B* 80 (7 Aug. 2009), p. 075116. DOI: `10.1103/PhysRevB.80.075116`. URL: `https://link.aps.org/doi/10.1103/PhysRevB.80.075116`.

[38] M. Jarrell. “Hubbard model in infinite dimensions: A quantum Monte Carlo study”. In: *Phys. Rev. Lett.* 69 (1 July 1992), pp. 168–171. DOI: `10.1103/PhysRevLett.69.168`. URL: `https://link.aps.org/doi/10.1103/PhysRevLett.69.168`.

[39] Martin C. Gutzwiller. “Effect of Correlation on the Ferromagnetism of Transition Metals”. In: *Phys. Rev. Lett.* 10 (5 Mar. 1963), pp. 159–162.

DOI: `10.1103/PhysRevLett.10.159`. URL: `https://link.aps.org/doi/10.1103/PhysRevLett.10.159`.

[40] Martin C. Gutzwiller. “Correlation of Electrons in a Narrow s Band”. In: *Phys. Rev.* 137 (6A Mar. 1965), A1726–A1735. DOI: `10.1103/PhysRev.137.A1726`. URL: `https://link.aps.org/doi/10.1103/PhysRev.137.A1726`.

[41] Nicola Lanatà et al. “Phase Diagram and Electronic Structure of Praseodymium and Plutonium”. In: *Phys. Rev. X* 5 (1 Jan. 2015), p. 011008. DOI: `10.1103/PhysRevX.5.011008`. URL: `https://link.aps.org/doi/10.1103/PhysRevX.5.011008`.

[42] K. M. Ho, J. Schmalian, and C. Z. Wang. “Gutzwiller density functional theory for correlated electron systems”. In: *Phys. Rev. B* 77 (7 Feb. 2008), p. 073101. DOI: `10.1103/PhysRevB.77.073101`. URL: `https://link.aps.org/doi/10.1103/PhysRevB.77.073101`.

[43] J.-P. JULIEN and J. BOUCHET. “AB-INITIO GUTZWILLER METHOD: FIRST APPLICATION TO PLUTONIUM”. In: *Recent Advances in the Theory of Chemical and Physical Systems*. Ed. by JEAN-PIERRE JULIEN et al. Dordrecht: Springer Netherlands, 2006, pp. 509–534. ISBN: 978-1-4020-4528-8.

[44] Gia-Wei Chern et al. “Mott Transition in a Metallic Liquid: Gutzwiller Molecular Dynamics Simulations”. In: *Phys. Rev. Lett.* 118 (22 June 2017), p. 226401. DOI: `10.1103/PhysRevLett.118.226401`. URL: `https://link.aps.org/doi/10.1103/PhysRevLett.118.226401`.

[45] Hidemaro Suwa et al. "Machine learning for molecular dynamics with strongly correlated electrons". In: *Phys. Rev. B* 99 (16 Apr. 2019), p. 161107. DOI: `10.1103/PhysRevB.99.161107`. URL: `https://link.aps.org/doi/10.1103/PhysRevB.99.161107`.

[46] Walter Metzner and Dieter Vollhardt. "Correlated Lattice Fermions in $d = \infty$ Dimensions". In: *Phys. Rev. Lett.* 62 (3 Jan. 1989), pp. 324–327. DOI: `10.1103/PhysRevLett.62.324`. URL: `https://link.aps.org/doi/10.1103/PhysRevLett.62.324`.

[47] H. Park, K. Haule, and G. Kotliar. "Cluster Dynamical Mean Field Theory of the Mott Transition". In: *Physical Review Letters* 101.18 (Oct. 2008). ISSN: 1079-7114. DOI: `10.1103/physrevlett.101.186403`. URL: `http://dx.doi.org/10.1103/PhysRevLett.101.186403`.

[48] Minh-Tien Tran. "Inhomogeneous phases in the Falicov-Kimball model: Dynamical mean-field approximation". In: *Phys. Rev. B* 73 (20 May 2006), p. 205110. DOI: `10.1103/PhysRevB.73.205110`. URL: `https://link.aps.org/doi/10.1103/PhysRevB.73.205110`.

[49] M Snoek et al. "Antiferromagnetic order of strongly interacting fermions in a trap: real-space dynamical mean-field analysis". In: *New Journal of Physics* 10.9 (Sept. 2008), p. 093008. ISSN: 1367-2630. DOI: `10.1088/1367-2630/10/9/093008`. URL: `http://dx.doi.org/10.1088/1367-2630/10/9/093008`.

[50] R. W. Helmes, T. A. Costi, and A. Rosch. "Mott Transition of Fermionic Atoms in a Three-Dimensional Optical Trap". In: *Physical Review Let-*

ters 100.5 (Feb. 2008). ISSN: 1079-7114. DOI: `10.1103/physrevlett.100.056403`. URL: `http://dx.doi.org/10.1103/PhysRevLett.100.056403`.

[51] Minh-Tien Tran. “Statistics of local density of states in the Falicov-Kimball model with local disorder”. In: *Phys. Rev. B* 76 (24 Dec. 2007), p. 245122. DOI: `10.1103/PhysRevB.76.245122`. URL: `https://link.aps.org/doi/10.1103/PhysRevB.76.245122`.

[52] Michael Potthoff and Matthias Balzer. “Self-energy-functional theory for systems of interacting electrons with disorder”. In: *Physical Review B* 75.12 (Mar. 2007). ISSN: 1550-235X. DOI: `10.1103/physrevb.75.125112`. URL: `http://dx.doi.org/10.1103/PhysRevB.75.125112`.

[53] “Strongly Correlated Systems”. In: *Springer Series in Solid-State Sciences* (2012). ISSN: 0171-1873. DOI: `10.1007/978-3-642-21831-6`. URL: `http://dx.doi.org/10.1007/978-3-642-21831-6`.

[54] G. Ehlers, S. R. White, and R. M. Noack. “Hybrid-space density matrix renormalization group study of the doped two-dimensional Hubbard model”. In: *Physical Review B* 95.12 (Mar. 2017). ISSN: 2469-9969. DOI: `10.1103/physrevb.95.125125`. URL: `http://dx.doi.org/10.1103/PhysRevB.95.125125`.

[55] Baoming Tang, Deepak Iyer, and Marcos Rigol. “Thermodynamics of two-dimensional spin models with bimodal random-bond disorder”. In: *Physical Review B* 91.17 (May 2015). ISSN: 1550-235X. DOI: `10.1103/`

physrevb.91.174413. URL: http://dx.doi.org/10.1103/PhysRevB.91.174413.

[56] Marcos Rigol, Tyler Bryant, and Rajiv R. P. Singh. “Numerical Linked-Cluster Approach to Quantum Lattice Models”. In: *Phys. Rev. Lett.* 97 (18 Nov. 2006), p. 187202. DOI: 10.1103/PhysRevLett.97.187202. URL: https://link.aps.org/doi/10.1103/PhysRevLett.97.187202.

[57] M. D. Mulanix, Demetrius Almada, and Ehsan Khatami. “Numerical linked-cluster expansions for disordered lattice models”. In: *Physical Review B* 99.20 (May 2019). ISSN: 2469-9969. DOI: 10.1103/physrevb.99.205113. URL: http://dx.doi.org/10.1103/PhysRevB.99.205113.

[58] Baoming Tang, Ehsan Khatami, and Marcos Rigol. “A short introduction to numerical linked-cluster expansions”. In: *Computer Physics Communications* 184.3 (Mar. 2013), pp. 557–564. ISSN: 0010-4655. DOI: 10.1016/j.cpc.2012.10.008. URL: http://dx.doi.org/10.1016/j.cpc.2012.10.008.

[59] Ehsan Khatami. “Three-dimensional Hubbard model in the thermodynamic limit”. In: *Physical Review B* 94.12 (Sept. 2016). ISSN: 2469-9969. DOI: 10.1103/physrevb.94.125114. URL: http://dx.doi.org/10.1103/PhysRevB.94.125114.

[60] Milica Milovanovi ć, Subir Sachdev, and R. N. Bhatt. “Effective-field theory of local-moment formation in disordered metals”. In: *Phys. Rev.*

Lett. 63 (1 July 1989), pp. 82–85. DOI: `10.1103/PhysRevLett.63.82`. URL: `https://link.aps.org/doi/10.1103/PhysRevLett.63.82`.

[61] Henrik Kajueter and Gabriel Kotliar. "New Iterative Perturbation Scheme for Lattice Models with Arbitrary Filling". In: *Phys. Rev. Lett.* 77 (1 July 1996), pp. 131–134. DOI: `10.1103/PhysRevLett.77.131`. URL: `https://link.aps.org/doi/10.1103/PhysRevLett.77.131`.

[62] Ralf Bulla, Theo A. Costi, and Thomas Pruschke. "Numerical renormalization group method for quantum impurity systems". In: *Rev. Mod. Phys.* 80 (2 Apr. 2008), pp. 395–450. DOI: `10.1103/RevModPhys.80.395`. URL: `https://link.aps.org/doi/10.1103/RevModPhys.80.395`.

[63] Antoine Georges and Gabriel Kotliar. "Hubbard model in infinite dimensions". In: *Phys. Rev. B* 45 (12 Mar. 1992), pp. 6479–6483. DOI: `10.1103/PhysRevB.45.6479`. URL: `https://link.aps.org/doi/10.1103/PhysRevB.45.6479`.

[64] Louis-François Arsenault, Patrick Sémon, and A.-M. S. Tremblay. "Benchmark of a modified iterated perturbation theory approach on the fcc lattice at strong coupling". In: *Physical Review B* 86.8 (Aug. 2012). ISSN: 1550-235X. DOI: `10.1103/physrevb.86.085133`. URL: `http://dx.doi.org/10.1103/PhysRevB.86.085133`.

[65] Rok Žitko. "Convergence acceleration and stabilization of dynamical mean-field theory calculations". In: *Phys. Rev. B* 80 (12 Sept. 2009),

p. 125125. DOI: `10.1103/PhysRevB.80.125125`. URL: `https://link.aps.org/doi/10.1103/PhysRevB.80.125125`.

[66] V. Dobrosavljevic. *Introduction to Metal-Insulator Transitions.* 2011. arXiv: `1112.6166 [cond-mat.str-el]`.

[67] P. W. Anderson. “Absence of Diffusion in Certain Random Lattices”. In: *Phys. Rev.* 109 (5 Mar. 1958), pp. 1492–1505. DOI: `10.1103/PhysRev.109.1492`. URL: `https://link.aps.org/doi/10.1103/PhysRev.109.1492`.

[68] Patrick A. Lee and T. V. Ramakrishnan. “Disordered electronic systems”. In: *Rev. Mod. Phys.* 57 (2 Apr. 1985), pp. 287–337. DOI: `10.1103/RevModPhys.57.287`. URL: `https://link.aps.org/doi/10.1103/RevModPhys.57.287`.

[69] N F Mott and R Peierls. “Discussion of the paper by de Boer and Verwey”. In: *Proceedings of the Physical Society* 49.4S (Aug. 1937), pp. 72–73. DOI: `10.1088/0959-5309/49/4s/308`. URL: `https://doi.org/10.1088/0959-5309/49/4s/308`.

[70] M. A. Paalanen et al. “Thermodynamic Behavior near a Metal-Insulator Transition”. In: *Phys. Rev. Lett.* 61 (5 Aug. 1988), pp. 597–600. DOI: `10.1103/PhysRevLett.61.597`. URL: `https://link.aps.org/doi/10.1103/PhysRevLett.61.597`.

[71] D. Belitz and T. R. Kirkpatrick. “The Anderson-Mott transition”. In: *Rev. Mod. Phys.* 66 (2 Apr. 1994), pp. 261–380. DOI: `10.1103/RevModPhys.`

66.261. URL: `https://link.aps.org/doi/10.1103/RevModPhys.66.261`.

[72] V. Dobrosavljevi ć and G. Kotliar. “Mean Field Theory of the Mott-Anderson Transition”. In: *Phys. Rev. Lett.* 78 (20 May 1997), pp. 3943–3946. DOI: `10.1103/PhysRevLett.78.3943`. URL: `https://link.aps.org/doi/10.1103/PhysRevLett.78.3943`.

[73] E. Miranda and V. Dobrosavljevi ć. “Localization-Induced Griffiths Phase of Disordered Anderson Lattices”. In: *Phys. Rev. Lett.* 86 (2 Jan. 2001), pp. 264–267. DOI: `10.1103/PhysRevLett.86.264`. URL: `https://link.aps.org/doi/10.1103/PhysRevLett.86.264`.

[74] E Miranda and V Dobrosavljević. “Disorder-driven non-Fermi liquid behaviour of correlated electrons”. In: *Reports on Progress in Physics* 68.10 (Aug. 2005), pp. 2337–2408. ISSN: 1361-6633. DOI: `10.1088/0034-4885/68/10/r02`. URL: `http://dx.doi.org/10.1088/0034-4885/68/10/R02`.

[75] Riku Yamamoto et al. “Electronic Griffiths Phase in Disordered Mott-Transition Systems”. In: *Phys. Rev. Lett.* 124 (4 Jan. 2020), p. 046404. DOI: `10.1103/PhysRevLett.124.046404`. URL: `https://link.aps.org/doi/10.1103/PhysRevLett.124.046404`.

[76] I. K. Kikoin et al. “Electrical Conductivity and Density of a Metal Vapor”. In: *JETP* 22 (1 1966), p. 89.

[77] N. F. Mott. “The electrical properties of liquid mercury”. In: *The Philosophical Magazine: A Journal of Theoretical Experimental and Applied*

Physics 13.125 (1966), pp. 989–1014. DOI: 10.1080/14786436608213149. eprint: https://doi.org/10.1080/14786436608213149. URL: https://doi.org/10.1080/14786436608213149.

[78] F. HENSEL and E. U. FRANCK. "Metal-Nonmetal Transition in Dense Mercury Vapor". In: *Rev. Mod. Phys.* 40 (4 Oct. 1968), pp. 697–703. DOI: 10.1103/RevModPhys.40.697. URL: https://link.aps.org/doi/10.1103/RevModPhys.40.697.

[79] Fumiko Yonezawa and Tohru Ogawa. "Metal-Nonmetal Transitions in Expanded Fluids: Electronic and Thermodynamic Properties". In: *Progress of Theoretical Physics Supplement* 72 (Jan. 1982), pp. 1–80. ISSN: 0375-9687. DOI: 10.1143/PTPS.72.1. eprint: https://academic.oup.com/ptps/article-pdf/doi/10.1143/PTPS.72.1/38664319/72-1.pdf. URL: https://doi.org/10.1143/PTPS.72.1.

[80] F. Hensel and H. Uchtmann. "The Metal-Insulator Transition in Expanded Fluid Metals". In: *Annual Review of Physical Chemistry* 40.1 (1989), pp. 61–83. DOI: 10.1146/annurev.pc.40.100189.000425. eprint: https://doi.org/10.1146/annurev.pc.40.100189.000425. URL: https://doi.org/10.1146/annurev.pc.40.100189.000425.

[81] Morrel H. Cohen and Joshua Jortner. "Conduction regimes in expanded liquid mercury". In: *Phys. Rev. A* 10 (3 Sept. 1974), pp. 978–996. DOI: 10.1103/PhysRevA.10.978. URL: https://link.aps.org/doi/10.1103/PhysRevA.10.978.

[82] T. E. Faber and J. M. Ziman. “A theory of the electrical properties of liquid metals”. In: *The Philosophical Magazine: A Journal of Theoretical Experimental and Applied Physics* 11.109 (1965), pp. 153–173. DOI: `10.1080/14786436508211931`. eprint: `https://doi.org/10.1080/14786436508211931`. URL: `https://doi.org/10.1080/14786436508211931`.

[83] N.F. Mott. “Electrons in disordered structures”. In: *Advances in Physics* 16.61 (1967), pp. 49–144. DOI: `10.1080/00018736700101265`. eprint: `https://doi.org/10.1080/00018736700101265`. URL: `https://doi.org/10.1080/00018736700101265`.

[84] N. F. Mott. “Conduction in non-crystalline materials”. In: *The Philosophical Magazine: A Journal of Theoretical Experimental and Applied Physics* 19.160 (1969), pp. 835–852. DOI: `10.1080/14786436908216338`. eprint: `https://doi.org/10.1080/14786436908216338`. URL: `https://doi.org/10.1080/14786436908216338`.

[85] Scott Kirkpatrick. “Percolation and Conduction”. In: *Rev. Mod. Phys.* 45 (4 Oct. 1973), pp. 574–588. DOI: `10.1103/RevModPhys.45.574`. URL: `https://link.aps.org/doi/10.1103/RevModPhys.45.574`.

[86] D. J. Phelps and C. P. Flynn. “Metal-insulator transition in rare-gas-alkali-metal thin films”. In: *Phys. Rev. B* 14 (12 Dec. 1976), pp. 5279–5288. DOI: `10.1103/PhysRevB.14.5279`. URL: `https://link.aps.org/doi/10.1103/PhysRevB.14.5279`.

[87] Takashi Odagaki, Naofumi Ogita, and Hirotsugu Matsuda. “Percolation Approach to the Metal-Insulator Transition in Super-Critical Fluid Metals”. In: *Journal of the Physical Society of Japan* 39.3 (1975), pp. 618–624. DOI: `10.1143/JPSJ.39.618`. eprint: `https://doi.org/10.1143/JPSJ.39.618`. URL: `https://doi.org/10.1143/JPSJ.39.618`.

[88] V M Nield, M A Howe, and R L McGreevy. “The metal-nonmetal transition in expanded caesium”. In: *Journal of Physics: Condensed Matter* 3.38 (Sept. 1991), pp. 7519–7525. DOI: `10.1088/0953-8984/3/38/023`. URL: `https://doi.org/10.1088/0953-8984/3/38/023`.

[89] P. Tarazona, E. Chacón, and J. P. Hernandez. “Simple Model for the Phase Coexistence and Electrical Conductivity of Alkali Fluids”. In: *Phys. Rev. Lett.* 74 (1 Jan. 1995), pp. 142–145. DOI: `10.1103/PhysRevLett.74.142`. URL: `https://link.aps.org/doi/10.1103/PhysRevLett.74.142`.

[90] T. Arai and R. L. McGreevy. “Percolation Aspects of the Metal-Insulator Transition in Expanded Cs”. In: *Physics and Chemistry of Liquids* 37.4 (1999), pp. 455–462. DOI: `10.1080/00319109908031449`. eprint: `https://doi.org/10.1080/00319109908031449`. URL: `https://doi.org/10.1080/00319109908031449`.

[91] A. Cadien et al. “First-Order Liquid-Liquid Phase Transition in Cerium”. In: *Phys. Rev. Lett.* 110 (12 Mar. 2013), p. 125503. DOI: `10.1103/`

PhysRevLett.110.125503. URL: https://link.aps.org/doi/10.1103/PhysRevLett.110.125503.

[92] Fumiko Yonezawa and Mitsuo Watabe. “Electron Correlation and Metal-Nonmetal Transition in a Disordered Binary System”. In: *Phys. Rev. B* 8 (10 Nov. 1973), pp. 4540–4551. DOI: 10.1103/PhysRevB.8.4540. URL: https://link.aps.org/doi/10.1103/PhysRevB.8.4540.

[93] Fumiko Yonezawa et al. “Electron correlations and metal-insulator transition in structurally disordered systems: General theory and application to supercritical alkali metals”. In: *Phys. Rev. B* 10 (6 Sept. 1974), pp. 2322–2332. DOI: 10.1103/PhysRevB.10.2322. URL: https://link.aps.org/doi/10.1103/PhysRevB.10.2322.

[94] S. Jüngst, B. Knuth, and F. Hensel. “Observation of Singular Diameters in the Coexistence Curves of Metals”. In: *Phys. Rev. Lett.* 55 (20 Nov. 1985), pp. 2160–2163. DOI: 10.1103/PhysRevLett.55.2160. URL: https://link.aps.org/doi/10.1103/PhysRevLett.55.2160.

[95] R. Winter et al. “The static structure factor of cesium over the whole liquid range up to the critical point”. In: *Berichte der Bunsengesellschaft für physikalische Chemie* 91.12 (1987), pp. 1327–1330. DOI: https://doi.org/10.1002/bbpc.19870911205. eprint: https://onlinelibrary.wiley.com/doi/pdf/10.1002/bbpc.19870911205. URL: https://onlinelibrary.wiley.com/doi/abs/10.1002/bbpc.19870911205.

[96] H. Fritzsche, D. Adler, and N. Mott. *Localization and metal-insulator transitions*. 1985.

[97] W. Freyland. “Magnetic susceptibility of metallic and nonmetallic expanded fluid cesium”. In: *Phys. Rev. B* 20 (12 Dec. 1979), pp. 5104–5110. DOI: `10.1103/PhysRevB.20.5104`. URL: `https://link.aps.org/doi/10.1103/PhysRevB.20.5104`.

[98] U. El-Hanany, G. F. Brennert, and W. W. Warren. “Enhanced Paramagnetism and Spin Fluctuations in Expanded Liquid Cesium”. In: *Phys. Rev. Lett.* 50 (7 Feb. 1983), pp. 540–544. DOI: `10.1103/PhysRevLett.50.540`. URL: `https://link.aps.org/doi/10.1103/PhysRevLett.50.540`.

[99] W. W. Warren, G. F. Brennert, and U. El-Hanany. “NMR investigation of the electronic structure of expanded liquid cesium”. In: *Phys. Rev. B* 39 (7 Mar. 1989), pp. 4038–4050. DOI: `10.1103/PhysRevB.39.4038`. URL: `https://link.aps.org/doi/10.1103/PhysRevB.39.4038`.

[100] Kurt Binder et al. “Molecular dynamics simulations”. In: *Journal of Physics: Condensed Matter* 16.5 (Jan. 2004), S429–S453. DOI: `10.1088/0953-8984/16/5/006`. URL: `https://doi.org/10.1088/0953-8984/16/5/006`.

[101] M.P. Allen, D.J. Tildesley, and Oxford University Press. *Computer Simulation of Liquids.* Computer Simulation of Liquids. Clarendon Press, 1987. ISBN: 9780198553755. URL: `https://books.google.com/books?id=ibURAQAAIAAJ`.

[102] D.C. Rapaport and D.C.R. Rapaport. *The Art of Molecular Dynamics Simulation*. Cambridge University Press, 2004. ISBN: 9780521825689. URL: `https://books.google.com/books?id=iqDJ2hjqBMEC`.

[103] E. Fermi et al. *Studies of Nonlinear Problems*. LA (Series) (Los Alamos, N.M.) Los Alamos Scientific Laboratory of the University of California, 1955. URL: `https://books.google.com/books?id=Thgk9gLXZ6AC`.

[104] Alexander D. MacKerell. "Empirical force fields for biological macromolecules: Overview and issues". In: *Journal of Computational Chemistry* 25 (2004).

[105] R. Car and M. Parrinello. "The unified approach to density functional and molecular dynamics in real space". In: *Solid State Communications* 62.6 (1987), pp. 403–405. ISSN: 0038-1098. DOI: `https://doi.org/10.1016/0038-1098(87)91043-X`. URL: `https://www.sciencedirect.com/science/article/pii/003810988791043X`.

[106] M. C. Payne et al. "Iterative minimization techniques for ab initio total-energy calculations: molecular dynamics and conjugate gradients". In: *Rev. Mod. Phys.* 64 (4 Oct. 1992), pp. 1045–1097. DOI: `10.1103/RevModPhys.64.1045`. URL: `https://link.aps.org/doi/10.1103/RevModPhys.64.1045`.

[107] G. Kresse and J. Hafner. "Ab initio molecular dynamics for liquid metals". In: *Phys. Rev. B* 47 (1 Jan. 1993), pp. 558–561. DOI: `10.1103/PhysRevB.47.558`. URL: `https://link.aps.org/doi/10.1103/PhysRevB.47.558`.

[108] Mark E Tuckerman. “Ab initiomolecular dynamics: basic concepts, current trends and novel applications”. In: *Journal of Physics: Condensed Matter* 14.50 (Dec. 2002), R1297–R1355. DOI: `10.1088/0953-8984/14/50/202`. URL: `https://doi.org/10.1088/0953-8984/14/50/202`.

[109] D. Marx and J. Hutter. *Ab Initio Molecular Dynamics: The Virtual Laboratory Approach*. John Wiley & Sons, Incorporated, 2010. ISBN: 9783527319619. URL: `https://books.google.com/books?id=1Ijmiw%5C_EchIC`.

[110] Claudio Attaccalite and Sandro Sorella. “Stable Liquid Hydrogen at High Pressure by a Novel Ab Initio Molecular-Dynamics Calculation”. In: *Phys. Rev. Lett.* 100 (11 Mar. 2008), p. 114501. DOI: `10.1103/PhysRevLett.100.114501`. URL: `https://link.aps.org/doi/10.1103/PhysRevLett.100.114501`.

[111] Martin Head-Gordon and John A. Pople. “Optimization of wave function and geometry in the finite basis Hartree-Fock method”. In: *The Journal of Physical Chemistry* 92.11 (1988), pp. 3063–3069. DOI: `10.1021/j100322a012`. eprint: `https://doi.org/10.1021/j100322a012`. URL: `https://doi.org/10.1021/j100322a012`.

[112] Martin J. Field. “Constrained optimization of ab initio and semiempirical Hartree-Fock wave functions using direct minimization or simulated annealing”. In: *The Journal of Physical Chemistry* 95.13 (1991), pp. 5104–5108. DOI: `10.1021/j100166a037`. eprint: `https://doi.`

org/10.1021/j100166a037. URL: https://doi.org/10.1021/j100166a037.

[113] Richard M. Martin. *Electronic Structure: Basic Theory and Practical Methods*. Cambridge University Press, 2004. DOI: 10.1017/CBO9780511805769.

[114] R. O. Jones. “Density functional theory: Its origins, rise to prominence, and future”. In: *Rev. Mod. Phys.* 87 (3 Aug. 2015), pp. 897–923. DOI: 10.1103/RevModPhys.87.897. URL: https://link.aps.org/doi/10.1103/RevModPhys.87.897.

[115] John P. Perdew and Yue Wang. “Accurate and simple analytic representation of the electron-gas correlation energy”. In: *Phys. Rev. B* 45 (23 June 1992), pp. 13244–13249. DOI: 10.1103/PhysRevB.45.13244. URL: https://link.aps.org/doi/10.1103/PhysRevB.45.13244.

[116] A. D. Becke. “Density-functional exchange-energy approximation with correct asymptotic behavior”. In: *Phys. Rev. A* 38 (6 Sept. 1988), pp. 3098–3100. DOI: 10.1103/PhysRevA.38.3098. URL: https://link.aps.org/doi/10.1103/PhysRevA.38.3098.

[117] J. P. Perdew and Alex Zunger. “Self-interaction correction to density-functional approximations for many-electron systems”. In: *Phys. Rev. B* 23 (10 May 1981), pp. 5048–5079. DOI: 10.1103/PhysRevB.23.5048. URL: https://link.aps.org/doi/10.1103/PhysRevB.23.5048.

[118] Takao Tsuneda and Kimihiko Hirao. “Self-interaction corrections in density functional theory”. In: *The Journal of Chemical Physics* 140 (Apr. 2014). DOI: 10.1063/1.4866996.

[119] V. I. Anisimov and O. Gunnarsson. "Density-functional calculation of effective Coulomb interactions in metals". In: *Phys. Rev. B* 43 (10 Apr. 1991), pp. 7570–7574. DOI: `10.1103/PhysRevB.43.7570`. URL: `https://link.aps.org/doi/10.1103/PhysRevB.43.7570`.

[120] Canio Noce. "The periodic Anderson model: Symmetry-based results and some exact solutions". In: *Physics Reports-review Section of Physics Letters - PHYS REP-REV SECT PHYS LETT* 431 (Aug. 2006), pp. 173–230. DOI: `10.1016/j.physrep.2006.05.003`.

[121] Martin C. Gutzwiller. "Effect of Correlation on the Ferromagnetism of Transition Metals". In: *Phys. Rev.* 134 (4A May 1964), A923–A941. DOI: `10.1103/PhysRev.134.A923`. URL: `https://link.aps.org/doi/10.1103/PhysRev.134.A923`.

[122] W. F. Brinkman and T. M. Rice. "Application of Gutzwiller's Variational Method to the Metal-Insulator Transition". In: *Phys. Rev. B* 2 (10 Nov. 1970), pp. 4302–4304. DOI: `10.1103/PhysRevB.2.4302`. URL: `https://link.aps.org/doi/10.1103/PhysRevB.2.4302`.

[123] Dieter Vollhardt. "Normal ^{3}He: an almost localized Fermi liquid". In: *Rev. Mod. Phys.* 56 (1 Jan. 1984), pp. 99–120. DOI: `10.1103/RevModPhys.56.99`. URL: `https://link.aps.org/doi/10.1103/RevModPhys.56.99`.

[124] Gia-Wei Chern. *Kinetics of thermal Mott transitions in the Hubbard model*. 2021. arXiv: `1907.05880 [cond-mat.str-el]`.

[125] Gabriel Kotliar and Andrei Ruckenstein. "New Functional Integral Approach to Strongly Correlated Fermi Systems: The Gutzwiller Approximation as a Saddle Point". In: *Physical review letters* 57 (Oct. 1986), pp. 1362–1365. DOI: `10.1103/PhysRevLett.57.1362`.

[126] J. Bünemann and F. Gebhard. "Equivalence of Gutzwiller and slave-boson mean-field theories for multiband Hubbard models". In: *Physical Review B* 76.19 (Nov. 2007). ISSN: 1550-235X. DOI: `10.1103/physrevb.76.193104`. URL: `http://dx.doi.org/10.1103/PhysRevB.76.193104`.

[127] Frank Lechermann et al. "Rotationally invariant slave-boson formalism and momentum dependence of the quasiparticle weight". In: *Phys. Rev. B* 76 (15 Oct. 2007), p. 155102. DOI: `10.1103/PhysRevB.76.155102`. URL: `https://link.aps.org/doi/10.1103/PhysRevB.76.155102`.

[128] Nicola Lanatà et al. "Slave Boson Theory of Orbital Differentiation with Crystal Field Effects: Application toUO2". In: *Physical Review Letters* 118.12 (Mar. 2017). ISSN: 1079-7114. DOI: `10.1103/physrevlett.118.126401`. URL: `http://dx.doi.org/10.1103/PhysRevLett.118.126401`.

[129] Emanuel Gull et al. "Continuous-time Monte Carlo methods for quantum impurity models". In: *Reviews of Modern Physics* 83.2 (May 2011), pp. 349–404. ISSN: 1539-0756. DOI: `10.1103/revmodphys.83.349`. URL: `http://dx.doi.org/10.1103/RevModPhys.83.349`.

[130] Walter Metzner and Dieter Vollhardt. “Ground-state properties of correlated fermions: Exact analytic results for the Gutzwiller wave function”. In: *Phys. Rev. Lett.* 59 (1 July 1987), pp. 121–124. DOI: `10.1103/PhysRevLett.59.121`. URL: `https://link.aps.org/doi/10.1103/PhysRevLett.59.121`.

[131] E. Müller-Hartmann. “The Hubbard model at high dimensions: some exact results and weak coupling theory”. In: *Zeitschrift für Physik B Condensed Matter* 76 (1989), pp. 211–217.

[132] M. Potthoff and W. Nolting. “Surface metal-insulator transition in the Hubbard model”. In: *Physical Review B* 59.4 (Jan. 1999), pp. 2549–2555. ISSN: 1095-3795. DOI: `10.1103/physrevb.59.2549`. URL: `http://dx.doi.org/10.1103/PhysRevB.59.2549`.

[133] H. Ishida and A. Liebsch. “Embedding approach for dynamical mean-field theory of strongly correlated heterostructures”. In: *Phys. Rev. B* 79 (4 Jan. 2009), p. 045130. DOI: `10.1103/PhysRevB.79.045130`. URL: `https://link.aps.org/doi/10.1103/PhysRevB.79.045130`.

[134] J. K. Freericks. “Dynamical mean-field theory for strongly correlated inhomogeneous multilayered nanostructures”. In: *Physical Review B* 70.19 (Nov. 2004). ISSN: 1550-235X. DOI: `10.1103/physrevb.70.195342`. URL: `http://dx.doi.org/10.1103/PhysRevB.70.195342`.

[135] Satoshi Okamoto. “Nonlinear Transport through Strongly Correlated Two-Terminal Heterostructures: A Dynamical Mean-Field Approach”. In: *Phys. Rev. Lett.* 101 (11 Sept. 2008), p. 116807. DOI: `10.1103/`

PhysRevLett.101.116807. URL: https://link.aps.org/doi/10.1103/PhysRevLett.101.116807.

[136] E. V. Gorelik et al. “Néel Transition of Lattice Fermions in a Harmonic Trap: A Real-Space Dynamic Mean-Field Study”. In: *Physical Review Letters* 105.6 (Aug. 2010). ISSN: 1079-7114. DOI: 10.1103/physrevlett.105.065301. URL: http://dx.doi.org/10.1103/PhysRevLett.105.065301.

[137] J. Hubbard and Brian Hilton Flowers. “Electron correlations in narrow energy bands”. In: *Proceedings of the Royal Society of London. Series A. Mathematical and Physical Sciences* 276.1365 (1963), pp. 238–257. DOI: 10.1098/rspa.1963.0204. eprint: https://royalsocietypublishing.org/doi/pdf/10.1098/rspa.1963.0204. URL: https://royalsocietypublishing.org/doi/abs/10.1098/rspa.1963.0204.

[138] J. Hubbard and Brian Hilton Flowers. “Electron correlations in narrow energy bands III. An improved solution”. In: *Proceedings of the Royal Society of London. Series A. Mathematical and Physical Sciences* 281.1386 (1964), pp. 401–419. DOI: 10.1098/rspa.1964.0190. eprint: https://royalsocietypublishing.org/doi/pdf/10.1098/rspa.1964.0190. URL: https://royalsocietypublishing.org/doi/abs/10.1098/rspa.1964.0190.

[139] Junjiro Kanamori. “Electron Correlation and Ferromagnetism of Transition Metals”. In: *Progress of Theoretical Physics* 30.3 (Sept. 1963), pp. 275–289. ISSN: 0033-068X. DOI: 10.1143/PTP.30.275. eprint:

https://academic.oup.com/ptp/article-pdf/30/3/275/5278869/30-3-275.pdf. URL: https://doi.org/10.1143/PTP.30.275.

[140] Hal Tasaki. “The Hubbard model - an introduction and selected rigorous results”. In: *Journal of Physics: Condensed Matter* 10.20 (May 1998), pp. 4353–4378. DOI: 10.1088/0953-8984/10/20/004. URL: https://doi.org/10.1088/0953-8984/10/20/004.

[141] Patrick Fazekas. *Lecture Notes on Electron Correlation and Magnetism.* WORLD SCIENTIFIC, 1999. DOI: 10.1142/2945. eprint: https://www.worldscientific.com/doi/pdf/10.1142/2945. URL: https://www.worldscientific.com/doi/abs/10.1142/2945.

[142] J. P. F. LeBlanc et al. “Solutions of the Two-Dimensional Hubbard Model: Benchmarks and Results from a Wide Range of Numerical Algorithms”. In: *Phys. Rev. X* 5 (4 Dec. 2015), p. 041041. DOI: 10.1103/PhysRevX.5.041041. URL: https://link.aps.org/doi/10.1103/PhysRevX.5.041041.

[143] Mingpu Qin et al. “Absence of Superconductivity in the Pure Two-Dimensional Hubbard Model”. In: *Phys. Rev. X* 10 (3 July 2020), p. 031016. DOI: 10.1103/PhysRevX.10.031016. URL: https://link.aps.org/doi/10.1103/PhysRevX.10.031016.

[144] Thomas Schäfer et al. “Tracking the Footprints of Spin Fluctuations: A MultiMethod, MultiMessenger Study of the Two-Dimensional Hubbard Model”. In: *Physical Review X* 11.1 (Mar. 2021). ISSN: 2160-3308. DOI:

10.1103/physrevx.11.011058. URL: `http://dx.doi.org/10.1103/PhysRevX.11.011058`.

[145] Elliott H. Lieb and F. Y. Wu. “Absence of Mott Transition in an Exact Solution of the Short-Range, One-Band Model in One Dimension”. In: *Phys. Rev. Lett.* 20 (25 June 1968), pp. 1445–1448. DOI: `10.1103/PhysRevLett.20.1445`. URL: `https://link.aps.org/doi/10.1103/PhysRevLett.20.1445`.

[146] John C. Tully. “Perspective: Nonadiabatic dynamics theory”. In: *The Journal of Chemical Physics* 137.22 (2012), 22A301. DOI: `10.1063/1.4757762`. eprint: `https://doi.org/10.1063/1.4757762`. URL: `https://doi.org/10.1063/1.4757762`.

[147] Nils Erik Dahlen and Robert van Leeuwen. “Solving the Kadanoff-Baym Equations for Inhomogeneous Systems: Application to Atoms and Molecules”. In: *Phys. Rev. Lett.* 98 (15 Apr. 2007), p. 153004. DOI: `10.1103/PhysRevLett.98.153004`. URL: `https://link.aps.org/doi/10.1103/PhysRevLett.98.153004`.

[148] M. Puig von Friesen, C. Verdozzi, and C.-O. Almbladh. “Successes and Failures of Kadanoff-Baym Dynamics in Hubbard Nanoclusters”. In: *Physical Review Letters* 103.17 (Oct. 2009). ISSN: 1079-7114. DOI: `10.1103/physrevlett.103.176404`. URL: `http://dx.doi.org/10.1103/PhysRevLett.103.176404`.

[149] N. Schlünzen et al. “Dynamics of strongly correlated fermions: Ab initio results for two and three dimensions”. In: *Phys. Rev. B* 93 (3 Jan.

2016), p. 035107. DOI: `10.1103/PhysRevB.93.035107`. URL: `https://link.aps.org/doi/10.1103/PhysRevB.93.035107`.

[150] Niclas Schlünzen, Jan-Philip Joost, and Michael Bonitz. "Achieving the Scaling Limit for Nonequilibrium Green Functions Simulations". In: *Phys. Rev. Lett.* 124 (7 Feb. 2020), p. 076601. DOI: `10.1103/PhysRevLett.124.076601`. URL: `https://link.aps.org/doi/10.1103/PhysRevLett.124.076601`.

[151] Niels Bode et al. "Scattering Theory of Current-Induced Forces in Mesoscopic Systems". In: *Physical Review Letters* 107.3 (July 2011). ISSN: 1079-7114. DOI: `10.1103/physrevlett.107.036804`. URL: `http://dx.doi.org/10.1103/PhysRevLett.107.036804`.

[152] Vincent F. Kershaw and Daniel S. Kosov. "Nonequilibrium Green's function theory for nonadiabatic effects in quantum electron transport". In: *The Journal of Chemical Physics* 147.22 (2017), p. 224109. DOI: `10.1063/1.5007071`. eprint: `https://doi.org/10.1063/1.5007071`. URL: `https://doi.org/10.1063/1.5007071`.

[153] Wenjie Dou, Gaohan Miao, and Joseph E. Subotnik. "Born-Oppenheimer Dynamics, Electronic Friction, and the Inclusion of Electron-Electron Interactions". In: *Phys. Rev. Lett.* 119 (4 July 2017), p. 046001. DOI: `10.1103/PhysRevLett.119.046001`. URL: `https://link.aps.org/doi/10.1103/PhysRevLett.119.046001`.

[154] Thomas D. Honeychurch and Daniel S. Kosov. "Timescale separation solution of the Kadanoff-Baym equations for quantum transport in

time-dependent fields". In: *Phys. Rev. B* 100 (24 Dec. 2019), p. 245423. DOI: `10.1103/PhysRevB.100.245423`. URL: `https://link.aps.org/doi/10.1103/PhysRevB.100.245423`.

[155] Vincent F. Kershaw and Daniel S. Kosov. "Non-equilibrium Green's function theory for non-adiabatic effects in quantum transport: Inclusion of electron-electron interactions". In: *The Journal of Chemical Physics* 150.7 (Feb. 2019), p. 074101. ISSN: 1089-7690. DOI: `10.1063/1.5058735`. URL: `http://dx.doi.org/10.1063/1.5058735`.

[156] X. Y. Zhang, M. J. Rozenberg, and G. Kotliar. "Mott transition in the d=∞ Hubbard model at zero temperature". In: *Phys. Rev. Lett.* 70 (11 Mar. 1993), pp. 1666–1669. DOI: `10.1103/PhysRevLett.70.1666`. URL: `https://link.aps.org/doi/10.1103/PhysRevLett.70.1666`.

[157] Norm M. Tubman et al. "Molecular-Atomic Transition along the Deuterium Hugoniot Curve with Coupled Electron-Ion Monte Carlo Simulations". In: *Phys. Rev. Lett.* 115 (4 July 2015), p. 045301. DOI: `10.1103/PhysRevLett.115.045301`. URL: `https://link.aps.org/doi/10.1103/PhysRevLett.115.045301`.

[158] W. R. Magro et al. "Molecular Dissociation in Hot, Dense Hydrogen". In: *Phys. Rev. Lett.* 76 (8 Feb. 1996), pp. 1240–1243. DOI: `10.1103/PhysRevLett.76.1240`. URL: `https://link.aps.org/doi/10.1103/PhysRevLett.76.1240`.

[159] T. Senthil. "Theory of a continuous Mott transition in two dimensions". In: *Phys. Rev. B* 78 (4 July 2008), p. 045109. DOI: `10.1103/PhysRevB.`

78.045109. URL: `https://link.aps.org/doi/10.1103/PhysRevB.78.045109`.

[160] Ryan V. Mishmash et al. "Continuous Mott transition between a metal and a quantum spin liquid". In: *Phys. Rev. B* 91 (23 June 2015), p. 235140. DOI: `10.1103/PhysRevB.91.235140`. URL: `https://link.aps.org/doi/10.1103/PhysRevB.91.235140`.

[161] Daniel Podolsky et al. "Mott Transition between a Spin-Liquid Insulator and a Metal in Three Dimensions". In: *Phys. Rev. Lett.* 102 (18 May 2009), p. 186401. DOI: `10.1103/PhysRevLett.102.186401`. URL: `https://link.aps.org/doi/10.1103/PhysRevLett.102.186401`.

[162] Ahmed Ibrahim and Thomas Vojta. "Emerging critical behavior at a first-order phase transition rounded by disorder". In: *Fortschritte der Physik* 65 (Feb. 2016). DOI: `10.1002/prop.201600018`.

[163] Michael Aizenman and Jan Wehr. "Rounding of first-order phase transitions in systems with quenched disorder". In: *Phys. Rev. Lett.* 62 (21 May 1989), pp. 2503–2506. DOI: `10.1103/PhysRevLett.62.2503`. URL: `https://link.aps.org/doi/10.1103/PhysRevLett.62.2503`.

[164] Kenneth Hui and A. Nihat Berker. "Random-field mechanism in random-bond multicritical systems". In: *Phys. Rev. Lett.* 62 (21 May 1989), pp. 2507–2510. DOI: `10.1103/PhysRevLett.62.2507`. URL: `https://link.aps.org/doi/10.1103/PhysRevLett.62.2507`.

[165] Jianhua Ma et al. "Machine learning electron correlation in a disordered medium". In: *Phys. Rev. B* 99 (8 Feb. 2019), p. 085118. DOI: `10.1103/`

`PhysRevB.99.085118`. URL: `https://link.aps.org/doi/10.1103/PhysRevB.99.085118`.

[166] M. Charlebois et al. “Impurity-induced magnetic moments on the graphene-lattice Hubbard model: An inhomogeneous cluster dynamical mean-field theory study”. In: *Phys. Rev. B* 91 (3 Jan. 2015), p. 035132. DOI: `10.1103/PhysRevB.91.035132`. URL: `https://link.aps.org/doi/10.1103/PhysRevB.91.035132`.

[167] Charles L. Cleveland and Rodrigo Medina A. “Obtaining a Heisenberg Hamiltonian from the Hubbard model”. In: *American Journal of Physics* 44.1 (1976), pp. 44–46. DOI: `10.1119/1.10537`. eprint: `https://doi.org/10.1119/1.10537`. URL: `https://doi.org/10.1119/1.10537`.

[168] P. W. Anderson. “New Approach to the Theory of Superexchange Interactions”. In: *Phys. Rev.* 115 (1 July 1959), pp. 2–13. DOI: `10.1103/PhysRev.115.2`. URL: `https://link.aps.org/doi/10.1103/PhysRev.115.2`.

[169] P. W. Anderson. “Antiferromagnetism. Theory of Superexchange Interaction”. In: *Phys. Rev.* 79 (2 July 1950), pp. 350–356. DOI: `10.1103/PhysRev.79.350`. URL: `https://link.aps.org/doi/10.1103/PhysRev.79.350`.

[170] Wiebe Geertsma and D. Khomskii. “Influence of side groups on 90° superexchange: A modification of the Goodenough-Kanamori-Anderson rules”. In: *Phys. Rev. B* 54 (5 Aug. 1996), pp. 3011–3014. DOI: `10.`

1103/PhysRevB.54.3011. URL: https://link.aps.org/doi/10.1103/PhysRevB.54.3011.

[171] P. -G. de Gennes. “Effects of Double Exchange in Magnetic Crystals”. In: *Phys. Rev.* 118 (1 Apr. 1960), pp. 141–154. DOI: 10.1103/PhysRev.118.141. URL: https://link.aps.org/doi/10.1103/PhysRev.118.141.

[172] Conrad Sanderson and Ryan Curtin. “Armadillo: a template-based C++ library for linear algebra”. In: *Journal of Open Source Software* 1.2 (2016), p. 26. DOI: 10.21105/joss.00026. URL: https://doi.org/10.21105/joss.00026.

[173] Conrad Sanderson and Ryan Curtin. “A User-Friendly Hybrid Sparse Matrix Class in C++”. In: *arXiv e-prints*, arXiv:1805.03380 (May 2018), arXiv:1805.03380. arXiv: 1805.03380 [cs.MS].

[174] Ronald Redmer and William W. Warren. “Magnetic susceptibility of Cs and Rb from the vapor to the liquid phase”. In: *Phys. Rev. B* 48 (20 Nov. 1993), pp. 14892–14906. DOI: 10.1103/PhysRevB.48.14892. URL: https://link.aps.org/doi/10.1103/PhysRevB.48.14892.

[175] Magnus Lipp et al. “Equation of state measurements by radiography provide evidence for a liquid-liquid phase transition in cerium”. In: *Journal of Physics: Conference Series* 500 (May 2014), p. 032011. DOI: 10.1088/1742-6596/500/3/032011.